UNIVERSIDAD
POLITECNICA
DE VALENCIA

MODIFICACIONES DEL ÁCIDO HIALURÓNICO COMO MATERIAL PARA LA REGENERACIÓN DEL SISTEMA NERVIOSO CENTRAL

……

HYALURONAN BASED BIOMATERIALS FOR CENTRAL NERVOUS TISSUE REGENERATION

Amparo Baiget Orts

Tesis Doctoral / enero 2012
Thesis Dissertation / *January 2012*

Director/*Supervisor* Manuel Monleón Pradas

“Science never solves a problem without creating ten more”

George Bernand Shaw

“La Tesis es eso que haces mientras pasa la vida”

Nuria B.

Quiero dedicar mi Tesis a mis padres, Carlos y Amparo. A mis hermanos, Nuria, Carlos y Begoña y a quienes se han convertido en tales, Jaume y Mª Jose. Han sido imprescindibles para hoy cerrar este trabajo con estas líneas y conforman la pared que me sostiene cuando el viento sopla fuerte…

Gracias por vuestro apoyo, consejos, soporte y compartir conmigo vuestra sabiduría.

Se la dedico también a Marc, Ada y Atila. Por que sin saberlo ellos todavía, han contribuido con sus pózimas mágicas de energía y sus sonrisas llenas de vida.

Os deseo la mejor vida que os podáis imaginar, la que vosotros escojáis.

Acknowledgements

I would like to express my gratitude to my supervisor, Dr. Manuel Monleón Pradas, for his support and dedication.

I really appreciated the help and encouragement of Prof. Manuel Salmerón Sánchez during my research and writing.

Thanks to the group of the Center for Biomaterials and Tissue Engineering for the comfortable and friendly environment. I would like to thank especially the ones who helped me daily in my personal and professional development during the more than six years I have been working there. Thanks to Elisa for sharing with me the first few years and the one p.m. coffee. Thanks to Myriam for withstanding my half sugar bags among so many other things. To Cristina M., Miriam H and Marco for their wholeheart support. In general to my collegues for their smiles and friendship,

I would like to thank Pedro and Patri for their frienship and the best Thesis cover ever seen. Good luck in your new project.

Thanks to Mª Jesús Vicent, who heads the Polymer Therapeutics Laboratory at the Prince Felip Research Center in Valencia, for her friendly welcome and support during the whole period I had the pleasure of working with her and her group. My special thanks to Vanessa and Inma to which I wish the best for their future defenses.

Very special thanks to Prof. C.J. Kirkpatrick and Dr. Ronald Unger, from the Institute of Pathology of the Johannes Gutenberg University of Mainz (Germany) for giving me the opportunity to work in their laboratory. Thanks to Anne Sartorius for her guidance, patience and friendliness and to Christian, Roman, Eva and Susana and all the guys of the lab for making every day as easy as staying at home.

Thanks to Ulises Alfonso Gomez Pinedo, from the Health Institute Carlos III of Madrid (Spain), for his support and guidance during the writing.

The financial support from the Spanish Science and Technology Minitry through the Project MAT2008-06434 and Convenio GVA-Instituto Nacional de Salud Carlos III “Programa de Medicina Regenerativa del Centro de Investigación Príncipe Felipe” is acknowledged and appreciated.

Last but not least, I want to give particular thanks to my friends: a mis amigos y amigas, los que me han acompañado siempre y los que he tenido la suerte de conocer mientras la Tesis ha sido mi vida: gracias! Por vuestro apoyo, comprensión y por todo el tiempo que hemos compartido y disfrutado juntos. Quiero hacer una mención especial para Pili y Ana, principio y final de mi aventura germana y compañeras incondicionales de este viaje que es la vida…

SUMMARY 11
RESUMEN 13
RESUM….. 15
CHAPTER 1. INTRODUCTION 17
1.1. TISSUE ENGINEERING 19
1.1.1. SCAFFOLDS FOR TE. 20
1.1.2. BIOMATERIALS AS SCAFFOLDS FOR TE APPLICATIONS 22
1.2. NEURAL TISSUE ENGINEERING 25
1.2.1. THE NERVOUS SYSTEM 26
1.2.2. THE BLOOD BRAIN BARRIER 28
1.2.3. NEUROLOGICAL DISEASES 31
1.3. HYALURONIC ACID 33
1.3.1. INTRODUCTION 33
1.3.2. MODIFICATION OF HYALURONIC ACID 36
1.3.3. HYALURONIC ACID IN TISSUE ENGINEERING 40
1.3.4. HYALURONIC ACID IN THE NERVOUS SYSTEM 42
1.3.5. SCAFFOLD INTEGRATION AND ANGIOGENESIS 43
1.3.6. ANGIOGENIC GROWTH FACTORS 45
HYPHOTESIS AND OBJETIVES 50
CHAPTER 2. MATERIALS AND METHODS 54
2.1 MATERIALS AND CELL LINES 56
2.2 METHODS 57
2.2.1. HYALURONAN CROSSLINKING 57
2.2.2. SCAFFOLDS FABRICATION. 59
2.2.3. MATERIALS CHARACTERIZATION 63
2.2.4. CELL CULTURE 71

CHAPTER 3.RESULTS 78
3.1. HYALURONAN CROSSLINKING 80
3.2. HA HYDROGELS CHARACTERIZATION 86
3.2.1. FOURIER TRANSFORMED INFRARED SPECTRA 87
3.2.2. WATER ABSORPTION CAPACITY 89
3.2.3. VOLUMETRIC SWELLING 91
3.2.4. COMPRESSION TESTS 92
3.2.5. ENZYMATIC DEGRADATION OF HA HYDROGELS 94
3.3. DEVELOPMENT OF HA BASED 3D STRUCTURES 96
3.3.1. STRUCTURES BASED IN HA-DEO 97
3.3.2. STRUCTURES BASED IN HA-DVS 100
3.4. HCMEC/D3 & U373 MONOCULTURES ON BIOMATERIALS. 106
3.4.1. HYALURONAN BASED BIOMATERIALS 106
3.4.2. ACRYLIC BASED BIOMATERIALS. 129
3.5. HCMEC/D3 & U373 CO-CULTURES ON BIOMATERIALS 139
3.5.1. HA BASED BIOMATERIALS 142
3.5.2. ACRYLIC BASED BIOMATERIALS. 149
CHAPTER 4. DISCUSSION 156
CONCLUSIONS 177
REFERENCES 181
LIST OF ABBREVIATIONS 199
LIST OF TABLES 201
LIST OF FIGURES 201

SUMMARY

The aim of this Thesis is to investigate the use of hyaluronic acid as a material for the design of scaffolds aimed at CNS regeneration. The motivation comes from the need of searching for new strategies that allow regeneration in the central nervous system. In degenerative diseases, such as Parkinson's disease, where the progressive loss of neuronal subpopulations occurs, a permissive environment able to support regeneration and connectivity of neurons from the host tissue may be a promising therapy to recover lost functionalities. In this Thesis we have focused on the development of structures able to integrate within the brain, supporting neural cells attachment and survival.

We hypothesized that hyaluronic acid provides an enabling environment and appropriate for regeneration due to its biocompatibility and diverses physiological applications. Biocompatible hydrogels based on modified hyaluronic acid were synthesized. Covalently crosslinked hyaluronic acid hydrogels, alone or in combination with acrylic polymers, were synthesized and permitted to develop different porous structures which may serve in different applications as cell supply, cell repopulation or tissue regeneration. Highly porous with interconnected spherical pores, hollow tubes or multichanneled scaffolds were developed. The processes allow for a wide range of shapes for different applications within the scope of central nervous system regeneration.

Furthermore, *in vitro* culture of human cell lines together with biomaterials was performed. A human microvascular endothelial cell line (hCMEC/D3) and a human glioma cell line (U373) were chosen for the studies. Experiments were focused on the interaction between hyaluronan based scaffolds and those cell lines composing the blood-brain-barrier (BBB) in the central nervous system. Biocompatibility, viability and phenotype characteristics were assessed. Hyaluronan based scaffolds did not elicit any

inflammatory response when cultured with endothelial cells and demonstrated to be a good cue to the growth of both cell lines in mono and co-culture. In addition, endothelial cells (ECs) exhibited reorganization into cord-like structures within the biomaterials. The reorganization of EC is necessary as response of angiogenic stimuli and the formation of new vascular sprouts which will guarantee a favourable integration of the scaffold with the host tissue. The influence of two different protein coatings prior to cell seeding was evaluated. On the one hand, laminin (LN), a protein derived from the basal lamina that participates in neuronal development, survival and regeneration; on the other hand, a coating of fibrin matrix (fb), which provides a suitable scaffolding for invading inflammatory, endothelial, and other tissue cells during the healing process. Results did not show noticeable differences between one protein and another in long periods of culture.

RESUMEN

El objetivo de esta tesis es investigar el uso de ácido hialurónico como material para el diseño de andamios “scaffolds” para su uso en la regeneración del sistema nervioso central (CNS de sus siglas en ingles: central nervous system). La motivación viene de la necesidad de buscar nuevas estrategias que permitan la regeneración del sistema nervioso central. En las enfermedades degenerativas, como la enfermedad de Parkinson, donde se produce una pérdida progresiva de las subpoblaciones neuronales, un ambiente permisivo capaz de apoyar la regeneración y la conectividad de las neuronas de los tejidos huésped puede ser una terapia prometedora para recuperar las funciones perdidas. En esta tesis nos hemos centrado en el desarrollo de estructuras capaces de ser integradas dentro del cerebro, que promuevan la adhesión celular y su supervivencia.

Nuestra hipótesis es que el ácido hialurónico proporciona un buen ambiente para la regeneración, debido a su biocompatibilidad y su gran diversidad de aplicaciones fisiológicas. A tal efecto se sintetizaron hidrogeles biocompatibles basados en ácido hialurónico modificado, covalentemente entrecruzados, solos o en combinación con polímeros acrílicos. Dichos materiales permitieron desarrollar diferentes estructuras porosas que pudieran servir para diferentes propósitos, tales como el suministro de células, la repoblación de células en zonas dañadas y la regeneración del tejido. Se prepararon estructuras altamente porosas, con poros esféricos interconectados, tubos huecos o scaffolds con multiples canales longitudinalmente dispuestos. Los hidrogeles sintetizados permitieron obtener una amplia gama de estrucuras para diferentes aplicaciones dentro del ámbito de la regeneración del sistema nervioso central.

Se llevaron a cabo cultivos *in vitro* de líneas celulares humanas con nuestros biomateriales basándonos en el uso de líneas celulares que componen la barrera hematoencefálica (BBB de sus siglas en inglés, blood-

brain-barrier) en el sistema nervioso central. Las células escogidas fueron una línea celular humana endotelial de la microvasculatura del cerebro (hCMEC) y una línea de células de glioma humano (U373). Los experimentos se centraron en la interacción entre el ácido hialurónico y dichas células y se evaluaron características como biocompatibilidad, viabilidad y fenotipo. Los biomaterials basados en ácido hialurónico no provocaron ninguna reacción inflamatoria cuando se cultivaron con hCMEC. Los resultados demostraron que los materiales empleados eran favorables para el crecimiento de ambas lineas celulares tanto en mono como en co-cultivo. Además, las células endoteliales mostraron reorganización de la matriz extracelular para formar estructuras en forma de cable creciendo en los biomateriales. La reorganización de las células endoteliales es necesaria como respuesta a estímulos angiogénicos y la formación de nuevos brotes vasculares que garantizan una integración favorable del scaffold con el tejido huésped. Se evaluaó asimimo la influencia del recubrimiento de dos proteinas diferentes antes de la siembra celular. Por un lado, laminina (LN), una proteína derivada de la lámina basal que participa en el desarrollo neuronal de supervivencia, y la regeneración, por otro lado, una red de fibrina (fb), que proporciona un andamiaje adecuado para la invasión de células endoteliales inflamatorias y células de otros tejidos durante el proceso de curación. Los resultados no mostraron diferencias notables entre una proteína u otra tras largos periodos de cultivo.

RESUM

L'objectiu d'aquesta tesi és investigar l'ús d'àcid hialurònic com a material per al disseny de bastides "esquelets" per al seu ús en la regeneració del SNC. La motivació ve de la necessitat de buscar noves estratègies que permetin la regeneració del sistema nerviós central. En les malalties degeneratives, com la malaltia de Parkinson, on es produeix una pèrdua progressiva de les subpoblacions neuronals, un ambient permissiu capaç de donar suport a la regeneració i la connectivitat de les neurones dels teixits hoste pot ser una teràpia prometedora per recuperar les funcions perdudes. En aquesta tesi ens hem centrat en el desenvolupament d'estructures capaços de ser integrades dins del cervell, que promoguin l'adhesió cel.lular i la seva supervivència.

La nostra hipòtesi és que l'àcid hialurònic proporciona un bon ambient per a la regeneració, per la seva biocompatibilitat i la seva gran diversitat d'aplicacions fisiològiques. A aquest efecte es van sintetitzar hidrogels biocompatibles basats en àcid hialurònic modificat, covalentment entrecreuats, sols o en combinació amb polímers acrílics. Aquests materials van permetre desenvolupar diferents estructures poroses que poguessin servir per a diferents propòsits, com ara el subministrament de cèl.lules, la repoblació de cèl.lules en zones danyades i la regeneració del teixit. Es van preparar estructures altament poroses, amb porus esfèrics interconnectats, tubs buits o esquelets amb múltiples canals longitudinalment disposats. Els hidrogels sintetitzats permetre obtenir una àmplia gamma de estructures per a diferents aplicacions dins l'àmbit de la regeneració del sistema nerviós central.

Es van dur a terme cultius *in vitro* de línies cel.lulars humanes amb els nostres biomaterials basant-nos en l'ús de línies cel.lulars que componen la barrera hematoencefàlica (BBB de les seves sigles en anglès, blood brain barrier) en el sistema nerviós central. Les cèl.lules escollides van ser una línia cel.lular humana endotelial de la microvasculatura del cervell

(hCMEC/D3) i una línia de cèl.lules de glioma humà (U373). Els experiments es van centrar en la interacció entre l'àcid hialurònic i les cèl.lules i es van avaluar característiques com biocompatibilitat, viabilitat i fenotip. Els biomaterials basats en àcid hialurònic no van provocar cap reacció inflamatòria quan es van cultivar amb la línea de cel.lules endotelial. Els resultats van demostrar que els materials emprats eren favorables per al creixement de les dues línies cel.lulars tant en mono com en co-cultiu.

A més, les cèl.lules endotelials van mostrar reorganització de la matriu extracelular per formar estructures en forma de cable creixent en els biomaterials. La reorganització de les cèl.lules endotelials és necessària com a resposta a estímuls angiogènics i la formació de nous brots vasculars que garanteixen una integració favorable del scaffold amb el teixit hoste. Es evaluó asimateix la influència del recobriment de dues proteïnes diferents abans de la sembra cel.lular. D'una banda, laminina, una proteïna derivada de la làmina basal que participa en el desenvolupament neuronal de supervivència, i la regeneración; d'altra banda, una xarxa de fibrina, que proporciona una bastida adequat per a la invasió de cèl.lules endotelials inflamatòries i cèl.lules de altres teixits durant el procés de curació. Els resultats no van mostrar diferències notables entre una proteïna o una altra després de llargs períodes de cultiu.

CHAPTER 1

INTRODUCTION

1.1. **Tissue Engineering**

Tissue Engineering (TE) was defined in 1993 by Robert Langer and Joseph P. Vacanti as “an interdisciplinary field that applies the principles of engineering and the life sciences toward the development of biological substitutes that restore, maintain, or improve tissue function”(Robert Langer & Joseph P Vacanti, 1993).

Biological tissues are made up of cells, their extracellular matrix and a complex of signalling systems (Lanza, Robert Langer, & J. Vacanti, 2007). When designing an artificial construct to be used in applications for TE, it is necessary to take into account all those areas of knowledge remembering that the goal is a successful integration of the construct.

Two different strategies are commonly used in tissue engineering: the use of acellular matrices or the use of matrices with cells (Atala, 2004). The success of acellular matrices depends on the natural ability of a body to regenerate creating a new own tissue. These matrices can be engineered scaffolds or tissues which have been treated to remove its cellular components. The use of matrices with cells requires the dissociation of a small piece of donor tissue into individual cells and commonly further expansion in culture. The source of the donor tissue can be allogenic (tissue from the same specie but from different individual) or autologous (from the same individual).

The engineered matrices used for scaffolding must be carefully chosen. The scaffold must provide the suitable environment for tissue building taking into account concepts such as biodegradation rate, signals needed for tissue building or integration with the host tissue without rejection. Otherwise, the scaffold will fail in its duty.

1.1.1. Scaffolds for TE.

To mimic the natural tissues in the body, 3D structures are needed to reconstruct the damaged tissue. For a successful integration, it must allow cell colonization and distribution as well as permit a good permeability and vascularization in it to ensure nutrients for every cell.

These 3D structures, commonly named scaffolds, can be defined as a structure intended to be used as substitute for a specified tissue either permanently or temporarily to restore its functionality. When a biomaterial is chosen for its application in TE, it must be considered in the context of its application taking into account their processing or ways of sterilization. In its design, some basic requirements must be accomplished (Atala, 2004):

- ✓ the scaffold must have high porosity with a proper pore size to give a high surface area which is needed for its application.
- ✓ the degradation rate must match with the formation of new tissue or be no degradable at all if needed.
- ✓ the scaffold must have the required mechanical integrity to maintain the predesigned tissue structure.
- ✓ the scaffold should positively interact with cells, including enhanced cell adhesion, growth, migration, and differentiated function.

Nowadays, due to the engineering improvements to fabricate materials in small dimension, it is possible to prepare different kinds of architectures with different shapes. Micro or nano-scaled patterns are used to study cell-biomaterial interaction in order to understand better the cell-surface interaction (Magnani, Priamo, Pasqui, & Barbucci, 2003).

Many methods have been reported for the development of scaffolds. Fiber bonding, solvent casting/particulate leaching, gas foaming and phase separation are methods widely described in literature.

Fibers, when bonded together in three-dimensions, provide a large surface area which supports cell attachment while creating paths for the rapid diffusion of nutrients for cell survival and growth (Mikos & Temenoff, 2000). However, they lack of structural stability limiting their use in vivo.

Solvent casting and particulate-leaching techniques are also widely used to obtain such structures. In this technique, a solid porogen is used to create a mold. Then, polymer solution is forced to soak the mold. After polymerization, porogen is removed by dissolving it in a good solvent leaving the desired porous structure. This method allows to control the pore size by selecting the appropriate porogen. Porosity may be controlled as well by varying the porogen/polymer ratio (M Monleón Pradas et al., 2001; Spanoudaki et al., 2006)

In order to avoid the use of organic solvents to prepare scaffolds for biological application, gas foaming techniques were developed. The organic solvents employed in others methods may have toxic effects *in vitro* and elicit an inflammatory response *in vivo*. This fabrication method creates porous matrices by employing a gas foaming technique that brings porous structures without the use of toxic solvents (Mooney, Baldwin, Suh, J P Vacanti, & R Langer, 1996).

In phase separtation based methods, freeze-drying and freeze-extraction, a solid-liquid demixing is created by freezing a polymer solution. Thus two phases are formed, frozen solvent and concentrated polymer phases. Then the frozen solvent is removed leading to a porous structure, corresponding to the volume occupied by the solvent. What makes different these techniques, freeze-drying and freeze-extraction, is the solvent removal strategy. The first method is based on the sublimation of the solvent while in the latter the solvent is revomed with a non-solvent of the polymer and without any drying step. Since the porous structure is obtained during the

freezing, similar porous structures may be obtained in both techniques. By changing the cooling rate, phase separation can occur via different mechanisms, resulting in scaffolds with various morphologies (M.-H. Ho et al., 2004).

Furthermore, injection molds have been employed to obtain complex structure shapes such as the butterfly-shaped of the spinal cord (Moore et al., 2006).

1.1.2. Biomaterials as scaffolds for TE applications

A biomaterial can be defined as a material intended to interface with biological systems to evaluate, treat, augment or replace any tissue, organ or function of the body (Williams, 1999).

Materials can be classified attending to their origin into naturally derived or synthetic. Taking into account the nature of their application, they can by consider as permanent or temporary materials (non degradable or degradable biomaterials respectively). A temporary structure is expected to provide the necessary support (mechanical or biological) to allow the new formed tissue to recover the expected shape and functionality. These biodegradable structures must accomplish some important properties (Nair & Laurencin, 2007) among which some must be highlighted:

- the biomaterial must not evoke inflammatory or toxic response upon implantation in the body, by itself or by their degradation products.
- the degradation products must be able to be metabolized and cleared from the body.

Biodegradable materials are currently employed for different applications such as bone screws (Dhillon, Prabhakar, & Prasanna, 2008) or biodegradable wound sealants (Tredwell, Jackson, Hamilton, V. Lee, & Burt, 2006). One handicap in the use of biodegradable materials is that in some cases they fail to meet the requirements due to the loss of their mechanical properties or inappropriate degradation rates.

Permanent structures are non biodegradable materials or those which have very low degradation rates. Some metals, as titanium, nickel and its alloys, are attractive materials due to its inertness and biocompatibility although they sometimes fail due to wear or provoking wear in bones. They are used in dental implants and in prosthesis (hips) (Donato et al., 2009). Ceramics are a good alternative to metallic implants but its use is so far limited. These kinds of materials have been employed in bone tissue engineering (Wilson, van Blitterswijk, Verbout, Dhert, & de Bruijn, 2011).

A diversity number of synthetic and natural materials have been employed in a wide range of applications in TE. Synthetic materials (polymers, ceramics and metals) are the classically described in literature. Applications for bone tissue engineering or other mineralized tissues widely employ these synthetic materials. Usually, for bone tissue engineering application, a stable porous structure is needed. A few polymers widely used as scaffolding biomaterials are poly(glycolic acid) (PGA), poly(lactic acid) (PLA), and their copolymers poly(lactic acid-co-glycolic acid) (PLGA) or poly(ε-caprolactone) (PCL).

Nowadays natural materials, most of them components found in the extracellular matrix, are gaining importance due to their properties such as bioactivity and biocompatibility. Fibrous proteins as collagen (Janakiraman, Kienitz, & Baskaran, 2007), a major component of the extracellular matrix (ECM) or silk (R E Unger et al., 2004), have been used for applications in tissue regeneration.

Alginate (Purcell, Singh, Tech, & Kipke, 2009), chitosan (Freier, Montenegro, Koh, & Shoichet, 2005) or hyaluronic acid (Antunes et al., 2010; Ibrahim, Q. K. Kang, & Ramamurthi, 2010; Y. Liu, Shu, Gray, & Prestwich, 2004) are examples of polisaccharides widely employed in tissue engineering scaffolds, alone or combined with other substances to improve their characteristics as biodegradability or mechanical properties.

Hydrogels represent an important and promising class of biomaterials because of their excellent biocompatibility, causing minimal inflammatory responses, thrombosis and tissue damage.

1.2. **Neural Tissue Engineering**

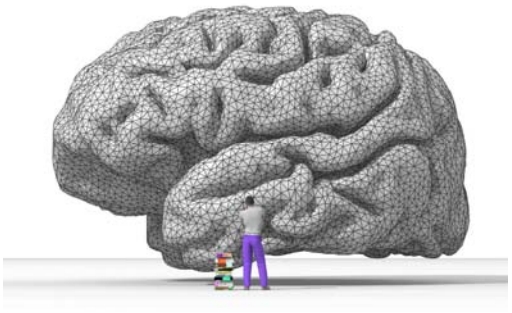

Figure 1.1. “Rendering of human brain” created by Nicolas Rougier (Bat. C. INRIA Nancy - Grand Est research center).

Since the first reconstitution of living tissues reported in the late seventies by E Bell and co-workers, too much work has been developed in the design of tissue engineering constructs or regeneration of the different tissues within the human body as breast, cardiovascular system or bone within others. The development of tissue engineering applied to the brain is a young but expanding field. A more detailed knowledge of mechanisms responses after damage or degeneration diseases has been accomplished by researchers in the field, thus, allowing the application of different therapies either in the central or in the peripheral nervous system. Therapies may be focused in the regeneration of the tissue with the consequent recovering of lost functions. Unfortunately, axonal outgrowth is limited in the central nervous system (CNS) and nowadays there is a lack of therapies to regenerate or slow down the degeneration of axonal pathways. Human brain is a complex system which is still far from being defined in terms of a complete description of cellular behaviour and the responses after damage or degeneration disease.

A brief introduction related to the nervous system is provided next. Without trying to be exhaustive, the composition of the nervous system, responses after damage and degeneration diseases are briefly described to help us to understand the scope of this thesis.

1.2.1. The Nervous system

The nervous system is comprised of two main divisions: the central nervous system, composed by the brain and the spinal cord, and the peripheral nervous system constituted of cranial, spinal and autonomic nerves that connect to the CNS. The special function of the nervous system is to establish communications with the brain and the whole organism and within the brain through electric stimulus.

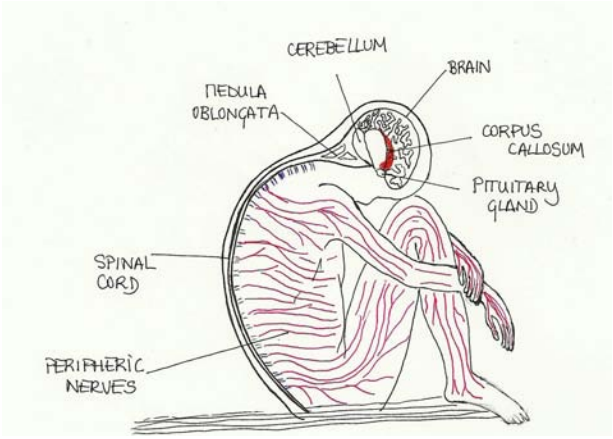

Figure 1.2. Central and Peripheric Nervous system representation in the human body.

Two main cell types are found in the nervous system: neurons and neuroglia. Neurons are the structural and functional cells of the nervous system. These cells do not have the ability to undergo mitosis although they can sprout new processes under certain conditions. They consist in the soma (cell body) and its extensions, named axons and dendrites. Axons are responsible of conducting the nervous impulse from the soma to other cells. Dendrites are implied in the reception of the stimulus.

Glial cells, or neuroglia, are the support cells of the nervous system. They aid in the function of neurons. Schwann cells are the support cells of the peripheral nervous system (PNS) while in the central nervous system (CNS) are astrocytes and oligodendrocytes. Unlike neurons, neuroglia has some capacity for cell division (Schmidt & Leach, 2003).

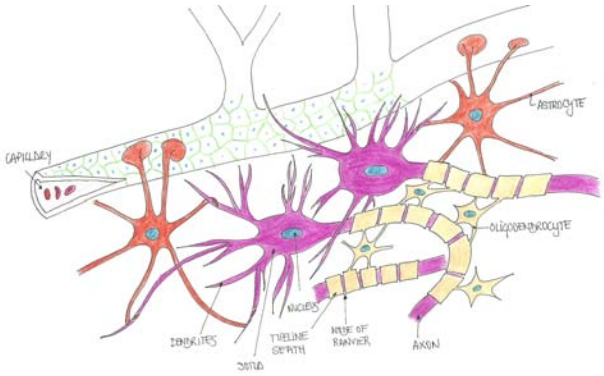

Figure 1.3. Schematic representation of the cells composing the central nervous system, neurons, oligodendrocytes and astrocytes and their conexión between them and capillaries.

Myelin is an insulating layer which surrounds the axons and aids to increase the speed at which impulses propagate along the myelinated fiber. In the PNS Schwann cells are the responsible of myelinization while in the CNS oligodendrocytes serve in this function. Astrocytes, the other type of microglia, contribute to the blood-brain barrier (BBB) (Schmidt & Leach, 2003). They are the most abundant cells in the CNS. During ages, astrocytes were thought to be passive cells only providing structural support to neurons but nowadays it is clear that they are more important in the homeostasis of the brain. Astrocytes have been shown to be involved in metabolic support of neurons, regulation of energy metabolism, development and maintenance of the BBB, guidance of neuronal migration and immune function (Markiewicz & Lukomska, 2006). There are two types of astrocytes, The radial glia is characterized by a long, radial process contacting the basal lamina at the pial surface (the innermost layer the membranes surrounding the brain and spinal cord named meninges). Glia expresses the astroglial cell cytoskeletal proteins vimentin (VIM) and glial fibrilliary acidic protein (GFAP) in their primary or mature state respectively (Briefings, 2010). The expression of GFAP by astrocytes has been reported to be essential for normal white matter architecture, BBB integrity as well as astrocyte-neuronal interactions (Eng, Ghirnikar, & Y. L. Lee, 2000).

1.2.2. The blood brain barrier

The blood brain barrier (BBB) is a natural barrier separating the blood flow and the brain. It is specific in the central nervous system and prevents the brain from bloodstream substances while allowing the access to nutrients and metabolites.

Physiologically, blood is separated by a layer of specialized endothelial cells which allows relatively free diffusion through paracellular spaces. Endothelial cells in the CNS are completely sealed by thight junctions, highly tighter compared to peripheral microvessels (Abbott, 2002). These tight junctions act as a barrier limiting the pass of non-lipophilic substances into the brain. Another cellular constituent of the BBB are the pericytes. They are separated from the ECs by a layer of basal lamina composed by matrix proteins. Perycites actively communicate with other cells envolved in the neurovascular unit such ECs, astrocytes and neurons. The functions of perycites include regulation of brain angiongenesis, the ECs tight junction formation and BBB differentiation within others (Balabanov & Dore-Duffy, 1998). Astrocytes complete the structure of the BBB playing a decisive role in the induction and maintenance of the BBB (Wolburg, Lippoldt, & Ebnet, 2007).

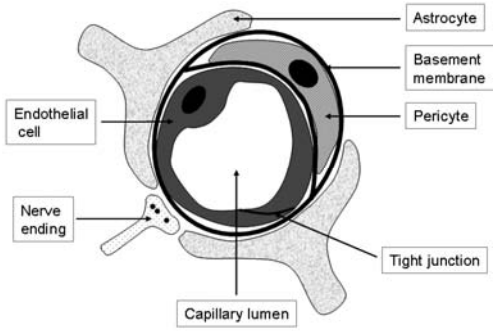

Figure 1.4. Cellular structure of the BBB (Figure from (Wilhelm, Fazakas, & Krizbai, 2011))

A triple co-culture of ECs, pericytes and astrocytes is thought to represent a good model to study the BBB *in vitro* (Nakagawa S, Deli MA, Kawaguchi H, Shimizudani T, Shimono T, Kittel A, Tanaka K, 2009). Couraud and co-workers (Weksler et al., 2005) developed the first stable and fully characterized endothelial human cell line (hCMEC/D3) to study a human model of the BBB *in vitro*.

Damage in the nervous system

As a response to damage in the nervous system, different processes occur in the central and peripheral nervous system which determine their different capacity to regenerate. When the PNS is damaged, support cells aid neuronal regeneration. Proliferating Schawnn cells, macrophages and monocytes are responsible of removing myelin debris, releasing of neurothophins, and lead axons toward their synaptic targets, resulting in restored neuronal function (Figure 1.5a). Typical treatments when injury occurs are based on the reconnection of the damaged nerve by surgery or by the use of an autologous nerve graft to guide the restoring of the PNS function (K.-kai Wang et al., 1998).

The physiological response to injury in the CNS is different. When an injury to the central nervous system occurs, a glial scar is formed as a protection barrier and so the healing process begins. This glial scar is composed of astrocytes and connective tissue elements. (Figure 1.5b). Although the glial scar is formed as a defense of the body to control and suppress further physical damage in the brain, it is the ultimate responsible of failure of the central nervous system regeneration. The glial scar stops macrophages infiltration to remove the myelin and debris from the damaged axons while blocks regenerating neurons to reach their synaptic targets (Schmidt & Leach, 2003)

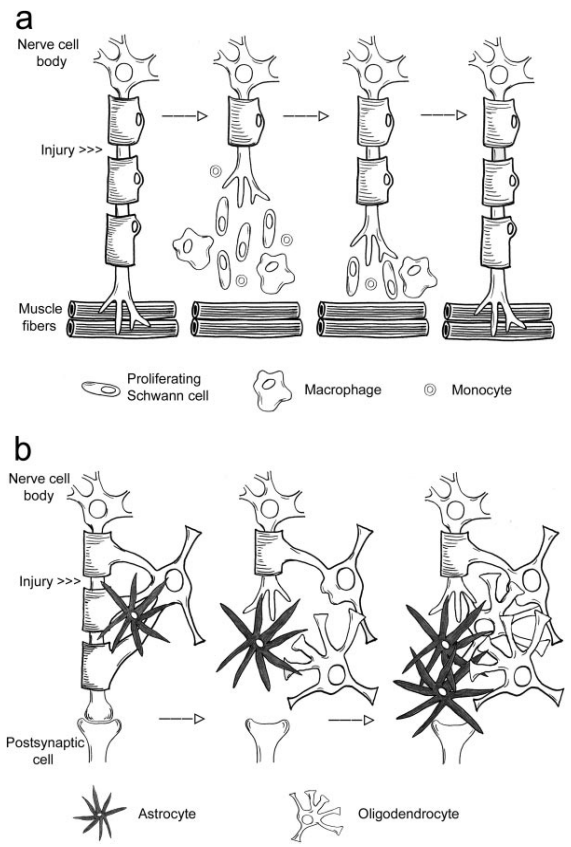

Figure 1.5. Regeneration in the peripheral (A) and central nervous system. (Figure from (Schmidt & Leach, 2003))

When the central nervous system is damaged functions such as memory, cognition, language and voluntary movement may be lost. Normally it is the result of the interruption of communication between nerve cell bodies and their targets. But not only transaction of nerve tracts may end in the loosing of this functions, the disruption of the interrelations between neurons and their supporting cells, and the destruction of the BBB can cause irreparable damages resulting in death or permanent disability (Ning Zhang, Yan, & Wen, 2005).

1.2.3. Neurological diseases

Neurological diseases such as Alzheimer, Parkinson or Huntington disease, result from the deterioration of neurons or their myelin sheaths, which may eventually lead to CNS-related dysfunction. Parkinson's disease (PD) is a neurodegenerative disorder characterized by a continuous and selective loss of dopaminergic neurons in the *substantia nigra pars compacta* with a subsequent reduction of neurotransmitter release mainly in the *striatum* (A. K. Meyer, Maisel, Hermann, Stirl, & Storch, 2010)**.** These two areas of the mid brain are connected by the nigrostriatal pathway, one of the major dopamine pathways in the brain (Figure 1.6). This pathway is particularly involved in the production of movement, as part of a system called the basal ganglia motor loop.

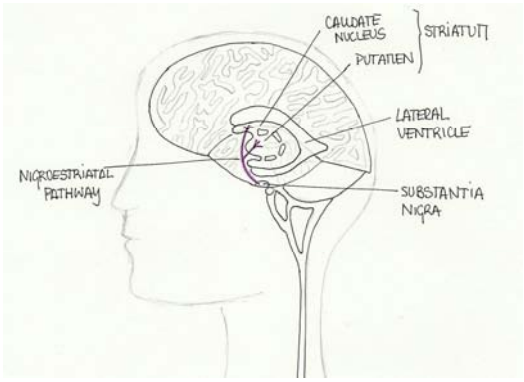

Figure 1.6. Nigrostriatal pathway, one of the major dopamine pathways in the brain.

Pharmacological treatment in the early stages of PD is based on the administration of "levodopa". L-dopa is transformed into dopamine in the dopaminergic neurons. The administration of this drug is just a symptomatic treatment and has a wide variety of side effects: the excess of dopamine produced by the exogenous administration of the synergic substance, which also results in a reduction of the endogenous formation of L-Dopa, makes the treatment eventually counterproductive. Besides, the treatment loses its effectiveness over time and does not slow the disease progression (Joyce et al., 2002).

Surgery treatments to control parkisonians effects consists in an electrode implant in both subtalamic nuclei (STN) but, while the treatment has good results in the recover of motor symptoms, it does not stop the evolution of the disease.

The ideal treatment for the PD may lie in the replacement of the lost cells in their original site. Indeed, cell-based strategies have been employed to overcome the limitations of the conventional symptomatic treatment. These strategies, focused on the transplantation of cells into the degenerated host brain, include bone narrow stromal cells (Naoyuki, Kakishita, & Itakura, 2007) or neurothopic growth factors (Reeves et al., 2005).

Clinical treatment for CNS regeneration is less promising. Even so, different approaches have been pursued in this area. After spinal cord injury, inflammation cell activation, reactive astrogliosis and the production of both growth promoting and inhibitory extracellular molecules occur. So when CNS is injured, anti-inflammatory drugs are administred to reduce swelling and secondary injury. Avoiding glial formation by inhibition of the involved molecular cascades, combined with the use of biomaterials in order to provide a biological environment that permits axons regeneration, seems to be a difficult but a promising strategy for CNS regeneration.

A mild inflammation response which, in any case, is an inevitable phase of any wound healing, could be beneficial to the use of scaffold implants. This fact will assure the recruitment of cells and signals to promote angiogenesis and thus a good integration of the construct.

1.3. Hyaluronic acid

1.3.1. Introduction

In 1934 Karl Meyer and John W. Palmer (Palmer & John, n d) working on the preparation of a supposed vitreous mucoid for further studies, obtained a free polysaccharide acid of high molecular weight, which was apparently in the vitreous humor in a salt-like combination. The polysaccharide was found to be very hygroscopic and not easily soluble in water. They showed that this substance contained uronic acid and an aminosugar, but no sulfoesters. They describe the procedure to obtain it from the vitreous humor of the eye and propose to name it *"Hyaluronic acid"* from hyaloids (vitreous) and uronic acid.

Until 1954, 20 years later, the structure of the molecule was not elucidated. Bernard Weissmann and Karl Meyer (Weissmann & K. Meyer, 1954) published the precise chemical structure for what they had named hyaluronic acid (Figure 1.7).

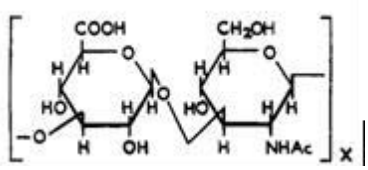

Figure 1.7. Molecule of HA as it was described for the first time by Bernard Weissmann and Karl Meyer in 1954 (Weissmann & K. Meyer, 1954).

Hyaluronic acid (HA) is described as a naturally occurring non-sulfated glycosaminoglycan (GAG) component of the ECM of connective, epithelial and neural tissues. Synovial fluid, vitreous humor, cartilage, blood vessels,skin and the umbilical cord are specific tissue types that contain significant amount of HA (Weissmann & K. Meyer, 1954).

During embryonic development, tissue regeneration and wound healing the ECM that surrounds migrating and proliferantig cells is rich in HA (Garg & Hales, 2004) Hyaluronan is widely distributed in a variety of tissue within the body (Table 1.1).

Table 1.1 Normal concentrations ($\mu g \cdot g^{-1}$) of HA in various organs of different species. Adapted from (J. R. E. Fraser, T. C. Laurent, & U. B. G. Laurent, 1997).

Organ or fluid	Man	Sheep	Rabbit	Rat
Umbilical cord	4100			
Synovial fluid	1400-3600	540	3890	
Dermis	200			
Vitreous body	140-338	260	29	
Lung		98-243		34
Kidneys			93-113	30
Renal Papillae			250	
Renal cortex			4	
Brain	35-115		54-76	74
Muscle			27	
Intestine				44
Thoracic lymph	8,5-1,8	1-34		5,4
Liver			1,5	4
Aqueous humour	0,3-2,2	1,6-5,4	0,6-2,5	0,2
Urine	0,1-0,3			
Lumbar CSF	0,02-0,32			
Plasma (serum)	0,01-0,1	0,12-0,31	0,019-0,086	0,048-0,26

Nowadays, hyaluronic acid, also referred to as hyaluronate or hyaluronan, is extensively studied for a wide range of applicatons intended to be biological (Jiang, Liang, & Noble, 2007) or not (coatings for electronic parts (Callegaro, 2002)).

Structure

The polymer was determined to be a repeating unit of D-glucuronic acid and N-acetilglucosamide linked together by alternating ß-1,4 and ß-1,3 glycosidic bonds. Hyalurononic acid is the only non-sulphated glucosaminoglycan (GAG), conferring to it unique properties. The long-chain polymer of HA is composed of repetitions of the disaccharide unit forming polymers with molecular weight between 10^5 and 10^7 Da (Garg & Hales, 2004) (MW_{sugar}= 417,1 g/mol).

In physiological solution, the backbone of the hyaluronan molecule is stiffened by a combination of the chemical structure of the disaccharide, internal hydrogen bonds, and interactions with the solvent. At physiological pH, the carboxyl groups of the molecule are predominantly ionized, making

the hyaluronic acid a polianion that associated exchangeable cations to maintain charge neutrality.

The concentration of HA in the human body varies depending on its location from 4 g/kg in the umbilical cord to 0.1-0.01 mg/l in normal serum. The total amount of HA in a 70kg human body is stimated to be around 15g (Garg & Hales, 2004).

Synthesis

In the inner surface of the plasma membrane of the cell, a group of membrane-bound synthases (HASs) synthesizes HA by cyclically adding the pertinent monomer units to the end of the forming polysaccharide chain. There are three different HAS required to synthesize HA which gives polymers of different molecular weighes (longer or shorter chains).

Degradation

Hyaluronidases, the enzymes responsible of hyaluronan degradation which cleave HA chains by hydrolysis into shorter fragments, may be classified into 3 types based on the end products that they generate. The first type of hyaluronidases (testis type, enzyme comission number (E.C.) 3.2.1.35) are endo-β-N-acetylhexosaminidases and cleaves ramdomly β 1-4-glycosidic linkages in the HA chains yielding tetra and hexa oligosaccharides as the main end products with N-acetylglucosamine at the reducing terminal. The second type (E.C. 3.2.1.36) are hyaluronate-3-glycanohydrolases, which cleaves glucuronate linkages and are inert towards other GAGs. The cleavage HA in tetrasaccharides and hexasaccharides as the main products with glucuronic acid at the reducing end. The third type (Microbial hyaluronidases, E.C. 4.2.99.1) cleave HA at β 1-4 glycosidic linkages using β elimination processes yielding 4-5 unsatured oligosaccharides (Girish & Kemparaju, 2007)

The production and degradation of hyaluronan may be enhanced or diminished under physiological or pathological conditions.

1.3.2. Modification of hyaluronic acid

Hyaluronan, in spite of being an interesting biomolecule to use for the fabrication of new biomaterials, has very poor biomechanical properties that make necessary its modification in order to obtain manipulable biomaterials with the desired properties.

The goal of cross-linking the hyaluronan molecule is usually to enhance its rheological properties or to produce forms of hyaluronan less soluble in water, such as solids or gels. Gels have been employed for tissue augmentation (Redbord, Busso, & Hanke, 2011) as injectable hydrogels but the interest of working with scaffolds based on HA as tissue regeneration guides drives the need of fabricating HA insoluble structures.

A variety of modifications have been done to the natural molecule of HA to obtain improvements in its chemical and mechanical properties. Many applications have been achieved by preparing hyaluronan derivates: crosslinked hyaluronan, hyaluronan-drug bioconjugates, hyaluronan-grafted-co-polymer and hyaluronan-liposome composites. Crosslinking has been performed with biepoxides (Zhao, 2006), divinilsulfone (Ibrahim, Q. K. Kang, & Ramamurthi, 2010), glutaraldehyde (Antunes et al., 2010), carbodiimides (Tomihata & Ikada, 1997) and hydrazides (Pitarresi, Craparo, Palumbo, Carlisi, & Giammona, 2007) among others.

Figure 1.8 shows the hyaluronic acid structure and the principal targets of covalent modifications.

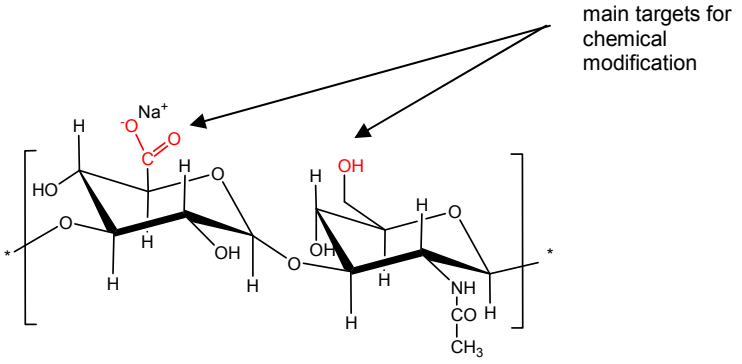

Figure 1.8. Molecular structure of hyaluronic acid showing the main targets for chemical modification.

Reactions through carboxyl groups

Typical reactions to cross-link hyaluronan through its carboxyl groups are esterification or carbodiimide-mediated reactions.

Esterification on hyaluronan has been carried out by alkylation of the tetra (n-butyl) ammonium salt of hyaluronan with an alkyl halide in dimethylformamide (DMF) solution. Under these conditions and with high percentages of esterification, a wide range of materials called HYAFF® , have been prepared. HYAFF® can be processed to obtain several types of devices such as tubes, membranes, non-woven fabrics, gauzes and sponges. These scaffolds are highly biocompatible, do not elicit any adverse reaction and are resorbed by the host tissues (Vindigni, Cortivo, Iacobellis, Abatangelo, & Zavan, 2009).

Carbodiimide-mediated reactions are frequently carried out by using dihydrize compounds. One typically used compound is adipic acid dihydrazide (ADH): in aqueous medium, a coupling reaction occurs between the glucuronic activated residue of the HA and the hydrazide group of ADH. The glucuronic acid residues are activated by reaction with soluble carbodiimides such as 1-ethyl-3(-3-dimethylaminopropyl) carbodiimide using hydroxybenzotriazole hydrate (HOBt) as precursor. One advantage of using ADH is that the molecule provides multiple pendant hydrazide groups for further derivatization with drugs (Luo & Prestwich, 1999), grafting on different surfaces (Mason et al., 2000) or further cross-linking reactions with the above mencioned carbodiimides (J. Kim et al., 2007).

Reactions with hydroxyl groups

Different reactions may be performed through the hydroxyl group of the molecule to modify the hyaluronic acid. A number of sulphated hyaluronic acid derivates, termed generically HyalS_x, have been developed by sulfation of the -OH groups present on hyaluronic acid molecule (Barbucci, Magnani, Rappuoli, Lamponi, & Consumi, 2000). Esterification, isourea coupling or

periodate oxidations are also strategies of modification through the hydroxyl group.

1.3.3. Hyaluronic acid in tissue engineering

Hyaluronic acid is a promising hydrogel for TE applications due to its biocompatibility and its ubiquitous localization in the organism; however, several improvements must be done to succeed.

Hyaluronan has been widely used in tissue engineering in a broad range of applications. Kim and partners employed acrylated hyaluronic acid scaffolds for regeneration of bone tissue. They found that in those hydrogels carrying hMSCs and growth factors, stem cells differentiated into specific cells such as osteoblasts and endothelial cells (J. Kim et al., 2007). Patterson and co-workers employing glycidyl methacrylate modified HA, concluded that these hydrogels, in spite of their poor mechanical properties which make their utilization as composite scaffold necessary, have potential for clinical application in bone defects (Patterson et al., 2010).

Xinqiao Jia and partners developed HA-based microgel systems to be employed in the treatment of vocal fold scarring (Jia et al., 2006). They suggested that their novel materials were promising injectable hydrogels due to their biocompatible filler properties and viscoelasticity similar to the natural tissue. These properties have been emploited by several authors for tissue augmentation in dermal applications (Y. Liu, Shu, Gray, & Prestwich, 2004; Redbord et al., 2011).

Hyaluronan has also been applied in cartilage tissue engineering. Chang and co-workers developed a tri-copolymer scaffold made of gelatine, chondroitin and hyaluronan to mimic the natural cartilage matrix (Chang, H.-C. Liu, C.-C. Lin, Chou, & F.-H. Lin, 2003). *In vitro* cultures with porcine chondrocytes showed that cells grew properly into the designed scaffold and furthermore started to secrete newly synthetized matrix, although not enough to form cartilage. Few years later, Nehrer and partners presented a three-year clinical assay testing hyaluronan matrices for cartilage repair [59]. They report favourable results compared with classic techniques of autologous chondrocyte transplantantion (ACT) suggesting Hyalurgraft® as an alternative to ACT.

1.3.4. Hyaluronic acid in the Nervous system

The nervous system has also been an important field for hyaluronan hydrogels applications. Periferal nerve regeneration has been assessed by Wang and partners by injecting hyaluronan solutions into nerve guides spanning a transected gap in the sciatic nerve (K.-kai Wang et al., 1998). They observed an increase in conduction velocities as well as an increase in myelinated axons in the hyaluronan containing group versus tubes filled with saline solutions (control group). Ten years later, Sakai and partners working on a photocrosslinked hyaluronic acid, reported that rat Schwann cells and neurospheres were grown onto HA conduits *in vitro* (Sakai et al., 2007). Furthermore, HA conduits mantained their shape after 3 weeks of cultivation.

In the last six years, hyaluronan has become an interesting biomaterial for central nervous system regeneration. Hyaluronan hydrogels modified with laminin (Shaoping Hou et al., 2005) or poly-D-Lysine (Wm Tian et al., 2005) were reported to support cell infiltration and angiogenesis in vivo. In the following two years, the use of protein sequences involved in cell adhesion gained importance and sequences such as RGD (arginine-glycine-aspartate) (I.S.Lee, 2006) or IKVAV (isoleucine-lysine-valine-alanine-valine) (Y. T. Wei et al., 2007) were employed by immobilization onto hyaluronan hydrogels. Considerable neural biocompatibility after implantation *in vivo* was reported showing that these materials formed a permissive interface that favoured cell ingrowth and angiogenesis. Bergman and co-workers prepared a scaffold of hyaluronan and collagen type I and demonstrated that neural stem/ progenitor cells (NS/PC) proliferated and formed neurons, astrocytes and oligodendrocytes in their synthetized scaffolds (Bergman, Wallenquist, Svahn, Bowden, & Bra, 2007). In the same year, Ma Jun and partners reported an experimental test of stroke recovery by implantation of HA hydrogel with the Nogo receptor antibody (NgR) in a rat model (Jun Ma et al., 2007). They reported that the hydrogels were invaded with some neurons and nerve fibers and suggested HA hydrogel as a promising scaffold material for the repair of defects in the brain.

Wang and Spector developed hyaluronan-collagen (HA-coll) sponges and cultured them with neural stem cells (NSCs) (Sakai et al., 2007)(T.-wei Wang & Myron Spector, 2009). They assured that HA and HA-Coll scaffolds favored the differentiation of NSCs to neuronal cells *in vitro*. Following the studies with the Nogo receptor, Pa Linjie and partners worked on an hyaluronan scaffold containing anti-NgR antibody (Pan, Ren, Fuzhai Cui, & Qunyuan Xu, 2009); they reported that hyaluronan-antiNgR prevented the action of inhibitory factors that would limit axon outgrowth and, in addition, promoted cell attachment. Recently, Yue-Teng Wei and co-workers developed a hyaluronan hydrogel modified with nogo-66 receptor antibody and poly-L-lysine (Y.-T. Wei et al., 2010) ; the hydrogel was shown to inhibit the formation of glial scar as well as to support angiogenesis and to promote axonal extension after implantation into a injured region of the spinarl cord.

1.3.5. Scaffold integration and angiogenesis

Apart from a good biocompatibility and a desired biodegradation rate, which depends on the final application, scaffolds must also allow connectivity with the host tissue. It is established that the maximum diffusion of nutrients and oxygen in tissues is not longer than 100 microns, making the formation of a new vascularization network within the 3D structure necessary. Thus, an adequate vascularization of the construct may be one of the most important issues to deal with to guarantee success after implantation.

Although angiogenesis is a very complex cascade of events, involving different cell types and protein signalling, several methods have been developed to test angiogenesis in biomaterials *in vitro*. J. Folkman and Christian Haudenschild were the first to decribe the development of capillary tube structures *in vitro* (Judah Folkman & Haudenschild, 1980). Then, Montesano and co-workers, improved the *in vitro* assays for the study of angiogenesis, providing a better understanding of the processes involved (Montesano, Orci, & Vassalli, 1983).

In vitro angiogenesis assays are based on the use of ECM compounds to mimic tissue conditions. The addition of angiogenic stimuli as basic fibroblast growth factor (bFGF) or vascular endothelial growth factor (VEGF) is also required.

New blood vessels can be formed by one of two distinct mechanisms namely vasculogenesis or angiogenesis. Vasculogenesis is the process of forming new blood vessels developed from angioblast precursor cells. However, angiogenesis requires the pre-existing blood vessels to outgrow new sprouts (Werner Risau, 1997).

The process of angiogenesis has been described as a three step mechanism: initiation, proliferation/invasion and maturation (Stromblad & Cheresh, 1996). The initiation process involves the release of growth factors or cytokines from tumor and/or inflammatory cells. A wide number of angiogenesis stimulators have been described namely angiopoietin-1 (Ang-1) (Koblizek, C. Weiss, Yancopoulos, Deutsch, & W Risau, 1998), basic fibroblast growth factor (bFGF) (Stromblad & Cheresh, 1996), and vascular endothelial growth factor (VEGF) (Breier & W Risau, 1996), among others. The released factors bind to specific receptors located on endothelial cells (ECs) in the nearby and EC turn into an activated state. ECs in turn begin to produce new molecules including enzymes that will be necessary in the further steps.

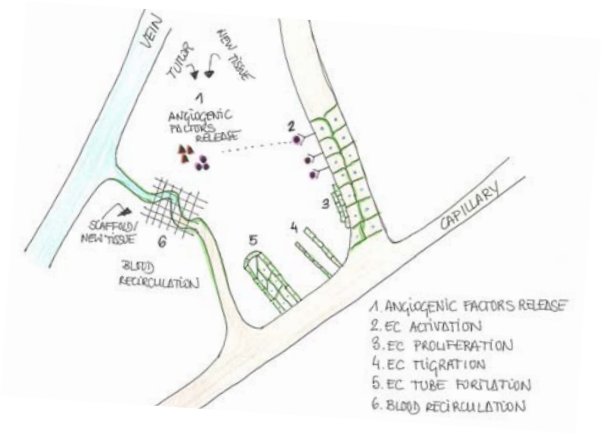

Figure 1.9. Angiogenesis process.

The enzymes dissolve tiny holes in the basement membrane surrounding all existing blood vessels. The ECs begin to proliferate and a migration out through the dissolved holes starts towards the target tissue, being normally a tumor. Specialized transmembrane proteins called integrins serve to pull the new blood vessel sprout forward. Enzymes named metalloproteinases (MMP) are now produced to dissolve the target tissue in order to accommodate the sprouting vessel. Sprouting ECs roll up to form a blood vessel tube growing from the host blood vessel. The individual sprouts fuse into loops, to allow the circulation of blood within them at the end of the process. To stabilise the new blood vessel, specialized muscle cells (smooth muscle cells, pericytes) are recruited, providing structural support to the vessel. Then, blood flow begins (Bunone et al., 1999; J Folkman & D'Amore, 1996; Werner Risau, 1997).

1.3.6. Angiogenic growth factors

In the adult, endothelial cells are in a quiescent stage until activation is required. Their angiogenic phenotype is stimulated under special conditions such as hypoxia. In addition, to facilitate migration the cell shape changes and a wide range of proteolytic enzymes are secreted in order to degrade the basement membrane, step needed during the development of new sproutings (Nomi, Atala, Coppi, & Soker, 2002).

Evidences suggest the existence of angiogenesis activators or inhibitors for capillary sprouting. Thus, the normally quiescent vasculature can be activated or desactivated by an on-off switch mechanism (Figure 1.10). The “balance” of the mentioned angiogenic inducers or inhibitors may activate the switch. Inhibitors (α–interferon or platelet factor-4) of endothelial cell chemotaxis and proliferation were first described in the early eighties (Cook & Figg, 2011; Hanahan & J Folkman, 1996).

A large list of angiogenic inducers has been described. Direct angiogenic molecules such as VEGF or bFGF can stimulate the activation of ECs. On the other hand, indirect angiogenic factors as angiopoietins, although they have been found to be very weakly mitogenic for ECs, are necessary during the new blood vessel formation.

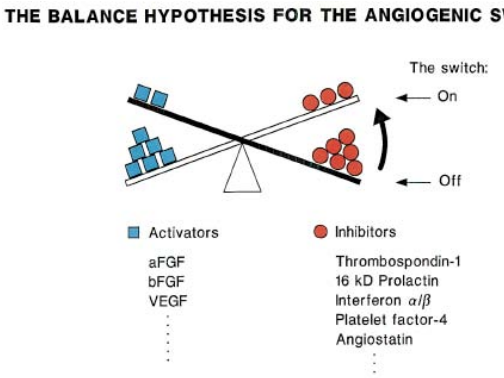

Figure 1.10. The balance hypothesis for the angiogenic switch (Hanahan & J Folkman, 1996)

Basic fibroblast growth factor (bFGF)

The basic fibroblast growth factor (bFGF) acts as a strong EC mitogen (J. A. Abraham et al., 1986). It is normally not secreted and it is still not clear how it is delivered into the extra-cellular matrix (ECM).

In contrast to VEGF, bFGF is not specific for ECs. ECs, fibroblasts, myoblasts and tumor cells express receptors to bind bFGF (Basilico & Moscatelli, 1992); it is mitogenic for neural cells such as oligodendrocytes, astrocytes and Schwann cells.

Vascular Endothelial growth factor (VEGF)

The vascular endothelial growth factor is a potent angiogenic factor. It is a specific mitogen for ECs, stimulating them to migrate and form tubes *in vitro* (Ferrara, 2001). A variety of cell types can express VEGF. Its

expression is up-regulated in tissues undergoing vascularization (Breier et al, 1992; Shweiki et al, 1993). Tumors secrete high levels of VEGF, while normal tissues do not, which is consistent with its role in tumor angiogenesis (Carmeliet, P., Ferreira, V., Breier, G., Pollefeyt, S., Kieckens, L., Gertsenstein, M., Fahrig, M., Vandenhoeck, A., Harpal, K., Eberhardt, C., Declercq, C., Pawling, J., Moons, L., Collen, D., Risau, W., Nagy, n d). There is evidence that VEGF acts as a survival factor for EC (Alon et al., 1995).

Angiopoietins (Ang)

The angiopoietins are protein growth factors with specific roles in the angiogenic process but do not seem to be mitogenic to ECs (Suri et al., 1996). The angiopoietins 1 and 2 (Ang-1, Ang-2) are competitive ligands that bind the same receptor, Tie-2, expressed on the surface of EC. While Ang-1 acts as agonist of the Tie-2 receptor to signal the recruitment of specialised cells that stabilize new formed blood vessels, the Ang-2 acts as antagonist (Cook & Figg, 2011). It is thought that the role of Ang-2 is to inhibit the interaction between EC and the supporting cells in order to facilitate EC migration from the vessel to form a new capillary (Cook & Figg, 2011). Analyses of supernatants containing Ang-1 were found to induce the formation of capillary sprouts while its depletion inhibited the sprouting (Koblizek, C. Weiss, Yancopoulos, Deutsch, & W Risau, 1998). Furthermore, some studies have been shown that neutralization of Ang-2 decreases tumor growth and angiogenesis as well as suppress EC proliferation (Oliner et al., 2004). The combined effect of Ang-1 and VEGF induce a synergistic angiogenic effect (Zacharek et al., 2007).

The aim of this work is the design of natural based scaffolds which seeded with neural cells in vitro or its precursors may be implanted in damaged areas in the brain and reach conectivitity with the host tissue ir order to provide a enable environment to recover lost functions.

Hypothesis

H1: Hyaluronic acid is a potencial biomaterial for scaffolding due to its biocompatibility to be used in neural regeneration,

H2: It is posible to produce hyaluronan based scaffolds with inner structures mimicking central nervous system tissue.

H3: The biomaterial will not produce any inmunologic response, alone or combined with the substances employed during its fabrication, thus giving a good support for neural tissue regeneration.

Objectives

O1. Development and physicochemical characterization of 3D materials (scaffolds) based on hyaluronic acid.

O2. Characterization of the biological performance of human neural cells on hyaluronic acid 2D supports and in 3D scaffolds.

O3. Study of co-cultures of human endothelial and astrocytic human cell lines in hyaluronic acid 3D scaffolds.

CHAPTER 2

MATERIALS AND METHODS

2.1 Materials and cell lines

2.1.1. Hyaluronan

Hyaluronic acid sodium salt from Streptococcus equi was supplied by Fluka (Spain) with a molecular weigh of 1.63 10^6 Dalton. Sodium hydroxide (NaOH, pellets, extra pure), hydrochloric acid (HCl, 37%), acetone (synthesis grade) and isopropyl alcohol (IPA, synthesis grade) were purchased from Scharlab, Spain.

Crosslinkers, 1,2,7,8-diepoxyoctane (DEO, 97%) and divinyl sulfone (DVS, 97%) were purchased from Sigma, Spain.

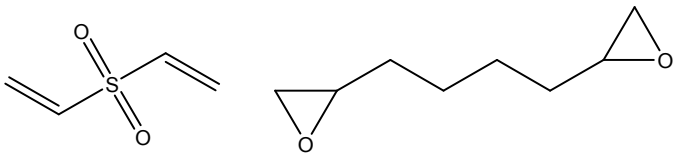

divinyl sulfone (DVS) | 1,2,7,8-diepoxyoctane (DEO)

Figure 2.1 Molecules of crosslinkers used for hyaluronan crosslinking.

2.1.2. Porogens

100 microns polypropilene fibres (PP) were supplied by Plasticel (Spain). Polymethyl methacrylate beads with mean particle size in the range of 80-110 microns (PMMA beads, Colacryl® DP300) were provided by Lucite International, UK.

2.1.3. Human brain microvessel endotelial cells (hCMEC/D3)

Human brain microvessel endothelial cell line, hCMEC/D3, developed by B.B. Weksler and co-workers(Weksler et al., 2005), were cultured in customer formulation endothelial cell BM (Promo Cell) containing 28 mM HEPES. The medium was supplemented with 15% of fetal calf serum (FCS; Gibco, Germany) + 100U/100μg/ml penicillin/streptomycin + 25 μg/ml

(1:500) sodium heparin (Sigma-Aldrich) + (1:5000) of basic fibroblast growth factor. Cells were sub-cultured and used between passages 30-33.

2.1.3. Human glioblastoma-astrocytoma cell line (U373)

Human glioblastoma-astrocytoma cell line U373-MG (Abcam, Germany) was cultured at 37°C in minimum essential media (MEM, Gibco) supplemented with 10% (v/v) fetal calf serum (FCS), 1% penicillin/streptomycin (10.000 units penicillin/ml 10.000 μg/ml streptomycin sulphate and 1% Glutamax (Gibco, Germany). Cells were subcultured in the same medium used to endothelial cells previously described. Cells were used in passages 10-15.

2.2 Methods

2.2.1. Hyaluronan crosslinking

Two different crosslinkers were employed to obtain non soluble hyaluronan hydrogels. 1,2,7,8-diepoxioctane (DEO) and divinylsulfone (DVS) were employed to crosslink the hyaluronan macromolecule expected to react through different functional groups n its structure.

Crosslinking with 1,2,7,8-diepoxioctane (DEO)

The crosslinking of hyaluronan with DEO was performed in a two step reaction. First, a 2% (w/w) aqueous solution of hyaluronan sodium salt was prepared. Films were obtained by solvent casting in Petri dishes by letting the solution evaporate at 37 ºC until dry. Samples were then cut and crosslinked in an acidic medium.

Samples were immersed in acetone/HCl 0.1N (70/30) (from now on referred to as “solvent”) solution and allowed to swell during one hour. Afterwards, the crosslinker was added. Different ratios of HA:solvent were assessed to crosslink hyaluronan, namely 1:50, 1:70 and 1:100 HA:solvent

(R_50, R_70 and R_100 respectively). Table 2.1 resume the different conditions of HA:solvent employed for HA crosslinking.

Table 2.1. Reaction conditions tested for hyaluronan crosslinking using 1,2,7,8-diepoxioctane

	R_50	R_70	R_100
acetone:HCl 0,1N	70:30	70:30	70:30
HA:(acetone:HCl)	1:50	1:70	1:100

Furthermore, different hyaluronan:crosslinker molar ratios were evaluated, namely from ratio 1:1 to 1:5 HA:crosslinker. Reaction time was in turn evaluated by leaving the reaction to continue during 24, 48 or 72h. Afterwards, samples were rinsed with isopropylalcohol/H_2O until the pH of the washings was neutral and further washed in water. Samples were left to dry at room temperature and then dried under vacuum at 60ºC during 48h.

Crosslinking with divinylsulfone (DVS)

5 g of HA were dissolved in 100 mL of 0,2M NaOH solution and mixed during 24h at room temperature. 10ml of the hyaluronan solution was mixed carefully with 77 μL of divinyl sulfone (1:0,64 molar ratio HA:DVS) assuring the complete diffusion of the crosslinker in the viscous solution. Then, the mixture was injected into a self-made mold consisting in two parallel glasses separated by a cable of known diameter, thus, giving a film with the desired thickness. Hyaluronan hydrogel was allowed to crosslink at RT during 4h. Afterwards, the resulting films were immersed in different solutions to end the crosslinking reaction. Five different ratios of acetone and water were mixed to rinse the hydrogels after the crosslink reaction, namely 100:0, 80:20, 50:50, 20:80 and 0:100 acetone:water (volume ratio).

2.2.2. Scaffolds fabrication.

Scaffolds with different inner porous structures were developed, both with DVS and DEO crosslinking procedures. Since the reaction of crosslinking is different in each case, different methodologies were employed.

Structures based in HA-DEO

Cylindrical tubes

Cylindrical silicone tubes were used to obtain cylinders made of hyaluronan. 2% HA aqueous solutions were injected in different molds. Bulk cylinders were obtained injecting the solution in 1mm inner diameter silicone tubes and lyophilized afterwards. Tubes of HA were manufactured by injecting in a mold consisting in a concentrically disposed cylinders. The internal diameter of the external cylinder was 2.2mm and the external of the inner cylinder was 1.2mm.

Channeled scaffolds

Multiple parallel-disposed channeled scaffolds were prepared with molds containing different inner channels diameters and external cylinders. Molds made of glass or silicon tubes were employed. Drilled cups were disposed in both endings. Filaments with external diameters of 100 or 200 microns, made of copper or polypropylene, were disposed following the paralelly drills from one end to the other. Hyaluronan 2% aqueous solution was injected and then lyophilized. Dry non-crosslinked 3D structures were obtained. Samples were then crosslinked with DEO by the protocol described and the conditions summarized in Table 2.2.

Table 2.2. Conditions for DEO crosslinking on hyaluronan 3D structures.

crosslinker	solvent (acetone:HCl 0,1N)	HA:(solvent) (w:w)	HA:X	time (h)
DEO	70:30	1:70	1:5	72

Scaffolds with different inner porous structures were prepared. Thus, interconnected spherical pores, interconnected cylindrical pores and non connected longitudinal cylindrical channels hyaluronan scaffolds were obtained. The specific methods used are explained in detail below.

Matrix of interconnected spherical pores structure

A particulate-leaching method was used to prepare constructs with interconnected spherical porous structure. Polymethylmethacrylate beads (PMMA) were used as porogen with particles ranging between 80-110 microns.

10 ml hyaluronan aqueous solution was mixed with PMMA in 1:20 ratio (w/w) solution:PMMA. The blend was carefully mixed to avoid air bubble formation. Once the mixture was homogeneous it was forced to fill a multidrilled Teflon® mold of empty cylinders of 7 millimetres diameter and 25 millimetres long (Figure 2.2) which permitted to obtain an amount of reproducible samples at once. The blend was lyophilized resulting in dry cylinders of hyaluronan containing the porogen. Cylinders obtained were cut into 1mm thickness disks and washed in acetone to remove the porogen. Thus, gentle washings in acetone was carried out under stirring. The acetone was changed daily until no residual porogen was appreciated as no residual white powder after acetone evaporation.

Samples were then crosslinked according to the conditions in Table 2.2 and kept immersed in acetone until further use.

Figure 2.2 Multidrilled Teflon® mold used to fabricate 3D structures of hyaluronan.

Matrix of longitudinal parallel cylindrical channels

Inner longitudinally channeled hyaluronan scaffolds were prepared by using a self-made mold. Thus, two pieces of microdrilled stainless steel with holes of 125 microns were disposed at the endings of Teflon® self made mold (Figure 2.3). These microdrilled pieces were used to support the fibers that will serve as template to obtain the longitudinal channels. Those pieces were fitted in both ends of a Teflon cylinder provided with a hole to inject the hyaluronan solution.

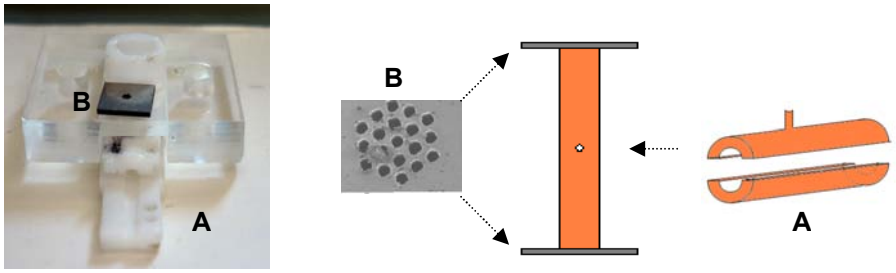

Figure 2.3 Self-made Teflon® device to fabricate hyaluronan multichanneled scaffolds.

Structures based in HA-DVS

Matrix with interconnected spherical pores

10 ml hyaluronan sodium hydroxide solution was mixed with the corresponding amount of DVS and rapidly mixed with PMMA beads in 1:20 ratio (w/w) solution:PMMA. Once the mixture was homogeneous it was forced to pass through multidrilled Teflon® mold as described for HA-DEO scaffolds. The blend was allowed to react during 4h to get a 7 mm diameter and 25 mm long HA-PMMA cylinders DVS crosslinked.

Immediately after demolding the cylinders, they were cut into disks of a 1mm thickness and thoroughly washed in acetone. Samples were kept in acetone to remove the porogen under stirring at room temperature. The solvent was changed every day until no porogen was left (samples were considered clean of porogen when no residual white powder was found after evaporation of the acetone used in the washings). Samples were kept in acetone until further use.

Longitudinal cylindrical channelled scaffolds

5% hyaluronan solution in 0,2M NaOH containing the crosslinker (DVS) was injected with a syringe to fill the mold described in Figure 2.3. The mold consisted in longitudinally disposed polypropylene filaments of 100 microns in diameter used as a template. The mixture was allowed to react during 4h at room temperature and a hyaluronan cylinder was obtained. Then the cylinder was immersed in acetone containing the filaments to maintain the template during dehydration of the structure avoiding the collapse of the walls. Samples were allowed to dry at room temperature and then at 60ºC and vacuum until dryness. The filaments were then removed.

HA coating on acrylic scaffolds

Acrylic matrices of interconnected cylindrical channels coated with hyaluronan were prepared following several steps. The matrix of a 3D mesh of cylindrical channels of poly(EA-co-HEA) 90/10 (v/v) were prepared employing a polyamide mesh template, protocol reported in (Rodriguez Hernández, Á. Serrano Aroca, José Luis Gómez Ribelles, & Manuel Monleón Pradas, 2008).

The acrylic 3D structures were then sterilized by gamma radiation (25kGy, ^{60}Co source). The coating of hyaluronan was performed by injecting under vacuum a solution of HA-DVS in 1:0,64 HA:DVS molar ratio. To ensure a correct filling of the inner structure, hydrophobic samples were first filled with water under vacuum to wet the whole inner surface of the construct. Then, the hyaluronan solution containing the crosslinker was injected in the same way twice. Samples were allowed to react during 4h and then immersed in acetone to remove the remaining products, washed several times with 70% ethanol and dried under vacuum. Scaffolds were kept dry until further use.

2.2.3. Materials characterization

Formulations which displayed the lower values of equilibrium water content (EWC) in both DEO and DVS crosslinking were chosen for further characterization. Their FTIR-ATR spectra were recorded and compression tests were performed in both hydrogels. The degree of crosslinking was evaluated by measuring their ECW. Finally structures were compared by in vitro degradation in presence of hyaluronidase.

To perform biological experiments HA-DVS hydrogels were cut into 7mm in diameter discs in swollen state. Samples were then dried at room temperature followed by vacuum drying at 60ºC. Discs were kept under dry conditions until their further use.

Fourier Transformed Infrared Spectra (FTIR-ATR)

The infrared spectra were recorded on a spectrophotometer (FT-IR Thermo Nicolet Nexus). The spectra were averaged on 60 scans in the range of 650-4400 cm^{-1} with a resolution of 16 cm^{-1}.

Scanning Electron Microscopy (SEM)

The morphology of the samples, surface and cross-section, was analyzed using a JEOL JSM 5410 scanning electron microscope (SEM), at an accelerating voltage of 15 KV at different magnifications. All specimens were pre-coated with a conductive layer of sputtered gold.

Equlibrium Water Content (EWC)

The equilibrium water content (EWC) was measured in each crosslinked hydrogel. Crosslinked samples were immersed in distilled water and allowed to swell until equilibrium for 24h. Afterwards, the fully swollen gels were weighed after the residual surface water was carefully removed using a fiberfree tissue. Samples were dried under vacuum and 60ºC and their weight was recorded. The equilibrium water content (EWC,%) was calculated according to equation 1:

$$EWC(\%) = w \cdot 100 \qquad \textbf{[1]}$$

$$w = \frac{w_{H_2O}}{w_d} = \frac{w_S - w_d}{w_d} \qquad \textbf{[2]}$$

where w_d weight of the dry sample (hyaluronan) and w_S the weight of swollen sample in equilibrium.

Volumetric swelling (Q)

The geometry of dry and swollen discs (n=3) was carefully measured to assess either the isotropic or anisotropic character of the swelling. The diameters of samples were measured with the help of a Vernier caliper and their thickness with a micrometer. The volumetric swelling is:

$$Q = \frac{V_{sw}}{V_{dry}} = \phi^{-1} \qquad \textbf{[3]}$$

where Q is the volumetric swelling of crosslinked hydrogels, V_{sw} is the volume of the dry sample, V_{dry} is the volume of the swollen sample and ϕ is the polymer volume fraction in the hydrogel.

The value of Q was determined according to equation 4 and calculated for the different crosslinked hydrogels.

$$Q = \frac{\rho_{HA}^{-1} + w \cdot v_{H_2O}}{\rho_{HA}^{-1}} \qquad \textbf{[4]}$$

If the volumetric swelling is isotropic, Q can be expressed in terms of the ratio between the diameter of the swollen and the dry sample (d_{sw} and d_{dry} respectively) expressed as the Λ the stretching ratio (equation 5)

$$Q_{isotropic} = \left(\frac{d_{sw}}{d_{dry}} \right)^3 = \Lambda^3 \qquad \textbf{[5]}$$

If the volumetric swelling is non isotropic, Q can not be calculated from the change in the diameter of the sample. Thus, a diference in the calculations values of Q following equation 4 or equation 5 is an indication of anisotropy of swelling.

Compression tests

The Young' modulus is a measure of the stiffness of an elastic material and it is widely employed to characterize materials. It can be obtained experimentally from strain-stress curves. The Young modulus (E) is defined as the ratio of the uniaxial stress over the uniaxial strain (equation 6).

$$E \cdot = \frac{\sigma}{\varepsilon} \qquad \textbf{[6]}$$

where σ is the stress applied in N/m^2 and ε the strain of the material resulting from the stress applied (m).

Strain-stress curves of the different crosslinked hydrogels were measured in their swollen state in unconfined compression (n=3). Tests were performed in a Seiko EXSTAR TMA/ss6000 Dilatometer (Seiko Instruments Inc., Chiba, Japan). Compression force was applied from 5 to 200 g at a rate of 5 $gmin^{-1}$ at 37ºC. Bulk samples were disk shaped, 7mm in diameter. The elastic moduli measured under compression in swollen state, E_{sw}, were calculated from initial linear slope of stress-strain curves.

Using the appropriate equations, the Young modulus (E), the density of chains ($\frac{n_c}{V_0}$) and the average molecular weight between crosslinkings can be calculated. Since the crosslinking is performed in the presence of a solvent, it is necessary to take into account the polymer volume fraction of the matrix, ϕ to relate the moduli in swollen state to the Young moduli in the dry rubbery state, E (equation 7).

$$E_{sw} = E \cdot \phi^{1/3} \qquad \textbf{[7]}$$

In turn, the Young modulus of the matrix (E, in the rubbery state) can be expressed as a function of the mol number of polymer chains (nc) and the volume of the matrix without deformation (equation 8):

$$E = 3 \cdot \frac{n_c}{V_0} \cdot R \cdot T \qquad \textbf{[8]}$$

where R is the ideal-gas constantt (R=8.31451 $JK^{-1}mol^{-1}$) ant T is the temperature (K).

Equation 8 can be rearranged and written as a function of the polymer's density (ρ_{HA}) and the molecular weight of the chains (M_c):

$$E = 3 \cdot \frac{\rho_{HA}}{\overline{M}_c} \cdot R \cdot T \qquad \textbf{[9]}$$

If E can be measured, the average molecular weight $\overline{M}_c$ can be calculated through equation 9.

Density

The density of non-crosslinked hyaluronan was measured gravimetrically in an analytical balance (Mettler Toledo analytical balance, sensitivity 0,00001 mg). The density can be measured in two steps, weighing the dry sample and the sample immersed in n-octane. The density of hyaluronan was calculated through equation 10,

$$\rho_1 = \frac{A}{P}\rho_0 \qquad \textbf{[10]}$$

where

ρ_1 =density of hyaluronan (g/cm^3)

ρ_0 = density of n-octane (g/cm^3)

A = weight of dry hyaluronan in air (g)

P = weight of hyaluronan in n-octane minus A (g)

Porosity

Porosity (Π) is defined as the the ratio between the volume of pores (V_{pores}) and the total volume of the structure (V_{total}):

$$\Pi = \frac{V_{pores}}{V_{total}} = \frac{V_{pores}}{V_{Polymer} + V_{pores}} \qquad \textbf{[11]}$$

where the volume of the pores and the volume occupied by the polymer (HA) can be calculated experimentally by weighing the dry and the swollen samples:

$$\mathrm{V_{pores}} = \mathrm{m}_{w\ pores} \cdot \upsilon_{\mathrm{w}} = \mathrm{m}_{\mathrm{w\ pores}} \cdot \frac{1}{\rho_{\mathrm{w}}} \qquad \textbf{[12]}$$

$$V_{HA} = m_{HA} \cdot \upsilon_{HA} = m_{HA} \cdot \frac{1}{\rho_{HA}} \qquad \textbf{[13]}$$

The expressions υ_w and υ_{HA} correspond to the specific volumes for water and hyaluronan respectively. In the same manner, the volume of hyaluronan can be obtained as a function of the mass of polymer (m_{HA}) and its apparent density (ρ_{HA}) calculated previously by equation 10. This method has the advantage of reducing the scatter of the results due to geometry irregularities of samples as the calculations are made directly from weight measurements.

The calculation of the porosity may be rearranged as

$$\Pi = \frac{(m_w \cdot \upsilon_w) - (EWC \cdot m_{HA})}{(m_w \cdot \upsilon_w) + (m_{HA} \cdot \upsilon_{HA})} \qquad \textbf{[14]}$$

where m_w refers to the total amount of water in the sample.

The inner porosity of hyaluronan scaffolds was calculated in samples cut into pellets of 1mm in high and 7 mm in diameter. Scaffolds were allowed to swell in water to equilibrium and then their weight was recorded. Afterwards, samples were lyophilized and weighed again. Same assay was performed by immersing similar samples in ethanol where the hyaluronan does not swell. The porosity was evaluated in the swollen and dry states of the polymer.

Degradation of hyaluronan

Hyaluronate lyase from *Streptomyces hyalurolyticus* (*3.2.1.35)* used for degradation studies was supplied by Sigma, Spain. The enzymatic degradation of hyaluronan crosslinked hydrogels was evaluated by in vitro tests. 5 mm disc shaped samples of each composition were introduced in individual vials containing 100U/ml of hyaluronidase in citrate buffer (pH=5). Each point time tested was evaluated by triplicate. Vials were incubated at 37 ºC and sampled at days 1, 2, 3, 8 and 14.

The enzymatic solution was refreshed weekely in order to assure the activity of hyaluronidase. The degradation rate of hyaluronan crosslinked hydrogels was quantified by measurement of the residual weight of the samples at different time points. Supernatants were boiled during 2 minutes to deactivate the enzyme and then kept at -80ºC. Samples were washed in distilled water prior to lyophilize and then weighed. The remaining mass (RM) was calculated for each sample as:

$$RM(\%) = \frac{m_{dayX}}{m_{day0}} \cdot 100 \qquad \textbf{[15]}$$

where m_{dayX} corresponds to the weight of the sample at day X and m_{day0} to the initial weight of the sample.

Molecular weight of degraded HA

Supernatants of hyaluronan enzymatic degradation were lyophilized and the molecular weight of hyaluronan released during degradation analyzed by gel permeation chromatography (GPC). Water styragel HR columns with water as mobile phase (0,8 mL/min) and 11 polyethyleneglycol (PEG) standards ranging from 106 to 79000 Da (Polymer Standard Service Win GPC software fit to a third order polynomial equation) as a reference for the number-average and weight-average molecular weight calculations, refractary index (RI, Waters 1525) detection.

Alcian blue assay

To evaluate whether the hyaluronan coating on acrylic samples was or not ubiquitous, samples were Alcian blue stained. The Alcian blue dye, which contains copper, stains acid mucopolysaccharides and glycosaminoglycans giving a blue color. It binds by electrostatic forces with the negatively charged macromolecules.

The assay consists in a two step protocol. First, samples were immersed during 10 minutes in Alcian blue solution (1% aqueous Alcian blue solution,

pH=1-2 was achieved with HCL 0,1M) forcing the liquid to fill the scaffold with a pipette. Then, samples were washed several times with fresh water and subsequently immersed in the neutral red solution (0,3 g of neutral red dye in 100 ml of water+0,1 ml glacial acetic acid) during 1min and washed again thoroughly with water. Samples without HA coating were used as controls.

2.2.4. Cell culture

Biomaterials preparation for cell culture.

Biomaterials were sterilized with 70% ethanol (3x10min washings) and protein coated, to prepare them for cell culture. 2D HA-DVS hydrogels were 7mm disc-shaped. 3D HA-DVS interconnected spherical pores structure was used as obtained after fabrication (7mm disc-shaped in non swollen state). HA-DVS coated acrylic scaffolds were 5x5 mm square shaped. Table 2.3 summarizes the shape, the protein coating and cultured cells onto the different HA-DVS biomaterials. Either laminin (LN) or fibrin (fb) protein coating was used on HA-DVS hydrogels. After the coating, biomaterials were conditioned by incubation 30 minutes with fresh medium, same as employed during cell culture. In 3D samples medium was forced to pass through the scaffold to enssure their filling with medium. Afterwards, cell seeding was carried out onto biomaterials in 48 well plates.

Table 2.3. Shape of samples, protein coating and cultured cells onto HA-DVS materials.

Structure	Sample shape	Protein coating		Cell culture		
		LN	fb	hCMEC	U373	co-CULTURE
2D HA-DVS hydrogels	disc	√	√	√	√	-
3D HA-DVS interconnected spherical pores	disc	√	√	√	√	√
HA-DVS coated acrylic scaffolds	square	√	-	√	√	√

Note. HA-DVS: hyaluronan hydrogels crosslinked with divinyl sulfone

LN coating.

Biomaterials were sterilized by being washed in 70% ethanol (3 times) and then rinsed in Dulbecco's phosphate buffered saline (DPBS) allowing then to swell to equilibrium. Then, laminin (laminin from Engelbreth-Holm-Swarm murine sarcoma basement membrane, LN, Sigma, Spain) coating was applied with a concentration of 20μg/ml in DPBS in an incubator at 37°C and 5% CO_2 overnight. Afterwards, materials were washed three times with DPBS prior to cell seeding.

Fibrin coating.

Fibrin coating was performed in a two-step procedure. First, biomaterials were immersed in a 400 μL solution of trisbuffersaline (TBS, Sigma) containing 2% fibrinogen (fibrinogen, Fraction I, Sigma) during 2h. Then, the solution was removed and 400 μL of thrombin (from human plasma, Sigma) in concentration 0.3 units/ml in TBS-$CaCl_2$ 20 mM were added. The fibrin matrix was allowed to polymerize for another two hours. Afterwards, the biomaterials were washed with DPBS and sterilized with ethanol (70% ethanol, 3 washings). Sterilized fibrin coated scaffolds were then rinsed in DPBS allowing them to swell to equilibrium prior to cell seeding.

hCMEC/D3 and U373 monocultures

A suspension containing either $2{,}2 \cdot 10^4$ hCMEC/well (50 μL) or $2{,}2 \cdot 10^4$ U373/well (50 μL) was added to each sample with the help of a micropipette. The seeding density of the 3D structures was incremented three fold with respect to the 2D structures due to the increase of the available surface for cell attachment. Cells were incubated at 37ºC and 5% CO_2 for 30 minutes to favor initial cell adhesion. Then 350μL of fresh medium was added to each well. The seeded biomaterials were incubated at 37°C and 5% CO_2 up to 21 days. The medium was refreshed every 2/3 days and replaced with fresh medium. The supernatants were kept at -20ºC for further studies. In the first refreshment of the medium, samples were moved to a new plate to keep

only the cells adhered to the scaffolds. Gelatin coated cover slides were employed as controls.

hCMEC/D3 and U373 co-culture

hCMEC/D3 and U373 were co-cultured by two different procedures either in a 1 to 10 ratio or in a 1 to 1 ratio (U373:hCMEC/D3) onto hyaluronan biomaterials.

Succesive cell seeding

A suspension containing $2{,}2 \cdot 10^5$ hCMEC/well (50 μL/well) was injected with the help of a micropipette. Cells were incubated at 37ºC and 5% CO_2 for 30 minutes to favor cell adhesion in the hydrogels. Afterwards fresh medium was added (350 μL). Endothelial cells were incubated at 37ºC and 5% CO_2 for 24h prior to addition of the astrocytes. Then, a suspension containing $2{,}2 \cdot 10^4$ U373/well (50 μL/well) was added by direct injection into the biomaterials with a micropipette. Cells were co-cultured in a 1 to 10 ratio (U373:hCMEC/D3) at 37ºC and 5% CO_2 onto biomaterials up to 21 days. Cell medium was collected and changed every 2/3 days. Gelatin coated plastic cover slides were used as controls.

Simultaneous cell seeding

A suspension of both cell lines was prepared containing $2{,}2 \cdot 10^4$ hCMEC/D3 and $2{,}2 \cdot 10^4$ U373 for 2D samples and $6{,}6 \cdot 10^4$ hCMEC/D3 and $6{,}6 \cdot 10^4$ U373 for 3D structures. Cells were seeded together by injection of 50 μL of the cell suspension with the help of a micropipette. Cells were incubated at 37ºC and 5% CO_2 for 30 minutes to favor the adhesion their adhesion to the biomaterials. Afterwards, fresh medium was added (350 μL). Cells were co-cultured up to 21 days. Cell medium was collected and changed every 2/3 days. Gelatin coated cover slides were used as controls.

Viability

To assess the viability of cells growing on hyaluronan based biomaterials individual cell lines, hCMEC/D3 and U373, were cultured on each biomaterial up to 8 days. At two times, 2 and 8 days, samples were incubated for 10 minutes in medium supplemented with 0,1 μM calcein-AM (1:1000, invitrogen). This acetomethoxy derivate can be transported through the cellular membrane of living cells by active esterases which transform the molecule by binding the calcium within the cell giving a strong fluorescence. The stained samples were observed in CLSM (Leica TCS NT) by placing them individually in microscope slides.

Inflammatory effects. E-selectin

Inflammatory effects of the materials to be used in *in vitro* studies were assessed by examining expression of E-selectin, a proinflammatory marker of endothelial cells. E selectin is expressed in cells upon activation by cytokines, as a response to an inflammatory stimulus.

With this aim, hCMEC/D3 cells were cultivated on two samples of each biomaterial for 72h. For each biomaterial set, one sample was stimulated with lipopolyssacharide [LPS from *Escherichia coli,* Sigma, Germany], a characteristic component of the cell wall of Gram– bacteria, as a model inflammatory substance serving as positive control. Stimulation was performed by adding 1μg/ml of LPS and cultured further 4h with the lipopolyssacharide. Subsequently samples fixed with paraformaldehyde (PFA) at 3,7% during 15 minutes at room temperature.

Samples were inmunostained against E-selectin. Shortly, after fixation with paraformaldehyde for 15 minutes at room temperature, constructs were washed 3 times with DPBS, and cells were permeabilized with 0,2x Triton-X during 10 minutes. Thereafter, constructs were washed and incubated with E-selectin antibody (Mouse anti-human, 1:100, ELAM-1) under mild shaking during 1h at room temperature. Samples were then washed 3 times with PBS and incubated with secondary antibody (1:1000, Alexa Fluor 488

antimouse, Molecular Probes) at RT in the dark under mild shaking. Samples were washed extensively with DPBS and the nucleus stained for 5 minutes with DAPI (1:10000). After 3 new washings samples were mounted with fluoromount and examined by CLSM.

Inmunofluorescent analysis

The expression of the platelet endothelial cell adhesion molecule (PECAM-1, CD-31) or von Willebrand Factor (vWF) were assessed in the cultures of endothelial cells. Astrocytes were evaluated by their expression of Glial Fribrillar Acid Protein (GFAP). Immunocytochemistry of these proteins was assessed at day 14 and 21 both in mono and co-cultures. For this end, after fixation with 3,7% paraformaldehyde (10min, RT) cultured samples were rinsed in PBS and the cell membranes were permeabilized with 0.3% Triton X-100 (10 min, RT). Samples were then incubated with the corresponding primary antibody diluted in PBS-BSA 1% at RT for 1h (mouse anti-human PECAM-1, 1:50, DAKO; rabbit anti-human vWF, 1:8000 respectively, DAKO and mouse anti-human GFAP, 1:200, Sigma, Germany). After extensive washing with PBS, samples were incubated with secondary antibody (PECAM and vWF: anti-mouse Alexa Fluor 488, 1:1000; GFAP: anti-mouse Alexa Fluor 654, 1:1000; Invitrogen, Germany) and newly rinsed before nucleus staining. This was done by incubating samples for 10 minutes with DAPI in DPBS. Samples were then washed with DPBS and mounted with Fluromount for visualization by confocal laser scanning microscopy (CLSM).

Growth factors release

Enzyme linked inmunosorbent assay (ELISA) was used for the detection and quantification of growth factors released by activated cells in culture medium. The supernatants of the cultured biomaterials were collected every 2-3 days during the period of culture; reserved supernatant was frozen and kept at -20ºC until further use.

DuoSet Elisas for Vascular Endothelial Growth Factor (VEGF, R&D Systems), Angiopoietin-1 (Ang-1, R&D Systems) and Angiopoietin-2 (Ang-2, R&D Systems) were used for the analysis of the collected supernatants at time points of 3, 7, 10, 14, 17 and 21d for each biomaterial both in mono and co-cultures. All Elisa kits were used according to the manufacturer's protocol.

CHAPTER 3

RESULTS

3.1. Hyaluronan crosslinking

Even though hyaluronan is widely used due to its biological properties, its application requires in the most of the cases modification by crosslinking or derivatization. Thus, hyaluronan may enhance its poor mechanical properties and be used in different aims. In this work hyaluronan chemical crosslinking was carried out with two different crosslinkers, namely 1,2,7,8-diepoxioctane (DEO) and divinylsulfone (DVS). The reaction medium was selected in convenience thus guiding the reaction through the desired functional group.

Crosslinking with 1,2,7,8-diepoxioctane

The crosslinking of hyaluronan with 1,2,7,8-diepoxioctane (DEO) was carried out in an acidic medium provided by a mixture of acetone and hydrochloride solution. The pH of the resulting solution was around 4-5.

Different volumetric ratios acetone:HCl 0,1N were examined, from ratios 50:50 (acetone:HCl 0,1 N) where the film dissolved completely to 100:0 (acetone:HCl 0,1 N) where it did not swell at all. A 70:30 ratio acetone:HCl 0,1N (volume) was chosen to perform further probes for an optimized crosslinking of hyaluronan.

Results showed the influence of different factors during crosslinking such as water content, crosslinker concentration or reaction time. As hyaluronan is a hydrogel, the measurement of the equilibrium water content of the crosslinked structures gives us information about the degree of crosslinking. A hydrophilic matrix with high degree of crosslinking is expected to retain small amounts of water; therefore, lower values of EWC will be measured.
In order to study the influence that crosslinker concentration employed have on the final hydrogel, the equilibrium water content measured after crosslinking was plotted as a function of reaction time (24, 48 and 72h) for the three different conditions independently (R_50, R_70 and R_100) (Figure 3.1). Moreover, the EWC was plotted as a function of the different

conditions to make evidence of the influence of crosslinker concentration within the same reaction times (Figure 3.2).

- ✓ **Same ratio HA:solvent, different reaction times**

Equilibrium water content for crosslinked hyaluronan samples under R_50 condition displayed differences for the different times evaluated. Samples which were crosslinked during 48 or 72 hours displayed low values of EWC (between 200 to 400 %) while samples crosslinked during shorter times (24 h) differ in the EWC depending on the crosslinker ratio. In those samples, the ones crosslinked with ratios HA:DEO of 1 to 1 or 1 to 2 resulted in hydrogels with considerably higher values of EWC while those samples crosslinked with ratios 1 to 3 to 1 to 5 (HA:DEO) showed similar values of swelling. EWC of samples crosslinked upon conditions R_70 displayed slightly lower values of EWC for samples crosslinked during 48 or 72 h. Those crosslinked during 24h revealed higher swelling in water for low ratios of HA:DEO (1:1 and 1:2) while for higher ratios the EWC was similar and lower. Samples crosslinked with R_100 conditions displayed lower values of EWC in longer reaction times which resulted in values of EWC between 250 and 350%, similar in the case of 48 and 72h. Samples crosslinked during shorter times (24h) displayed the higher values of EWC for lower HA:DEO ratios (1 to 1) while values decreased below 400% afterwards. Plotted results can be found in Figure 3.1.

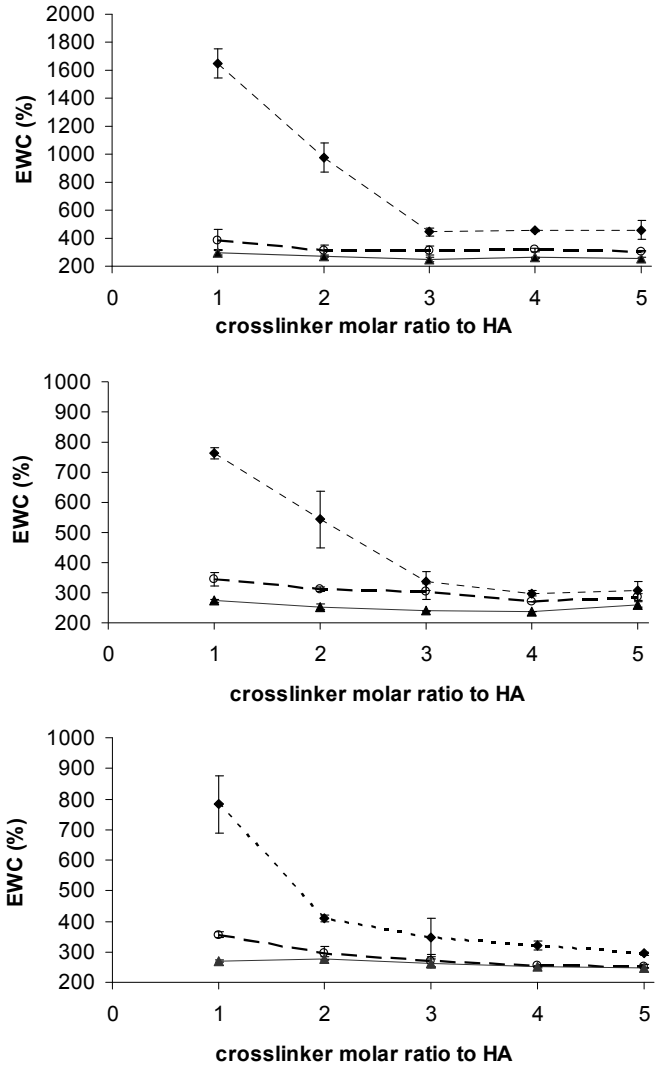

Figure 3.1. EWC in HA-DEO crosslinked samples using a 1:50 ratio (w/w) (acetone:HCl 0,1N):HA during different times reactions. (72h —▲—, 48h −−○−−, 24h ····♦···). B) EWC in HA_DEO crosslinked samples using a 1:70 ratio (w/w) (acetone:HCl 0,1N):HA during different timed reactions. (72h —▲—, 48h −−○−−, 24h ····♦···); C) EWC in HA_DEO crosslinked samples using a 1:100 ratio (w/w) (acetone:HCl 0,1N):HA during different timed reactions. (72h —▲—, 48h −−○−−, 24h ····♦···)

- ✓ **Same reaction time, different HA:solvent ratios**

Same results were plotted as a function of the reaction time for every ratio HA:crosslinker employed. The EWC measured for 24h reaction showed the lower values for 1:70 and 1:100 (HA:solvent) compared with 1:50 for ratios of crosslinker higher than 1:3 (HA:DEO). High EWC values were measured for low crosslinker concentrations. Those samples crosslinked in a 1:50 ratio HA:solvent showed the higher EWC values. In general, 24h reaction resulted in high values of EWC for ratios of crosslinker equal or lower than 2, the lower the content of water in the reaction medium the lower the value of EWC. For ratios equal or higher than 3 value stabilized displaying slight differences within them. The higher values of swelling were observed for samples crosslinked with 1:1 ratio (HA:DEO) and conditions R_50 reaching 1700% of EWC. Those samples were very difficult to manage. Figure 3.2 collects the plotted data for measured EWC.

48h reaction showed to be less influenced by crosslinker concentration. Except to 1:1 HA:DEO ratio, the measured EWC values were between 250 and 400%. The larger reaction time evaluated (72h) showed slight differences in the EWC values demonstranting less dependence with concentration of crosslinker or solvent employed in longer times (note the small scale in Y axis in Figure 3.2).

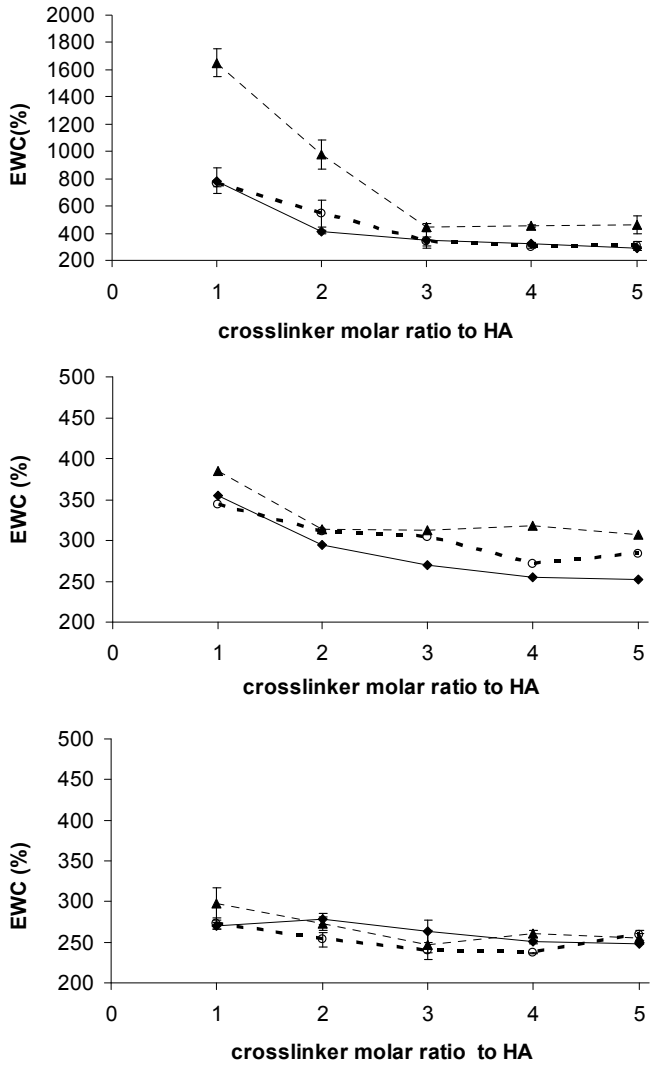

Figure 3.2. EWC in 24h crosslinking reaction of HA_DEO hydrogels. (1:100 HA :solvent —▲—; 1:70 HA:solvent −−○−−; 1:50 HA:solvent ····♦···) B) EWC in 48h crosslinking reaction of HA_DEO hydrogels. (1:100 HA :solvent —▲—; 1:70 HA:solvent −−○−−; 1:50 HA:solvent ····♦···) C) EWC in 72h crosslinking reaction of HA_DEO hydrogels. (1:100 HA :solvent —▲—; 1:70 HA:solvent −−○−−; 1:50 HA:solvent ····♦···)

Summarizing, samples crosslinked during shorter times (24h) showed a higher dependence with crosslinker concentration than those crosslinked during 48 or 72h. The longer the reaction time the lower the EWC. Within the same reaction times, the higher the water content on the reaction the lower the swelling values. Figure 3.3 shows the lower values of EWC for every condition as a function of reaction time.

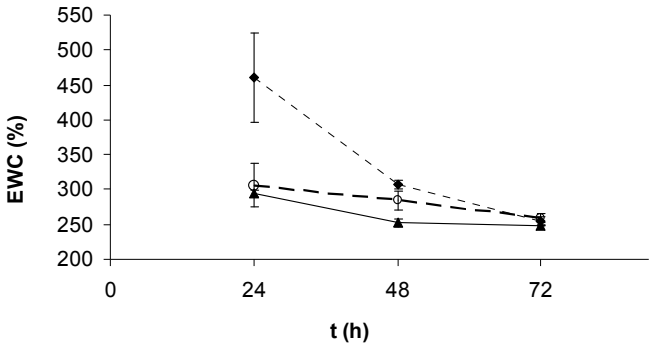

Figure 3.3. The lower EWC for 1:5 HA_DEO molar ratio employed to crosslink hyaluronan during three times, 24, 48 and 72 h. R_50 (····♦···), R_70 (−−○−−) and R_100 (—▲—).

Crosslinking with divinylsulfone

Hyaluronan divinylsulfone crosslinked samples were obtained by mixing a basic solution of hyaluronan (5% HA in 0,1M NaOH) and the crosslinker were left to react for 4h.

To end the crosslinking reaction, the hydrogel was gently rinsed with solvent to eliminate the unreacted divinylsulfone. The solution employed for the washing was noticed to influence the properties of the crosslinked hydrogel. In order to assess the effect of the solvent composition employed for the rinsing, the hydrogel was exposed to solutions containing different acetone-water ratios. Immersion time in the different solutions was evaluated as well. The EWC measured are in the graph Figure 3.4.

Results may be arranged into two different groups. A first group composed of those samples rinsed with acetone alone or with low contents of water. A second range, grouping those samples immersed in acetone

solutions with high ratios of water or only water. Samples, all of them crosslinked in equal conditions, showed lower rates of EWC when washed with solvent containing high concentrations of acetone or only acetone after 10 minutes of immersion to keep the value of swelling low afterwards (group 1). Besides, samples rinsed with solvents containing 50% or more water in volume showed similar behaviour in terms of swelling, displaying high values of retained water.

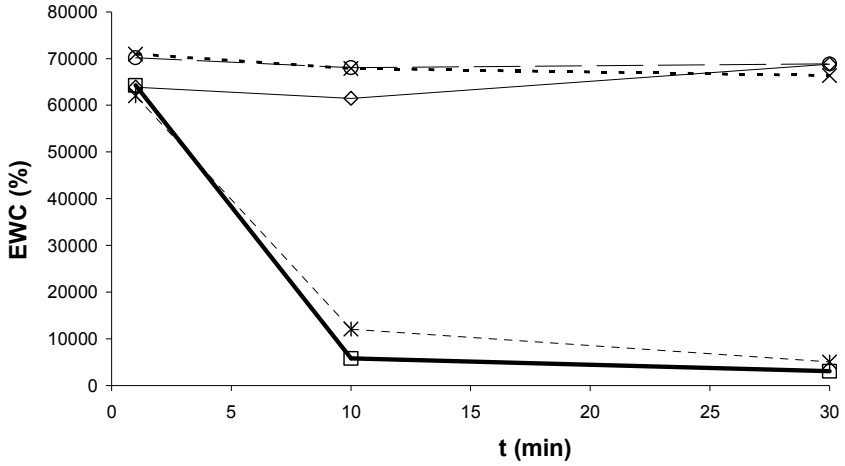

Figure 3.4. EWC of hyaluronan crosslinked films with DVS after ending the reaction by rinsing with different acetone-water solutions. (—□— acetone; ···∗···80:20 acetone:water; −−○−− 50/50 acetone:water; —◊— 20:80 acetone:water; ▪▪▪x▪▪▪ water)

3.2. HA hydrogels characterization

Those samples which displayed the lower rates of EWC for each crosslinker were selected for further characterization. The crosslinked hydrogels were characterized by their FTIR-ATR spectra, EWC in fixed conditions, volumetric swelling and Young modulus measured in compression. Biodegradability of hydrogels in presence of hyaluronidase was also evaluated as well as the fragments resulted from the enzymatic degradation. Table 3.1 summarizes the conditions and crosslinkers selected for its characterization.

Table 3.1. Selected conditions for Hyaluronan crosslinking with 1,2,7,8-diepoxioctane (HA-DEO) and divinylsulfone (HA-DVS) for characterization.

X	HA:X	reaction phase	medium	time (h)
DEO	1:5	solid	acid	72
DVS	1:0,64	liquid	basic	4

X: crosslinker; DEO: 1,2,7,8-diepoxioctane; DVS: divinylsulfone; molar ratios

3.2.1. Fourier Transformed Infrared Spectra (FTIR-ATR)

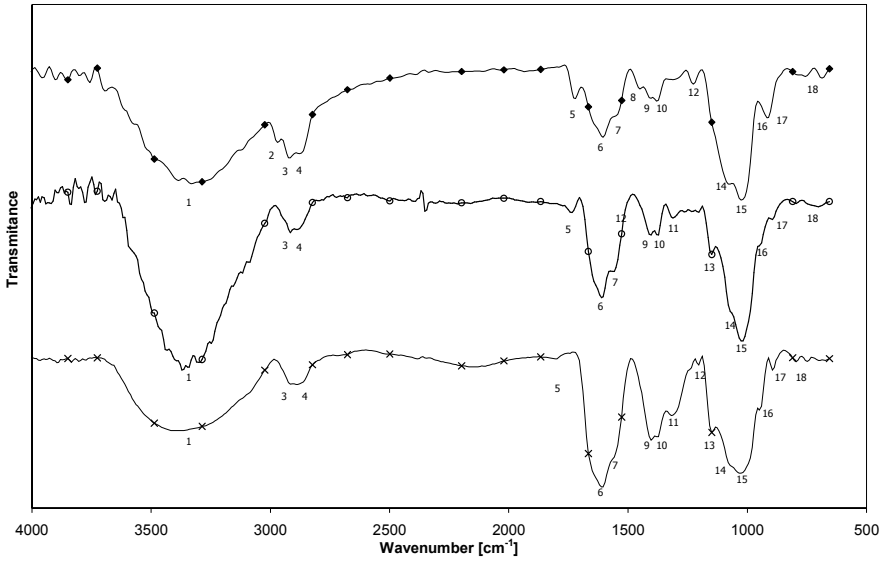

Figure 3.5. FTIR spectra of Hyaluronic acid and crosslinked derivates synthetized. (natural HA ─x─; HA-DVS ─♦─ ; HA-DEO ─○─)

Figure 3.5 shows the infrared spectra measured in the range of 600-4000 cm^{-1} for natural hyaluronan and chemically crosslinked derivates.

In a general view there is a broad band with a maximum in 3340cm^{-1} due to the N-H stretching and O-H stretching. Bands in 2931cm^{-1} and 2893cm^{-1} correspond to the C-H bond stretching. Band with maximum in 1836cm^{-1} correspond to the mixture of the vibrations of several bonds. In one side

there is the C=O carboxyl from amide I and from ester bond, giving a slight shoulder in higher frequencies for the later. The shoulder in lower frequencies may correspond to the amide II bond. Amide I and amide II bands are schematically represented in Figure 3.6 for a better understanding.

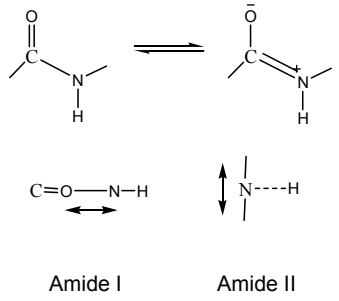

Figure 3.6. Different bond vibrations in the amide group.

Continuing toward lower band frequencies CH_2, CH_3 deformation and the combination of C-O with C=O bond (1412cm^{-1}, 1404cm^{-1}) and the stretching of C-O-C, C-O and C-O-H (1149, 1080 and 1049 cm^{-1}) appears. Finally, in the lower frequencies of the spectra there are the bands corresponding to C-O-C stretching, O-H deformation and C=O deformation (957, 895 and 810 cm^{-1}).

The typical bands describing the IR spectra of natural HA and both crosslinked hydrogels are collected in Table 3.2.

Table 3.2. Peaks in FTIR-ATR spectra for natural hyaluronan and their crosslinked structures HA-DEO and HA-DVS.

	HA	HA-DEO	HA-DVS	band description
1	3440	3379	3348	N-H, O-H stret
2	-	-	2978	Csp3-H DVS
3	2931	2931	2931	C-H stret
4	2893	2893	2893	
5	1836	1759	1728	C=O carboxyl amide I
6	1620	1620	1620	
7	1574	1581	1574	
8	-	-	1466	Asim stret S=O
9	1412	1412	1419	CH_2, CH_3, COH def C-O and C=O
10	1404	1396	1404	
11	-	1327	1334	
12	1227	1234	1234	
13	1149	1157	-	
14	1080	1072	1088	C-O-C; C-O; C-O-H stretching
15	1049	1034	1034	
16	957	957	-	
17	895	918	926	C-O-C stret, O-H def, C=O def
18	810	818	810	

3.2.2. Water absorption capacity

The amount of water retained in a hydrogel is associated with the amount of hydrophilic groups and the crosslinking density of the matrix among other factors. Crosslinking may be considered as an opposed force to the solvatation of the matrix. If the polymer was not crosslinked, the result of its immersion in solution will be its dissolution.

Hydrogels, in their crosslinked state, are able to retain high amounts of water. The total amount of water in a hydrogel, result of taking together the primary bound water (water hydrating the most polar hydrophilic groups) and secondary water (responsible of the swelling of the matrix) will determine the absortion and diffusion of solutes through the hydrogel. The water absorbed in the hydrogel matrix depends mainly on the crosslinking density which can be estimated by their equilibrium water content (EWC).

Water vapour absorption and water swelling by immersion was evaluated for the different crosslinked matrices. On the one hand, the capacity of the

material for gainning and keeping water vapour will give us information about the intrinsic hydrofilicity of the molecules making up the matrix. The amount of vapour gained depends on the nature of the material. On the other hand, the total capacity of the hydrogel for absorbing water was evaluated by immersion of the samples in distilled water. In this situation, both the chemical affinity for water of the HA molecules and the ability of the materials to lodge a pure water phase are taken into account together.

The EWC was measured for the different crosslinked matrices (HA-DEO and HA-DVS) and the different values obtained were compared. Swelling was higher for the DVS crosslinked matrices reaching values higher than 600% (weight) versus the 140% of HA-DEO matrices. The values of EWC in water vapour, compared with swelling under immersion, were slightly lower for HA-DEO (131%) while quite noticeable for HA-DVS hydrogels (400%). The evidences in the results showed different behaviour depending on the matrix. HA-DEO hydrogels revealed high hydrophilicity displaying low differences between the immersion and vapour water retention which may be interpreted as a high crosslinked matrix. Besides, HA-DVS matrices behave noticeably different under such conditions demonstrating a higher hydrophilic matrix compared with HA-DEO. The HA-DVS matrix displays favourable characteristics for the desired applications as a highly open matrix which may permit a proper diffusion through the hydrogel. The different hydrophilicity of the crosslinker chains may affect the amount of water gained by exposition to water vapour. The longer hydrophobic chains resulting from diepoxioctane crosslinking will retain less primary bound water than the higher hydrophilic chains resulting from the divinyl sulfone.
The EWC of the different hydrogels are plotted in Figure 3.7.

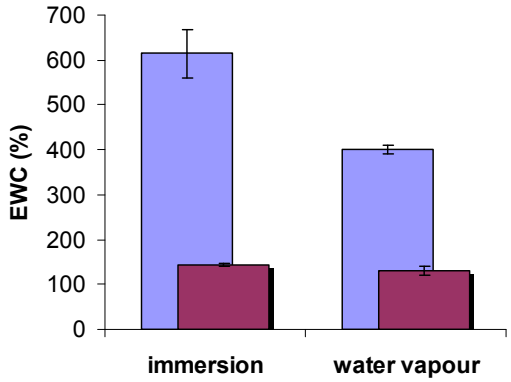

Figure 3.7. EWC of HA-DEO (■) and HA-DVS (■) hydrogels by immersion (water) or by water vapour absorption at 37°C.

3.2.3. Volumetric swelling

To assess the isotropy or anisotropy of the swelling in hyaluronan crosslinked matrices, swollen samples were geometrically measured. HA-DVS hydrogels become larger compared to the HA-DEO samples fact that is in agreement with the values of EWC measured for each matrix. The Q values were calculated considering both an isotropic or non isotropic swelling. HA-DEO hydrogels displayed lower Q values both for isotropic or anisotropic calculations in the order of 3. In those hydrogels, the Q values do not greatly differ, displaying approximately an isotropic swelling. In the case of HA-DVS hydrogels, Q values calculated in both considerations were very different ($Q = 4$ versus $Q = 8$ considering an isotropic and anisotropic swelling respectively) thus demonstrating a non isotropic swelling. For better a better understanding of the result visualize the data graphed in Figure 3.8.

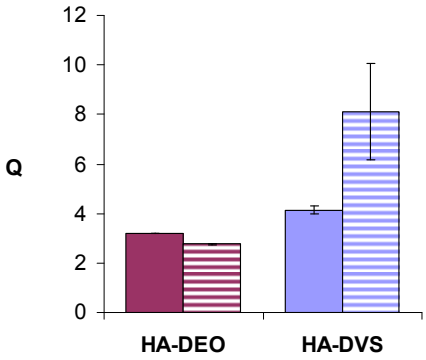

Figure 3.8. Volumetric swelling for HA-DEO (■) and HA-DVS (■) crosslinked hydrogels. Q values for isotropic calculation according to equation 5 (solid colour); Q values according to equation 4 (striped colour)

3.2.4. Compression tests

Isothermal mechanical analysis is useful to assess the mechanical properties of materials. Analyzing the strain during unconfined compression with significant load in thin films, the Young modulus can be measured and the crosslinking density evaluated.

The stress-strain curves indicated different responses for HA-DEO and HA-DVS crosslinked hydrogels. HA-DVS matrices displayed higher capacity of deformation without breaking as well as a higher yield strain. In HA-DEO matrices, yield values up to 140% were calculated while HA-DVS reached values higher than 220%.

The Young modulus in swollen state, E_{sw}, can be calculated for each hydrogel from the initial slope of the elastic deformation on stress-strain curves. The value of Young modulus allows us to evaluate the crosslinking degree of each matrix in the terms of density of chains, $\frac{n_c}{V_0}$ and the molecular weight between crosslinks, $\overline{M}_c$.

Lower values of E_{sw} were obtained for HA-DVS compared to HA-DEO. This value gives us an approximation of the stiffness of the matrices, the

higher the value the lower the stiffness of the matrix. Higher elastic behaviour was found in HA-DVS matrix versus a more rigid structure measured for HA-DEO matrices.

The physical characteristic of the matrices as density of chains and molecular weight between crosslinks were estimated from the calculated values for E_{sw}. Calculations demonstrated longer chains of polymer between crosslinks for HA-DVS compared to the HA-DEO structure.

Figure 3.9 shows stress-strain curves for hyaluronan crosslinked hydrogels both with DEO and DVS. The physical properties of hydrogels both calculated and stimated for those crosslinked matrices are collected in Table 3.3.

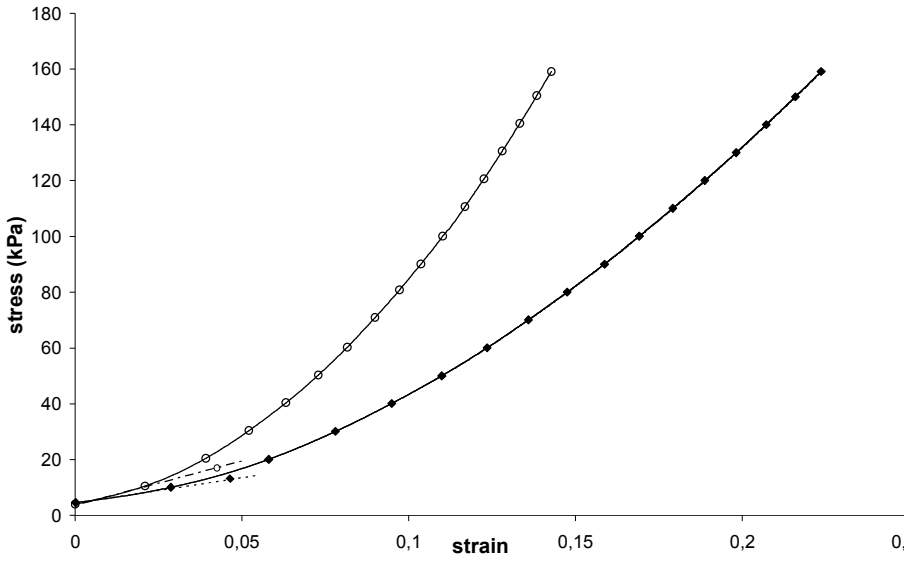

Figure 3.9. Typical stress-strain curve for hyaluronan crosslinked hydrogels. HA_DVS —♦— ; HA_DEO —○—.

Table 3.3. Physical properties for hyaluronan crosslinked matrices.

matrix	EWC (%)	Q	E_{sw} (kPa)	$\overline{M}_c$ (g/mol)
HA-DEO	144±4	3±0	311±35	41400
HA-DVS	615±54	8±2	164±23	139000

Note. Abreviations: equilibrium water content (EWC); volumetric swelling ratio (Q); Measured Young modulus in swollen state (E_{sw}); Average molecular weight between crosslinks (M_c)

3.2.5. Enzymatic degradation of HA crosslinked hydrogels

Although there are non-enzymatic mechanisms which degrade hyaluronan, it is thought that hyaluronidases are the main cause responsible for hyaluronan degradation within the body. The stability of crosslinked hydrogels synthetized in this work was assessed *in vitro* by immersing the samples in aqueous solutions containing 100U/ml of hyaluronidase (testis. type).

The remaining weight of samples exposed to *in vitro* degradation in presence of hyaluronidase was recorded and are graphed in Figure 3.10. According to the results, both the HA-DVS and HA-DEO matrices degraded following the same pattern but, within the time evaluated, HA-DEO matrix were slightly more stable (35% remaining weight of HA-DVS versus 50% of the HA-DEO hydrogels in day 14). Samples maintained their bulk integrity while becoming degraded losing weight but displaying their cylindrical shapes.

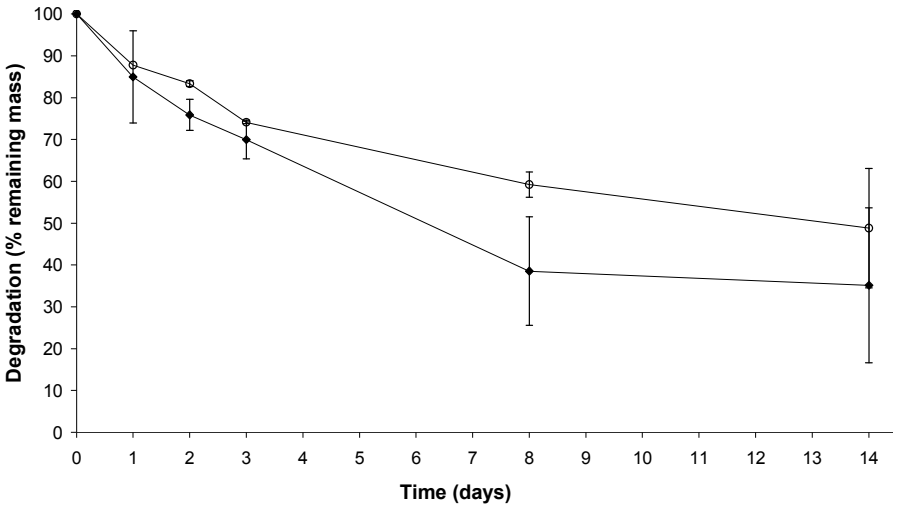

Figure 3.10. In vitro enzymatic degradation of hyaluronan crosslinked hydrogels. HA-DVS (♦) and HA-DEO (○).

Molecular weight of degraded hyaluronan

The molecular weights of hyaluronan polymers released to the medium in the *in vitro* enzymatic degradation studies were assessed and analyzed by GPC with the help of PEG standards. HA-DVS crosslinked hydrogels were found to be broken into polymer chains of different lengths thus, in high molecular weight hyaluronan (HMW-HA, higher than 50000 g/mol) and low molecular weight hyaluronan (LMW-HA, lower than 10000 g/mol). The molecular weights of DEO crosslinked hydrogels were a mix of both high and low molecular weight in most of the days evaluated although during the first 24 hours only low molecular weight was released. Table 3.4 contains the results obtained for both crosslinked matrices.

Table 3.4. GPC measured molecular weighes for HA matrices by enzymatic degradation.

molecular weight (GPC)						
	Hydrogel					
	HA-DVS			HA-DEO		
days	M_n (g/mol)	M_w (g/mol)	M_w/M_n	M_n (g/mol)	M_w (g/mol)	M_w/M_n
1	51719	54502	1,05381001	9194	9443	1,02708288
	4202	4409	1,04926226			
2	55679	57678	1,03590223	20805	21610	1,03869262
	4380	4624	1,05570776			
3	52416	53962	1,02949481	28995	30259	1,04359372
	4308	4617	1,07172702	3227	3372	1,04493337
8	52071	53447	1,02642546	30338	31850	1,04983849
	4209	4421	1,05036826	3240	3390	1,0462963

3.3. Development of HA based 3D structures

With the compromise to produce different geometric scaffolds made on crosslinked hyaluronan, several 3D structures with different inner porosities were prepared. Hyaluronan scaffolds were performed by crosslinking either with DEO or DVS. Different methods were employed, adapting the procedure to the conditions of crosslinking for each substrate.

Generally, porogens employed were easily removed from the structures. The porosity and interconnection of the matrix in spherical pores distribution, were able to be tuned by changing the ratio of porogen:polymer, from matrices in which there were not observed interconnection of the pores to highly interconnected matrices which are further characterized below. The method provided reproducible samples to carry out further assays.

Figure 3.11 shows images of the cylinders obtained after demolding the hyaluronan mixtures and detail of disc cut for further studies.

Figure 3.11. Optic microphotographs of a complete cylinder obtained by porogen leaching in a mold (a); b and c correspond to details of dry discs cut from the cylinder used for further studies.

3.3.1. Structures based in HA-DEO

Cylinders

Cylinders made of HA were obtained by lyophilisation of hyaluronan solutions. Afterwards those cylinders were crosslinked with DEO following the described protocols. The pores within the structure had sizes in the range of 30 microns. Two different architectures were developed, highly porous cylinders 1mm in diameter and tubes with inner diameter of 1,2mm and outer diameter of 2,2mm (Images A and B respectively in Figure 3.12). The thickness of the tube wall was around 500 microns displaying a highly open structure with high microporosity. Figure 3.12 collects the SEM microphotographs of different cylinders made on HA-DEO where it can be most appreciated of its detailed bulk porosity.

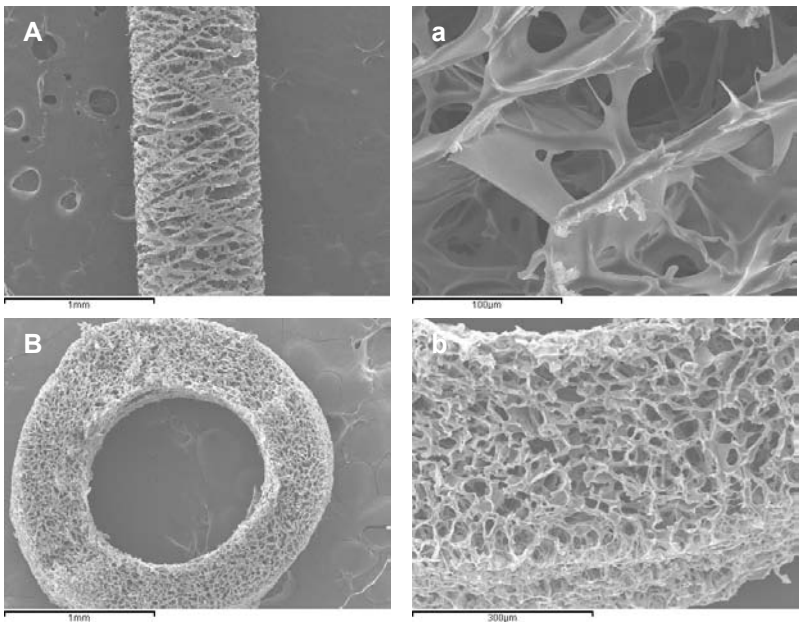

Figure 3.12. Scanning electron microscopy of 1mm diameter porous cylinders made on HA-DEO. A) 1mm in diameter highly porous bulk cylinder; B) tube with large inner diameter.

Interconnected spherical porous structures

Hyaluronan scaffolds with inner interconnected spherical pores were prepared by a porogen leaching technique. Those structures displayed highly open matrix with micro and macroporosity. Figure 3.13 shows the SEM photographs were the pores can be observed in detail (photographs a.1 and a.2). The microporosity, obtained as result of lyophilyzation, had sizes around 2 microns.

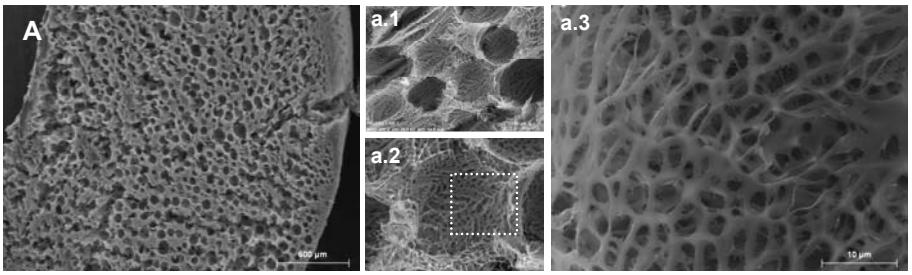

Figure 3.13. Scanning electron microscopy of lyophylized HA-DEO scaffolds obtained by porogen leaching with low interconnection between pores. A) Panoramic view of the scaffold; a.1) detail of the pores; a.1) detail of the pores showing the microporosity of the walls; a.3) detail of the microporosity of the bulk hyaluronan.

Channelled scaffolds

Multiple parallel-disposed channelled scaffolds were prepared following a fiber molding method employing metallic or polymeric filaments. Structures with different architectures and pore sizes were built. Porosity was originated either by lyophilization (A and C in Figure 3.14) or by the use of porogen (B in Figure 3.14) obtaining smaller or bigger porous sizes respectively. The pores provoked by the lyophilization process had sizes in the range of 30 microns while the pores obtained with porogen had higher sizes in the range of 120 microns approximately. There were differences observed by the use of polypropylene, stainless steel or copper filaments (filaments diameters: 100, 200 and 100 microns respectively). The composition of the tube used as a mold, either made of silicon or glass, thus resulted in differences in the final structures. Scaffolds fabricated into glass tubes and coper filaments

(photograph C in Figure 3.14) presented aligned disposition of porosity resulted from lyophilization. Those gradients were not observed when using stainless steal or polymeric filaments and silicon tubes as a mold (photographs A and B in Figure 3.14). This fact is thought to appear due to the temperature gradients produced by conductivity of filaments which were not found with non conductive filaments. In Figure 3.14 there are collected the SEM photographs of those structures including detail of the cylinders created within the scaffold.

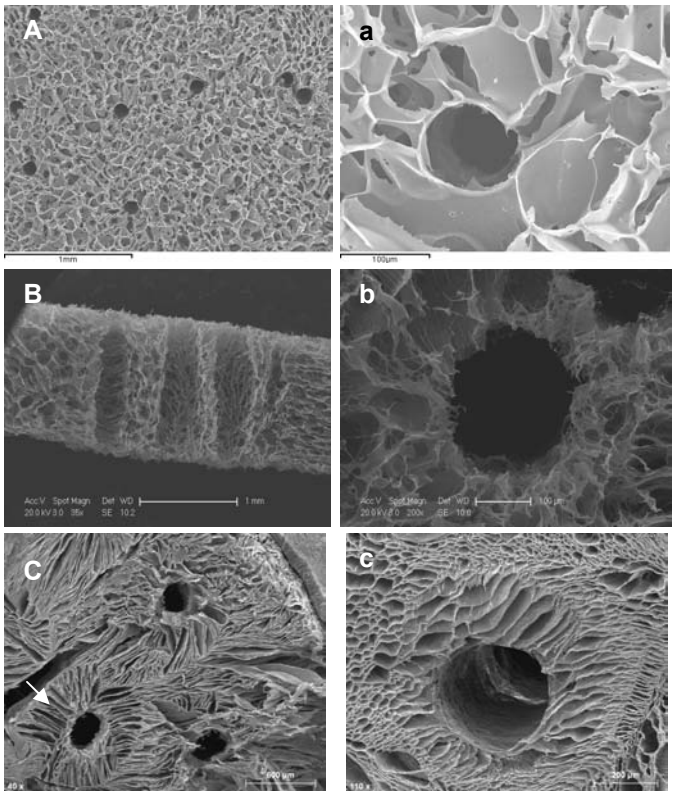

Figure 3.14. Scanning electron microscopy of 3D structures with multiple parallel-like distributed channels made on HA-DEO. Scaffolds were fabricated using different filaments: A) 100 microns polypropylene filament; B) 200 microns metallic filament; C) 100 microns copper filament. Images a, b and c show higher magnification of the correspondent panoramic images. White arrow in figure C shows the aligned porosity provoked by gradients of temperature from the metallic filament.

3.3.2. Structures based in HA-DVS

HA-DVS structures were prepared both by a porogen leaching technique and fiber molding. Furthermore, non degradable structures made of acrylates were coated with HA-DVS hydrogel to study their biological response afterwards.

Interconnected spherical porous structures.

Scanning Electron Microscopy (SEM) images show the inner structure observed in interconnected spherical pores HA-based scaffolds (Figure 3.15). The structure displayed randomly distributed pores within the matrix as well as high connectivity between the pores with throats with an average of 36 microns in size. The pore's sizes observed were corresponding with the dimensions of the particles employed as porogen in the fabrication of scaffolds with sizes ranging between 100 to 150 microns. The thickness of the walls separating the pores was estimated to be around 5 microns.

To improve the biological characteristics of hyaluronan scaffolds, a fibrin coating was applied to those structures by polymerizing a solution of fibrinogen deposited throughout the matrix and crosslinked with thrombin. Fibrin (fb) was randomly deposited on the hyaluronan both covering and filling the pores. Nonetheless it was observed to still be an open pore structure filled with fb which is thought to improve the biological properties of the scaffolds. The scaffold containing a polymerized fibrin matrix can be observed in Figure 3.16.

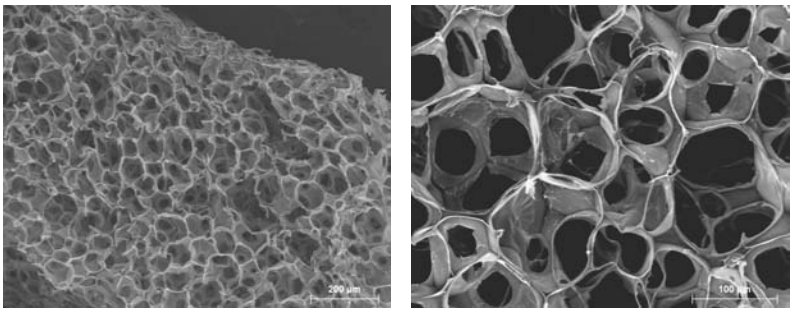

Figure 3.15. 3D matrix of HA-DVS with interconnected spherical porous inner structure. the matrix was obtained by a porogen leaching technique with pores sizes between 100 and 130 microns.

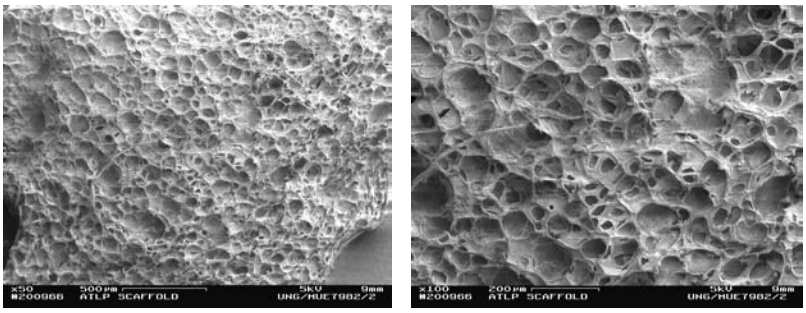

Figure 3.16. 3D matrix of HA-DVS with interconnected spherical porous inner structure showing the fibrin coating. Fibrin coating, obtained by polymerizing a solution of fibrinogen deposited throughout the matrix and crosslinked with thrombin, is thought to enhance the biological properties of HA-DVS scaffolds.

Porosity

The total porosity of spherical interconnected porous scaffolds was measured by volumetric calculations. The calculated porosity of scaffolds gave evidence of a highly porous structure both in swollen and not swollen state (higher than 94% in both cases). The highly open structures obtained assures enough space for cells to grow and a proper diffusion of nutrients and waste to adequate cell supply within the scaffold.

Table 3.5. Porosity and standard deviation of scaffolds. The porosity in swollen state was measured by equilibrium swelling in water and the non swollen porosity by immersion in absolute ethanol were hyaluronan do not swells.

Sample	Porosity (%) ± SD
swollen	94,4 ± 0,8
no swollen	96,5 ± 0,5

Hyaluronan cylindrical channelled scaffolds

Figure 3.17 shows the structure of a hyaluronan cylindrical channelled scaffold obtained by fiber molding. The channels were uniformly distributed in a parallel way and separated by a thin wall of hyaluronan. The channels (100 microns in diameter) were well defined with smooth walls in the inner side of the channel, those surfaces which were in contact with the filament during fabrication. A detail of the filament employed as a mold to build the scaffold is shown in Figure 3.17-B (white arrow). The filaments were easily removed from the structure and did not stick to the inner surface of the walls forming the channels. The external surface of the scaffold displayed rough micro porous walls (Figure 3.17-a.3). The walls manifested into two different structures. The surfaces corresponding to those in contact with the filaments presented a wall approximately of 3 microns in thickness without porosity (white arrows in Figure 3.17-a.2). Within those solid surfaces separating the channels there were observed high porosity bulk with pores ranging 10 microns in size (white head arrows in Figure 3.17-a.2).

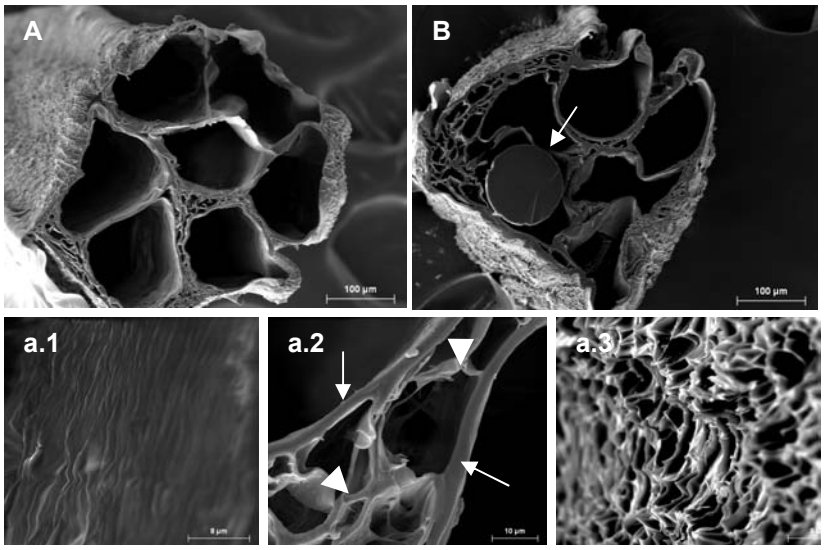

Figure 3.17. Tubular channeled scaffold made on HA-DVS. A) Apical panoramic view of the scaffold; B) same view showing a remaining filament employed as mold to built the scaffold, the white arrow shows a detail of the filament employed to construct the scaffold. a.1) higher magnification of the scaffold showing a detail of the inner wall of the channel; a.2) detail of the porosity between parallel channels, arrows shows the wall in contact with the filaments and arrow heads the porosity within the wall; a.3) detail of the outer surface of the scaffold showing high porosity.

Hyaluronan coated acrylic scaffolds

Non degradable acrylic scaffolds made as 3D mesh of cylindrical channels were coated with a thin layer of hyaluronan. The regular pattern of the structures and their connection sites between the cylinders may be seen in Figure 3.18. The hyaluronan coating was examined first by scanning electron microscopy. Alcian blue assay, a test to analyze the presence of GAGs, was used to investigate the distribution into the matrix. The thin layer of hyaluronan coating was easily distinguishable from the primary acrylic structure as can be appreciated by the different texture present in the walls of the scaffold when seen in a scanning electron microscope (Figure 3.19). In the figure, images B and C show in detail the hyaluronan coating into the acrylic scaffold. Images A and a.1 show a panoramic view with more or less magnification where the HA-DVS coating may be appreciated.

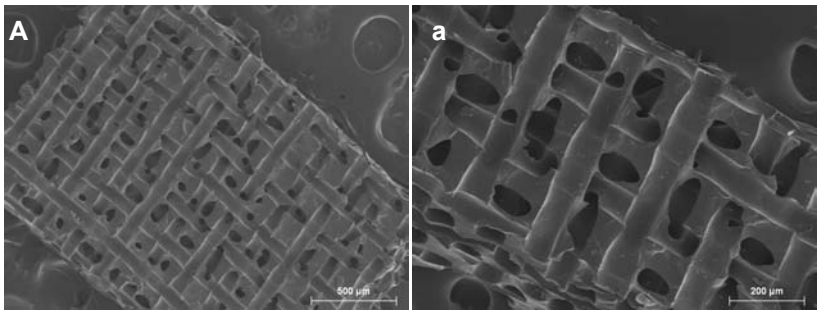

Figure 3.18. Interconnected cylindrical channelled scaffold made on a co-polymer of poly(ethylacrylate-co-hydroxyethylacrylate) in a 9 to 1 ratio. A) Panoramic view of the scaffold. Scale bar corresponds to 500 microns; a) higher magnification showing the channels and the interconnections between them.

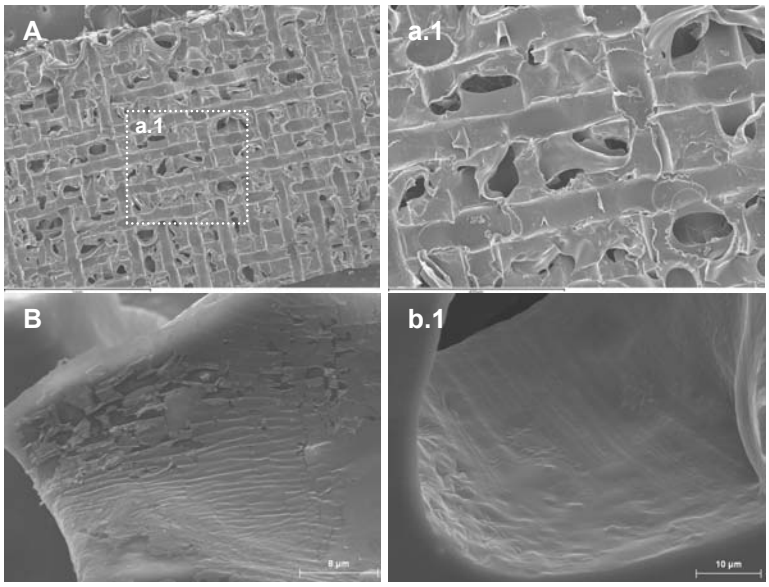

Figure 3.19. Microphotographs of acrylic co-polymer scaffold coated with hyaluronan DVS crosslinked layer. Images A and B show a panoramic view of the hyaluronan coated scaffold (scale bar correspond to 1mm and 400μm respectively). Images a.1 and b.1 show detail of the hyaluronan coating (scale bar correspond to 8 and 10μm respectively).

Alcian blue assay

The presence of hyaluronan within the acrylic scaffold was assessed by alcian blue staining. Alcian blue only stained the acrylic scaffold coated with hyaluronan which turned to a dark blue colour (assay positive) while the acrylic scaffold employed as a control (without hyaluronan coating) did not. The distribution of the staining seemed homogeneous in the 3D matrix turning the whole sample into blue without an apparent appearance of white spots indicating areas without coating. Figure 3.20 shows optic images of a non hyaluronan coated acrylic scaffold (left) and hyaluronan coated acrylic scaffold (right).

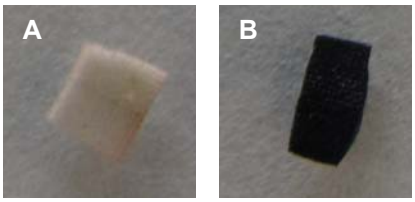

Figure 3.20. Evaluation of hyaluronan content in acrylic scaffolds after HA coating by alcian blue assay. Images correspond to the alcian blue staining on acrylic scaffold without HA-DVS coating (A) and with HA-DVS coating (B).

Hyaluronan content on acrylic coated matrix

The amount of hyaluronan coating within the acrylic scaffold was evaluated by weight. To calculate the amount of hyaluronan, dry samples with and without HA were weighted. The average value obtained for hyaluronan content on acrylic matrices was 0,79±0,13 mg. This value supposed an average of 30% of the total weight of the acrylic scaffold which is thought to be noticeable. The coating was considered to be reproducible ($s = \pm 0.13$). The total volume occupied by hyaluronan within the channels was estimated in 6,6% of the total free volume which may assure space enough for cells to grow within the scaffold.

3.4. hCMEC/D3 and U373 monocultures on biomaterials.

3.4.1. Hyaluronan based biomaterials

Biomaterials were assayed in terms of their biological interaction using different cell lines. In the case of hyaluronan based biomaterials samples used for *in vitro* culture characterization were disc shaped, both for the 2D (films) and 3D structures (scaffolds with interconnected spherical pores).

To favour cell adhesion, biomaterials were subjected to different protein coating, either laminin (LN) or fibrin (fb), and the influence of the coating on cell behaviour was analyzed.

An endothelial cell line from the microvasculature, named hCMEC/D3, and an astrocytic cell line (U373) were chosen to mimic the conditions of the BBB for the *in vitro* characterization of the biomaterials. To assess the phenotype of those cells growing onto the hyaluronan based biomaterials, different experiments were performed. On the one hand, viability was qualitatively assayed by calcein staining. On the other hand, the inflammatory effects elicited by biomaterials were analyzed by E-selectin expression in ECs. The phenotype of ECs growing on HA based biomaterials were assessed by immunocytochemistry of the expressed PECAM-1 and vWF while in the case of astrocytes it was followed by GFAP expression. Results permitted to analyze the invasion of the 3D structure by cells, their morphology within the pores and surfaces and their specific protein expression. *In vitro* culture was followed up to 21 days in physiological environment. For better understanding, Table 3.6 and Table 3.7 summarize the different experiments performed.

Table 3.6. Shape of samples, protein coatings and human cell lines assayed on HA-DVS hydrogels.

Structure	Sample shape	Protein coating		Cell culture	
		LN	fb	hCMEC	U373
2D HA-DVS hydrogels	disc	√	√	√	√
3D HA-DVS interconnected spherical pores	disc	√	√	√	√

Note. HA-DVS: hyaluronan hydrogels crosslinked with divinyl sulfone

Table 3.7. Assays performed to biological characterization of both hCMEC/D3 and U373 cell lines growing onto 2D and 3D HA-DVS based hydrogels.

Cell line	Assays performed			
	Viability	Inflammatory effects	Inmunocytochemistry	cytokine release
hCMEC/D3	√	√	√	√
U373	√	-	√	√

Note. hCMEC/D3: Human brain microvessel endothelial cell line (Weksler et al., 2005)
U373: Human glioblastoma-astrocytoma cell line

3.4.1.1 HA-DVS films. Assays in 2D hydrogels.

Viability

Calcein staining was employed to assess the viability of cells growing onto HA-based hydrogels. The acetomethoxy derivate of calcein (Calcein-AM) readily passes through the cell membrane of viable cells because of its enhanced hydrophobicity as compared to calcein. The AM masks the part of the molecule that chelates calcium and, when it is transported into living cells, esterases cut off the AM groups resulting in a strong green fluorescence. Due to the lack of sterases on dead cells, only living cells are stained.

Both the endothelial and the astrocytic cell lines showed viable cells in day 8 of *in vitro* culture. At this time, hCMEC/D3 showed no appreciable differences by the use of distinct protein coatings onto biomaterials performed prior to cell seeding. Cells growing on 2D biomaterials displayed organized morphologies of cells with oriented extracellular matrices. Cells invaded completely the surface of the disc shaped samples with extended cytoplasm and establishing contacts with each other (Figure 3.21).

The astrocytic cell line, U373, showed different cell morphologies depending on the protein coating. In the case of LN coated biomaterials, high density of astrocytes spread throughout the material showing fusiform morphologies and completely expanded cytoplasms. When fibrin coating was used, a lower density of cells was observed and cells displayed an aligned parallel-like distribution of their cytoskeleton with not completely expanded distribution (Image B in Figure 3.22).

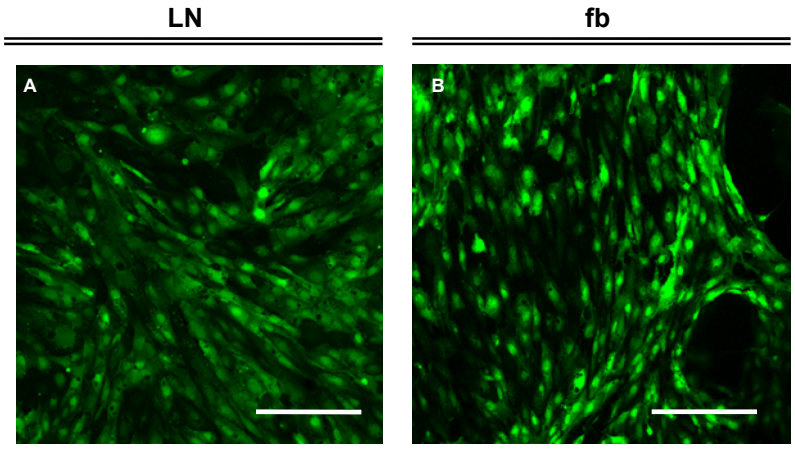

Figure 3.21. 8 days calcein stained hCMEC/D3 growing onto films of HA-DVS hydrogels LN (left column, A) or fb (right column, B) coated. The acetometoxy calcein derivate readily passes through the cell membrane of living cells where the AM groups are cut off by esterases resulting in a strong green fluorescence. Dead cells lack esterases therefore only living cells are marked. Scale bars in images A and B correspond to 150 microns.

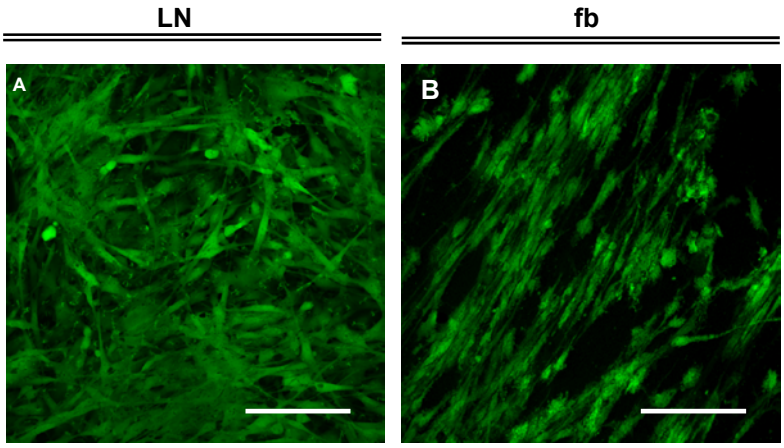

Figure 3.22. 8 days calcein stained U373 cells growing onto films of HA-DVS hydrogels LN (left column, A) or fb (right column, B) coated. Scale bars in images A and B correspond to 150 microns.

Inflammatory markers. E-selectin

Lipopolysaccharides (LPS) are large molecules consisting of a lipid covalently bonded to a polysaccharide. They are found in the outer membrane of Gram-negative bacteria and act as endotoxins. LPS elicit strong immune responses in many cell types. Endothelial cells transform into an activated state evoked by released cytokines and express the specific cell adhesion molecule E-selectin which is involved in inflammation.

To assess the compatibility of HA-based biomaterials and the normal phenotype of endothelial cells growing on them, the expression of E-selectin in absence and presence of LPS was evaluated.

Endothelial cells growing onto HA-DVS hydrogels pre-coated either with LN or fb before the cell seeding demonstrated no expression of the inflammatory marker E-selectin (absence of green fluorescence). Thus, it was demonstrated a good cell-biomaterial compatibility in terms of toxicity. Besides, ECs expressed the proinflammatory marker after LPS stimulation assuring their phenotypic characteristics growing on the hyaluronan biomaterials. Figure 3.23 shows the confocal micrographs for E-selectin immunostaining including detail of its expression in individual cells.

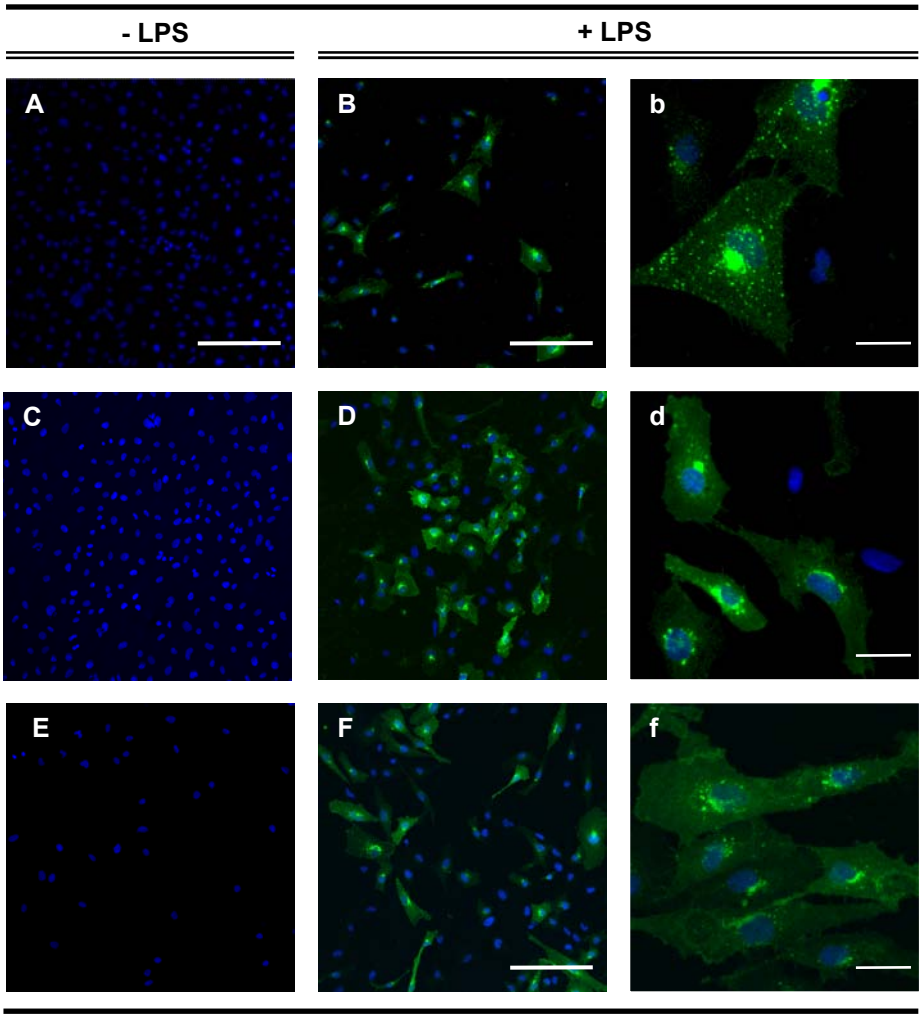

Figure 3.23. Expression of the endothelial specific cell adhesion molecule, E-selectin, by hCMEC/D3 growing on HA-DVS hydrogels without and upon activation by LPS as inflammatory response. LPS are endotoxins found in the outer membrane of Gram-negative bacteria. E-selectin expressed by EC was stained in green fluorescence. ECs were grown in LN or fb coated HA-DVS hydrogels during 48h in absence (left) or presence (right) of LPS stimulation. Cell nuclei were stained with DAPI. A) hCMEC/D3 cultured in cover slides as control; B) control of hCMEC/D3 LPS stimulated; C) hCMEC/D3 cultured on HA-based hydrogels LN coated; D) hCMEC/D3 cultured on HA-based hydrogels LN coated LPS stimulated; E) hCMEC/D3 cultured on HA-based hydrogels fb coated; F) hCMEC/D3 cultured on HA-based hydrogels fb coated LPS stimulated. Scale bar corresponds to 150 microns in images A to F. Scale bar in images b, d and f which show a detail of images B, D and F, corresponds to 25 microns.

Immunocytochemistry

To assess the phenotype of ECs growing onto HA-based biomaterials, two cell protein markers were employed. On the one hand, the platelet/endothelial cell adhesion molecule-1 (PECAM-1), which is expressed on the surface of ECs at cell-cell junctions and which is thought to play an important role in embryogenesis and development. On the other hand, von Willebrand factor (vWF), a large multimeric glycoprotein produced in the endothelium, concretely in the Weibel-Palade bodies, which becomes available when the endothelium is damaged (for example in inflammation).

CONTROL

The expression of specific proteins in cells growing on plastic cover slides was used as control. Cells demonstrated high expression of vWF in day 14 of *in vitro* culture. Green spots can be appreciated within the endothelium corresponding to the stained vWF aggregates. ECs spanned throughout the complete surface of the cover slides establishing contacts with one each other and reaching confluence. PECAM-1 expression was stained in ECs at day 21 of culture. ECs widely expressed this protein at cell-cell junctions, thus describing the cell cytoskeleton with a green fluorescence lining as can be appreciated in Figure 3.24b. Higher magnification shows a detail of the distribution of the specific markers within endothelial cells.

The astrocytic cell line, U373, was immunoassayed against GFAP expression in red fluorescence. Astrocytes highly expressed GFAP in day 14 of culture displaying bipolar morphologies and long processes. A parallel-like distribution of the intermediate filament was observed, indicating a kind of cytoskeleton orientation. Taking into account the planned co-cultures, astrocytes were grown in the same medium as ECs instead of using the specific for astrocytes; despite this, high rate of survival and lack of apoptotic cells were observed (Figure 3.25).

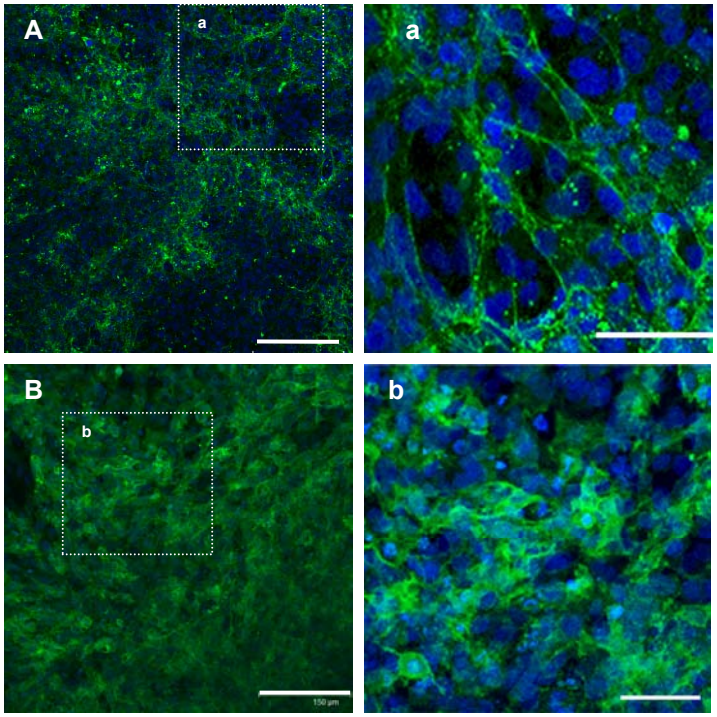

Figure 3.24. Endothelial cell specific markers expressed by hCMEC/D3 cultured in vitro in cover slides as control during 14 days (A) and 21 days (B). Protein expression was immunoassayed in green fluorescence. Cell nuclei were stained with DAPI. A) vWF expression; B) PECAM-1 expression; a and b show a detail of A and B respectively. Scale bar corresponds to 150 microns in images A and B and to 50 microns in images a and b.

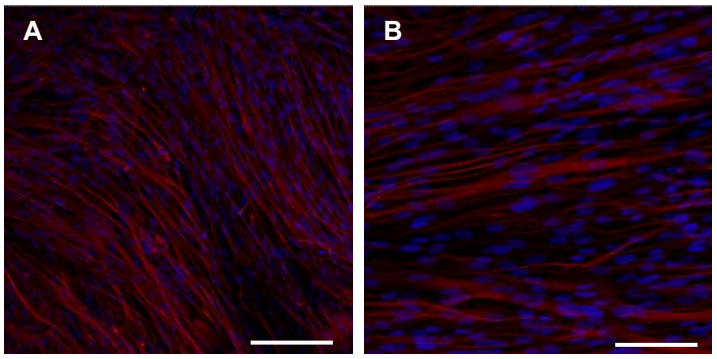

Figure 3.25. GFAP, an intermediate filament expressed by astrocytes thought to maintain astrocyte mechanical strength and shape in the CNS, was assayed in the U373 cell line. The protein was marked in red fluorescence. A: U373 growing onto cover slides as control during 14 days; B: detail of GFAP expression in controls. Scale bar corresponds to 150 microns in image A and to 75 microns in image B.

BIOMATERIALS

The phenotype of hCMEC/D3 growing onto hyaluronan based hydrogels was followed by PECAM-1 and vWF expression up to 21 days in culture. The response upon the two different protein employed to favour cell adhesion was evaluated.

vWF expression by hCMEC/D3 growing on HA-DVS hydrogels, either LN or fb pre-coated, was evaluated in two time points. Figure 3.26 and Figure 3.27 collect the confocal photographs results of the vWF and PECAM-1 staining. In day 14 of culture, ECs spanned throughout the surface of the hydrogel and displayed high expression of vWF both in LN and fb coated hydrogels. After 21 days of culture, high density of adherent cells were still found displaying less vWF expression as can be interpreted from a lower rate of green aggregates observed (Figure 3.26). Apparently, the distribution of the cell cytoskeleton was different showing a kind of orientation in fb coated hydrogels while in LN coated biomaterials cells spread randomly. The PECAM-1expression (Figure 3.27) showed the ECs forming cord-like organization with some differences apparently which may be effected by protein coating. In LN coated hydrogels there were observed wider spaces between ECs while in fb coated hydrogels the density of cells was noticeably lower and the contacts between cells were weaker in terms of PECAM-1 expression. In both cases cells displayed elongated morphologies which may be a consequence of migration to form those structures.

The phenotype of the astrocytic cell line, U373, was followed by GFAP expression. Hydrogels precoated with LN displayed a randomly distribution of astrocytes throughout surface and high rate of apoptotic cells in day 14 of culture while fibrin coated biomaterials showed elongated cytoplasm with long extensions of their processes and no appreciable apoptotic cells. In day 21 of culture LN coated hydrogels displayed higher organization of the filaments while cells on fb did the opposite showing less organization than the previous time point evaluated (Figure 3.28).

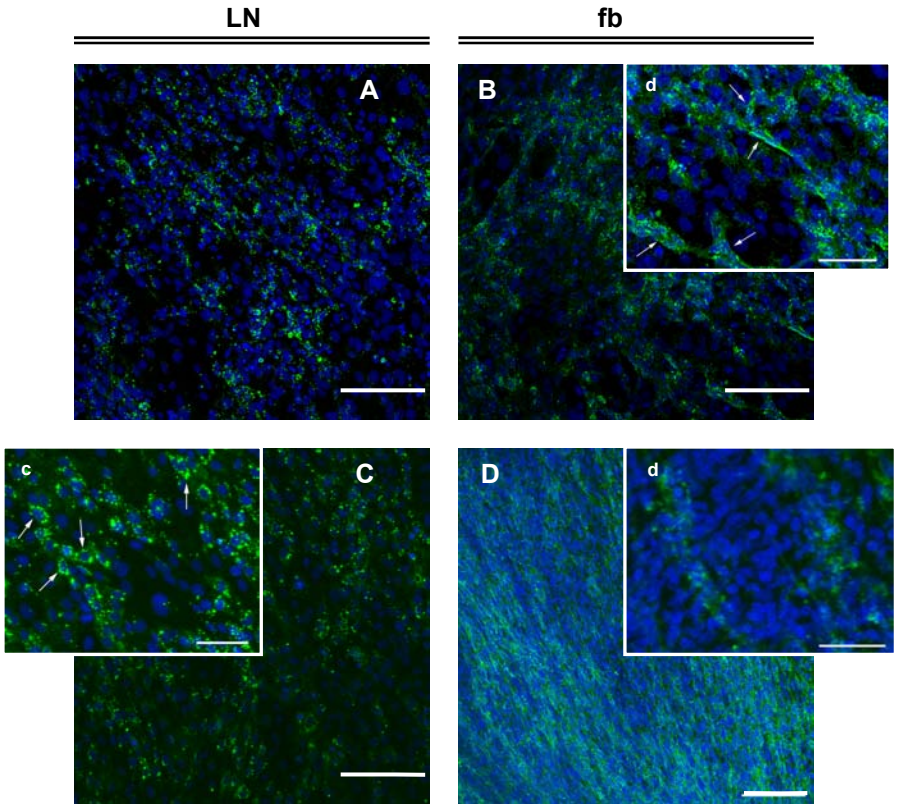

Figure 3.26. vWF expression (green fluorescence) by hCMEC/D3 cultured onto HA-DVS hydrogels coated either with LN (left) or fb (right). Images A and B correspond to 14 days of culture; images C and D to 21 days culture. Nuclei were stained with DAPI. Scale bar corresponds to 150 microns. White arrows in images b and c point at sites with vWF expression.

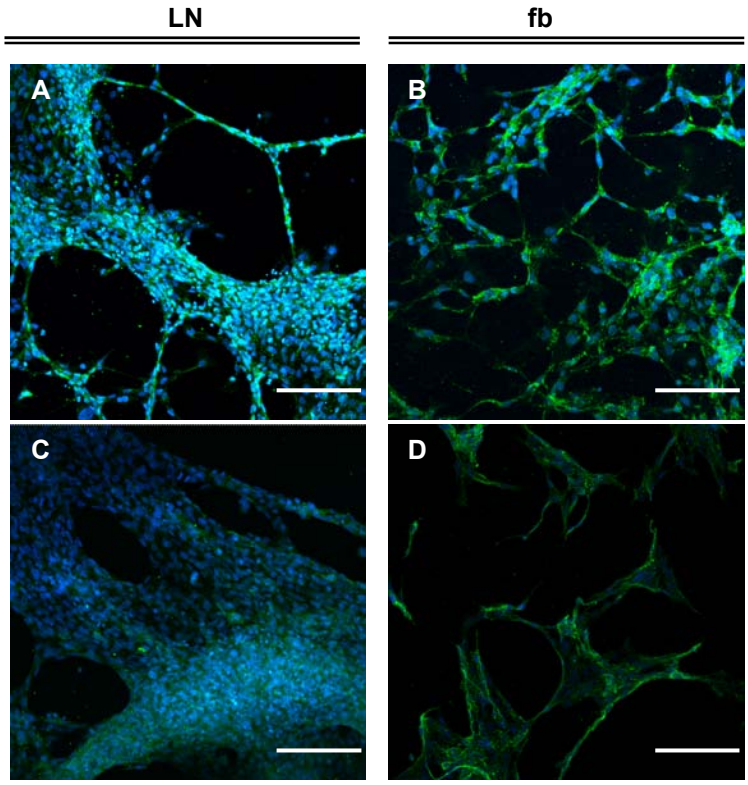

Figure 3.27. PECAM expression (green fluorescence) by hCMEC/D3 cultured onto HA-DVS hydrogels coated either with LN (left) or fb (right). Images A and B correspond to 14 days of culture; images C and D to 21 days culture. Nuclei were stained with DAPI. Scale bar corresponds to 150 microns.

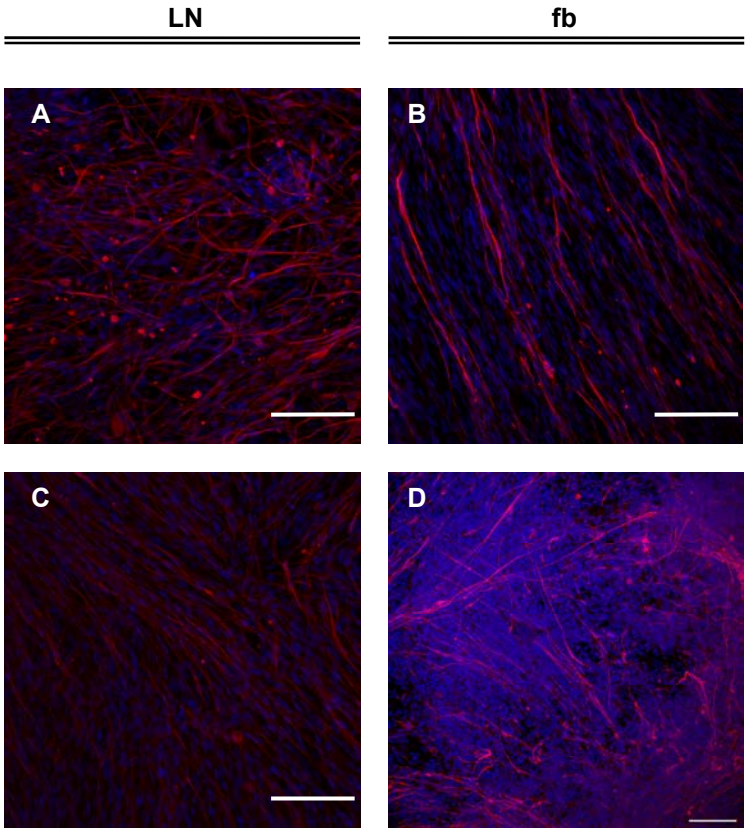

Figure 3.28. GFAP expression (red fluorescence) by U373 cultured onto HA-DVS hydrogels coated either with LN (left) or fb (right). Images A and B correspond to 14 days of culture; images C and D to 21 days culture. Nuclei were stained with DAPI. Scale bar corresponds to 150 microns.

Cytokine release

Growth factors (cytokines) are substances capable of stimulating cellular growth, proliferation and cellular differentiation. While growth factors imply a positive effect on cell division, cytokines may act by promoting or inhibiting it, therefore the measurement of some cytokines are used as “death” signals (apoptosis). Angiopoietins (Ang-1 and Ang-2) are cytokines involved in angiogenesis. They bind the same receptor (Tie-2) on ECs when they become activated by present angiogenic signals as the basic fibroblast growth factor (bFGF). The balance between both cytokines synergistically

with presence of vascular endothelial growth factor (VEGF) is thought to be a good way to evaluate whether ECs are able to reorganize and lead to the formation of new sprouts when cultured onto our HA based biomaterials.

Released cytokines either by hCMEC/D3 or U373 into the supernatants growing onto HA-based hydrogels were evaluated. The release by cells cultured in plastic cover slides were used as control.

The two coatings employed did not elicit differences in the concentration of Ang-1 released by ECs growing on biomaterials. Similar levels of cytokine were registered in controls in which the concentration increased with time in culture. The release of Ang-2 displayed clear differences between the controls and coated biomaterials supernatants. While the concentration of the cytokine started to increase from the beginning of the culture in controls, in the case of biomaterials it was delayed to day 14 of culture. Biomaterials were changed to new wells after 3 days of culture to assure only the cells attached to the scaffold are considered. Thus, it may be expected that lower concentration of cytokines in early times or a delay in reaching the same concentrations as controls due to the lower density of cells. LN or fb coated biomaterials displayed differences in the release of the cytokine, which was found in higher concentrations in the case of LN coated hydrogels. In both cases the release increased with time displaying a maximum in day 21. VEGF was almost undetectable during the period of culture evaluated for controls and the same behaviour was found in the supernatants of biomaterials.

The release of Ang-1 by U373 was similar for both coated biomaterials. The concentration was lower than controls in early times but it became similar in longer times even slightly higher in day 21 of culture.

No detection of Ang-2 was found in biomaterials while control did in low concentrations. VEGF was released in high concentrations in the supernatants of both control and biomaterials although the latter displayed a delay. The cytokine increased its concentration in day 14 in biomaterials while in controls did from day 8. Figure 3.29 summarizes the results for

growth factors (VEGF) and cytokines (Ang-1 and Ang-2) secreted by hCMEC/D3 or U373 in the supernatants of *in vitro* cultures (left and right column respectively).

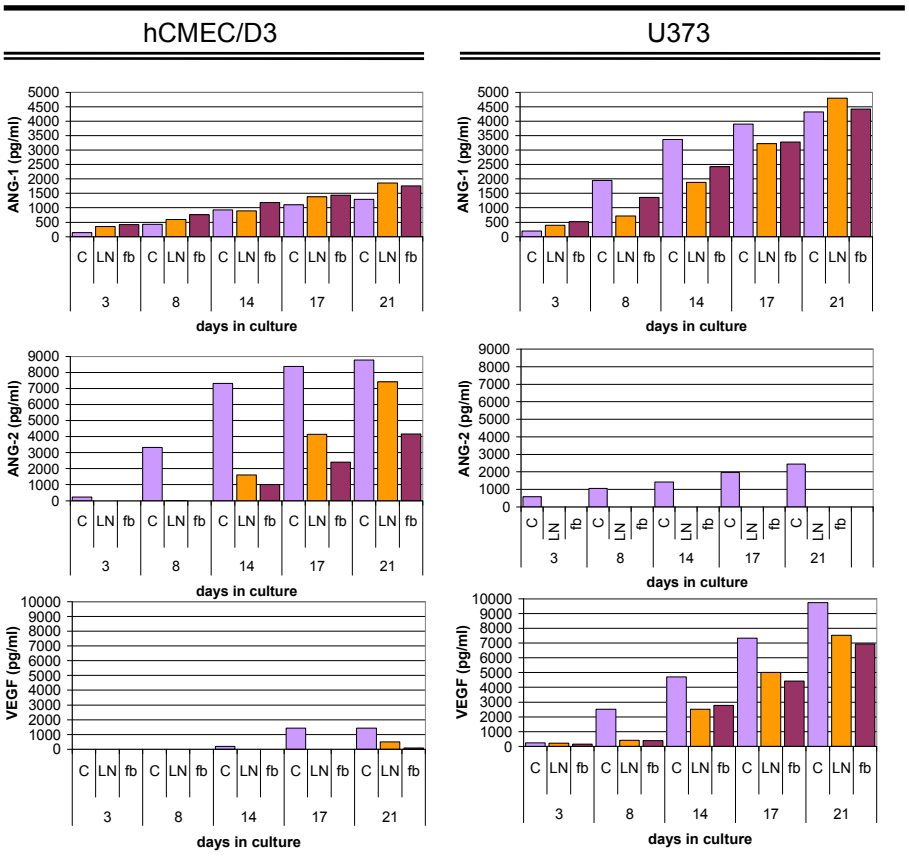

Figure 3.29. Vascular Endothelial Growth Factor (VEGF) and Angiopoietins (Ang-1 and Ang-2) released by hCMEC/D3 (left column) and U373 (right column) into the supernatants growing in monoculture onto 2D hyaluronan crosslinked hydrogels. The release was evaluated during 21 days of culture and detected by enzyme-linked inmunosorbent assay (ELISA). Control (■), LN coated hyaluronan scaffolds (■) and fb coated hyaluronan scaffolds (■).

3.4.1.2 HA-DVS spherical interconnected porous scaffolds. Assays in 3D structures.

Viability

The viability of endothelial and astrocytic cell lines was assessed in 3D hyaluronan scaffolds to evaluate whether the inner structure or the chemical processes employed may affect the survival of cells growing within them.

Viability assays performed on day 8 of culture showed viable cells in both cases, displaying higher cell density in fb coated biomaterials (Figure 3.30) ECs exhibited rounded-like shaped morphology in LN coated scaffolds while in fb coated hydrogels exhibited a more spread morphology. In both cases cells established contacts to each other and formed a 3D network. U373 spanned throughout the porous structure, showing high density of viable cells. In the LN coated biomaterials, astrocytes were found in longer fusiform disposition of their cytoskeleton, rather than the more rounded shapes found in HA hydrogels fb coated. The formation of bundles of astrocytes were apparent in LN coated biomaterials while in fb coated ones, astrocytes formed aggregates. Figure 3.30 and Figure 3.31 collects the confocal images for calcein stained endothelial and astrocytic cell lines respectively.

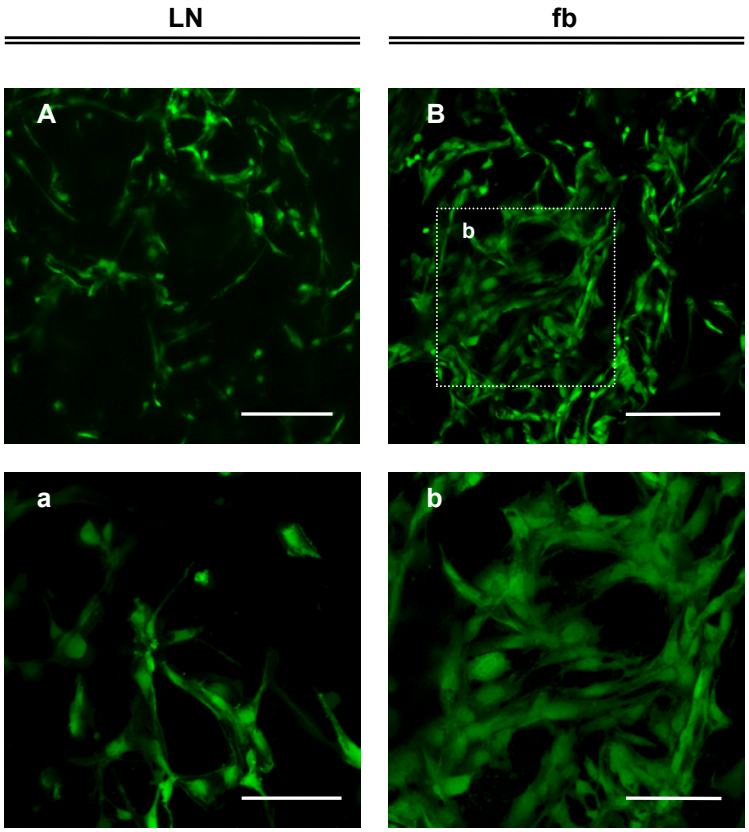

Figure 3.30. 8 days calcein stained hCMEC/D3 growing onto HA-DVS spherical interconnected porous scaffolds LN (left column) or fb (right column) coated. The acetomethoxy calcein derivate readily passes through the cell membrane of living cells where the AM groups are cut off by esterases resulting in a strong green fluorescence. Dead cells lack esterases therefore only living cells are marked. A) HA-DVS spherical interconnected porous scaffolds LN coated; B) HA-DVS spherical interconnected porous scaffolds fb coated. Images a and b show detail of A and B respectivelyl. Scale bar corresponds to 150 microns in images A and B and to 75 microns in images a and b.

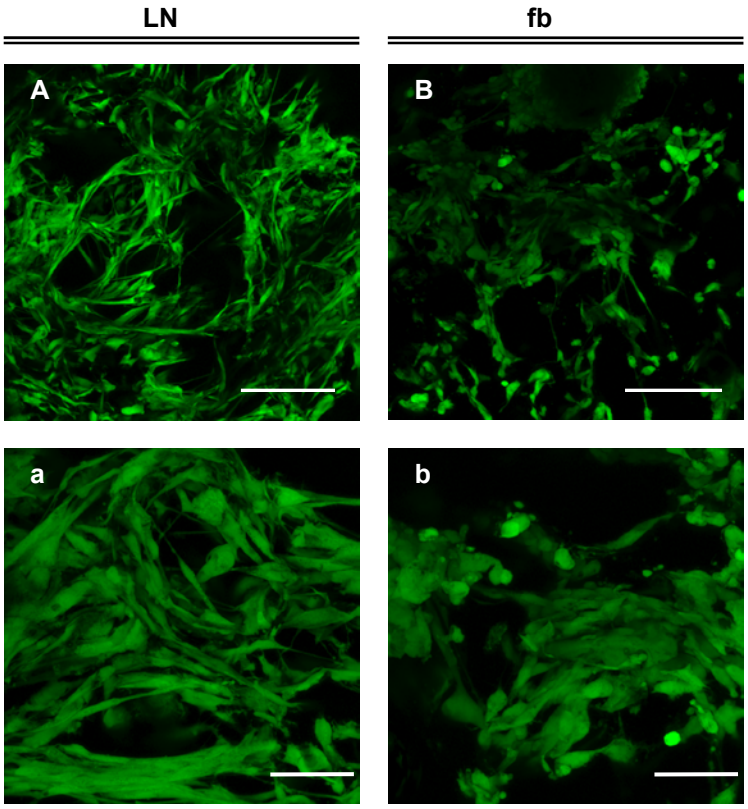

Figure 3.31. 8 days calcein stained U373 cells growing onto HA-DVS spherical interconnected porous scaffolds LN (left column) or fb (right column) coated. A) HA-DVS interconnected porous scaffolds LN coated; B) HA-DVS interconnected porous scaffolds fb coated. Images a and b show detail of A and B respectively. Scale bar in images A and B corresponds to 150 microns and in images a and b to 75 microns.

Immunocytochemistry

Specific endothelial and astrocytic markers were immunoassayed in cells growing onto HA-DVS scaffolds. To assess the phenotype of the endothelial cell line, the expression of vWF and PECAM-1 was examined. The endothelium-specific vWF protein was observed distributed on cells growing within the scaffold and displayed a high rate of expression both in early and longer times of culture (Figure 3.32). Higher magnification shows detail of the vWF expression where the autofluorescence of the hyaluronan scaffold is less evident seeing more clearly the green staining of the protein. PECAM-1 expression elicited some more information about the distribution of cells within the scaffold (Figure 3.33). Cells were observed to be reorganized following a different pattern to the one defined by the scaffold itself. Cells assembled to form what seem to be capillary-like distributions, although this can only be confirmed by further characterization (for example, with transmision electronic microscopy techniques). Figure 3.33 contains the transmitted photographs of the scaffold which has been merged with the confocal images of the nuclei (blue fluorescence) for better visualization. In both LN and fb precoated scaffolds cells assemble in cord-like shapes which did not correspond with the structure defined by the scaffold. These images demonstrate that ECs are not following any pattern dictated by the scaffold and reorganize themselves establishing contacts with each other, leaving spaces where other cells may accommodate. Results did not demonstrate clear differences between the two coatings used. Nonetheless, higher rate of cord-like assembling was found in the fibrin coated hyaluronan scaffolds.

The phenotype of astrocytes was assessed by their GFAP expression on HA-DVS protein coated scaffolds. Cells grew and spread in high densities throughout the inner structure in both LN and fb coated scaffolds. The expression of GFAP was lower in both cases for longer times of culture. Furthermore, while in short times the GFAP filaments were thick and randomly distributed in both cases, in longer times there were differences. LN coated biomaterials displayed a high rate of organization forming bundles

of thick filaments (see Figure 3.35c) while wider filaments with no bundles assembling was observed for fb coated hydrogels.

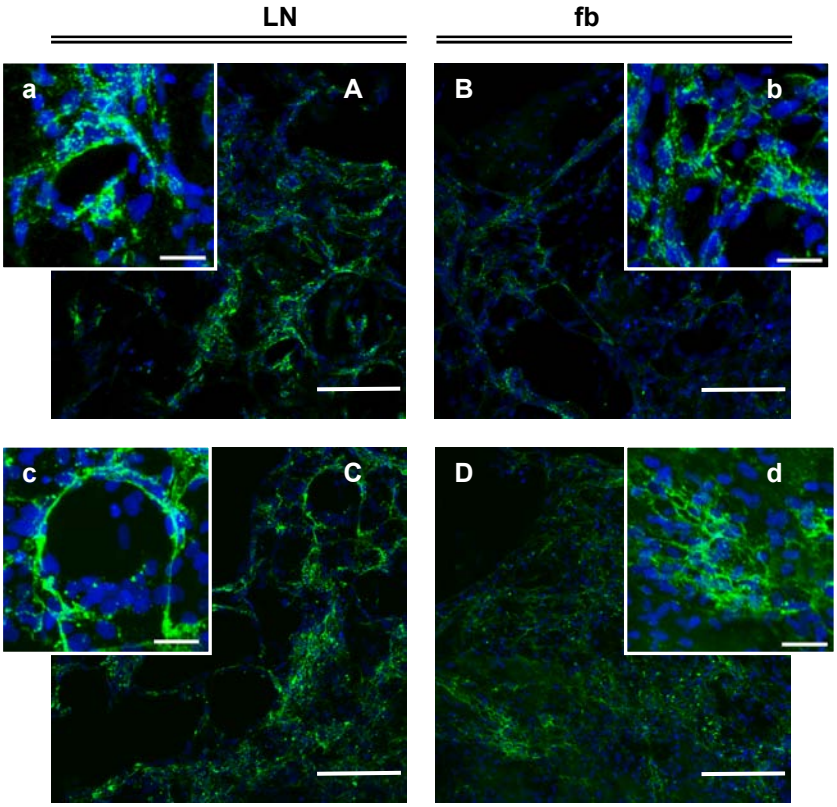

Figure 3.32. vWF expression (green fluorescence) by hCMEC/D3 cultured onto HA-DVS scaffolds coated either with LN (left) or fb (right). Images A and B correspond to 14 days of culture; images C and D to 21 days culture. a to d images correspond to detail of images A to D respectively. Nuclei were stained with DAPI (blue fluorescence). Images a, b c and d show detail of the corresponding capital letters. Scale bar corresponds to 150 microns in images A to D and to 75 microns in a to d.

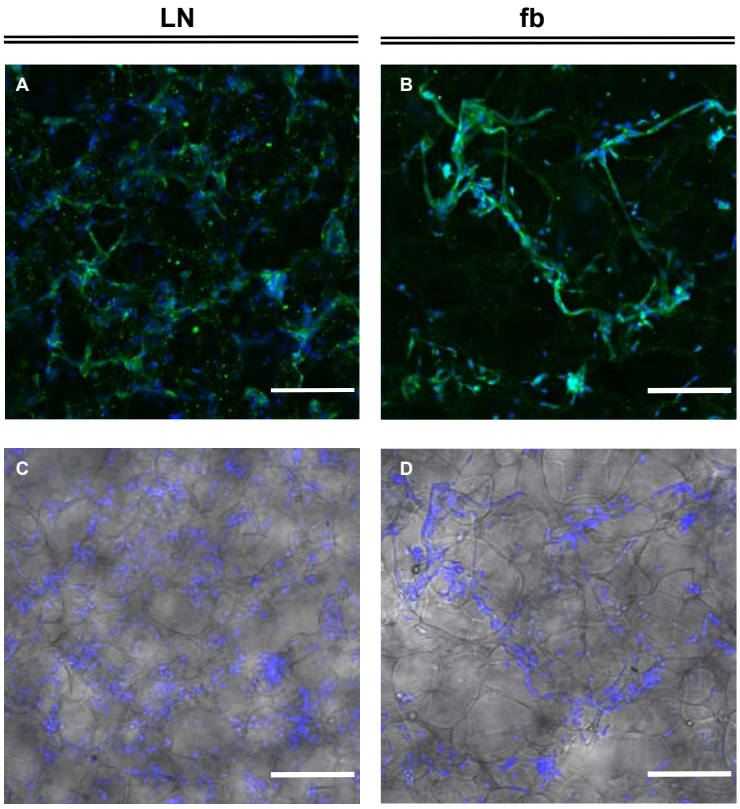

Figure 3.33. PECAM-1 expression (green fluorescence) by hCMEC/D3 cultured onto HA-DVS spherical interconnected scaffolds coated either with LN (left) or fb (right). Images A and B correspond to 14 days of culture; images C and D correspond to transmitted photographs of scaffolds with cells. Nuclei were stained with DAPI (blue fluorescence). Bar corresponds to 150 microns.

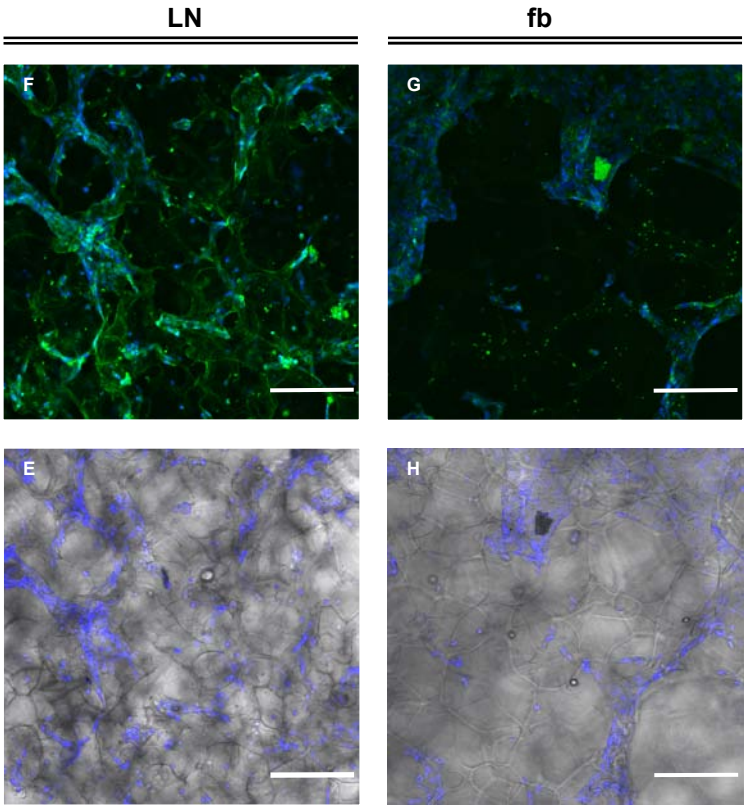

Figure 3.34. PECAM-1 expression (green fluorescence) by hCMEC/D3 cultured onto HA-DVS spherical interconnected scaffolds coated either with LN (left) or fb (right). Images A and B correspond to 21 days of culture; images C and D correspond to transmitted photographs of scaffolds with cells. Nuclei were stained with DAPI (blue fluorescence). Bar corresponds to 150 microns.

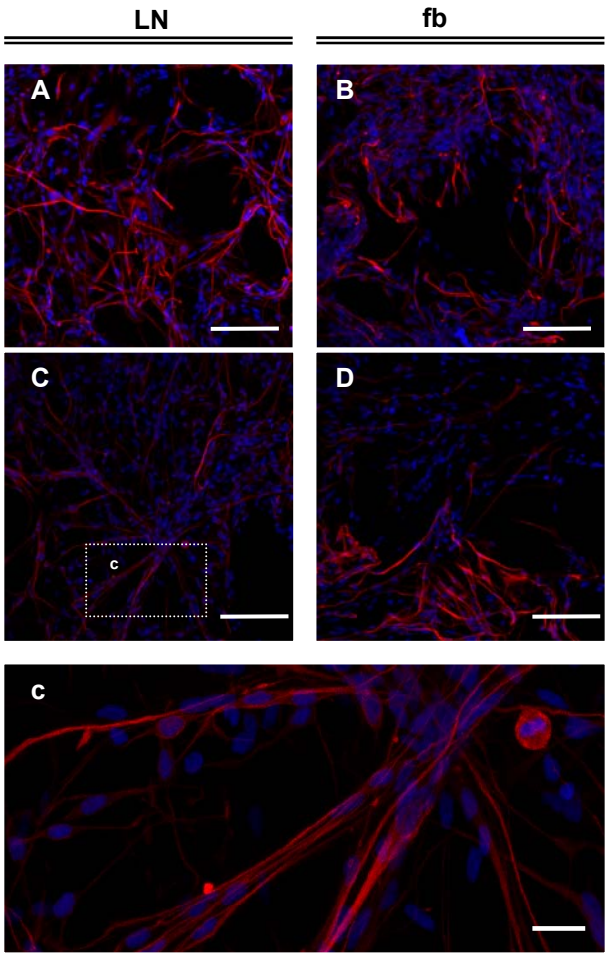

Figure 3.35. GFAP expression (red fluorescence) by U373 cultured onto hyaluronan DVS crosslinked hydrogels coated either with LN (left) or fb (right). Images A and B correspond to 14 days of culture; images C and D to 21 days culture. Image c show the formation of bundles of GFAP filaments in better detail. Nuclei were stained with DAPI (blue fluorescence). Scale bar corresponds to 150 microns in images A to D and 25 microns in image c.

Cytokine release

Angiopoietin-1 (Ang-1), angiopoietin-2 (Ang-2) and vascular endothelial growth factor (VEGF) released by Hcmec/D3 or U373 into the supernatants of HA-DVS scaffolds were examined up to 21 days in culture.

Ang-1 release by ECs was considerably higher in biomaterials compared with control release, both in LN and fb coated scaffolds. The concentration of cytokine released increased with days in culture displaying a maximum in day 21. No relevant differences were found for LN or fb coated biomaterials. The release of Ang-2 was low in almost every time evaluated compared with the release in control. LN and fb coated materials presented slight differences in their release presenting the latter the lower values. The concentration of VEGF was almost undetectable during the period evaluated although low rates were found in long times of culture.

In the case of astrocyte monoculture, the release of Ang-1 was slightly higher in fb than in LN coated biomaterials and in turn both presented higher release when compared with controls. Ang-2 concentration was quite similar in biomaterials and controls, and it was released in low concentrations taking into account the release of this cytokine by endothelial cells. VEGF was highly expressed during the period evaluated again in higher concentrations than controls did. Both coated biomaterials presented similar release.

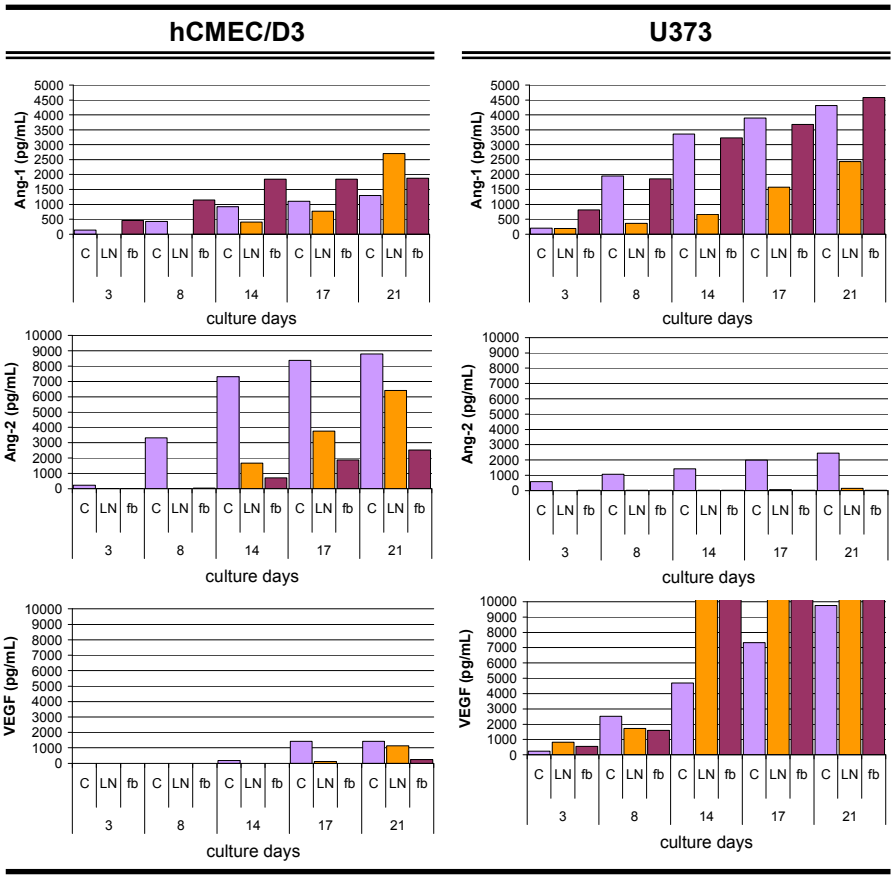

Figure 3.36. Angiogenic cytokines (Ang-1, Ang-2 and VEGF) released by hCMEC/D3 (left column) and U373 (right column) into the supernatants growing in monoculture onto 3D hyaluronan spherical interconnected porous scaffolds. The release was evaluated during 21 days of culture and detected by enzyme-linked inmunosorbent assay (ELISA). Control (■), LN coated hyaluronan scaffolds (■) and fb coated hyaluronan scaffolds (■).

3.4.2. Acrylic based biomaterials.

The influence of hyaluronan in the integration of cells in acrylic scaffolds was assessed with endothelial and astrocytic cells. (hCMEC/D3 and U373 respectively)

Viability

The viability of both the endothelial and the astrocytic cell lines was examined in acrylic cylindrical interconnected channelled scaffolds containing or lacking hyaluronan. ECs were viable in acrylic scaffolds both with and without hyaluronan in the time evaluated. Higher density of cells was found in hyaluronan coated biomaterials and cells showed higher affinity with the biomaterial displaying more expanded morphologies. However, U373 exhibited apparently similar viability at the same time point (8d) in both structures which were invaded by cells in a higher rate. In the next figures, (Figure 3.37 and Figure 3.38 for hCMEC/D3 and U373 respectively) there are photograps in which a detail of calcein staining may be observed.

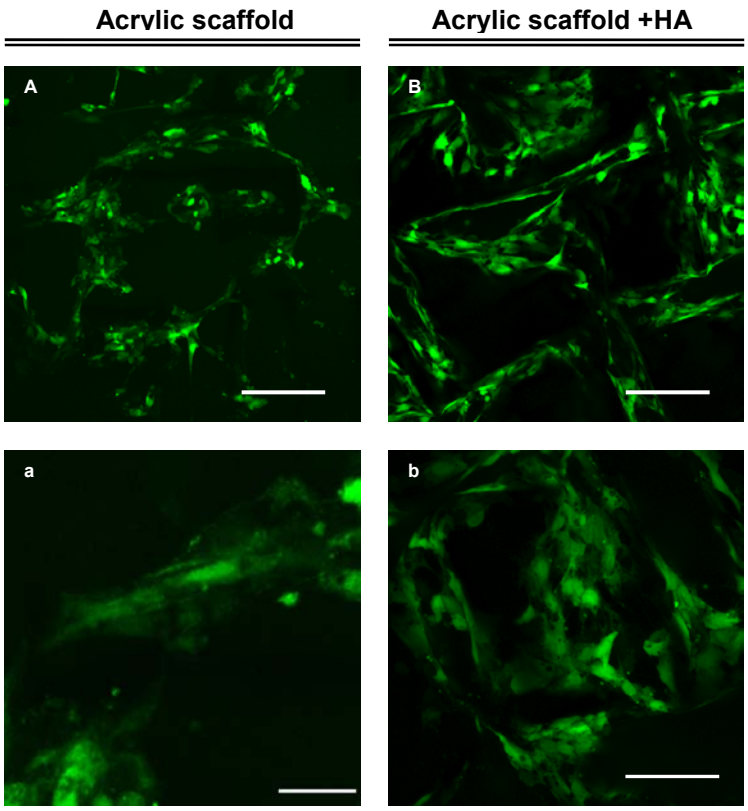

Figure 3.37. 8 days calcein stained hCMEC/D3 growing onto acrylic based biomaterials both without (left) and with (right) HA-DVS coating. The acetometoxy calcein derivate readily passes through the cell membrane of living cells where the AM groups are cut off by esterases resulting in a strong green fluorescence. Dead cells lack esterases therefore only living cells are marked. a and b correspond to detail of images A and B respectively. Scale bar corresponds to 150 microns in A and B, to 75 in b and to 30 in a.

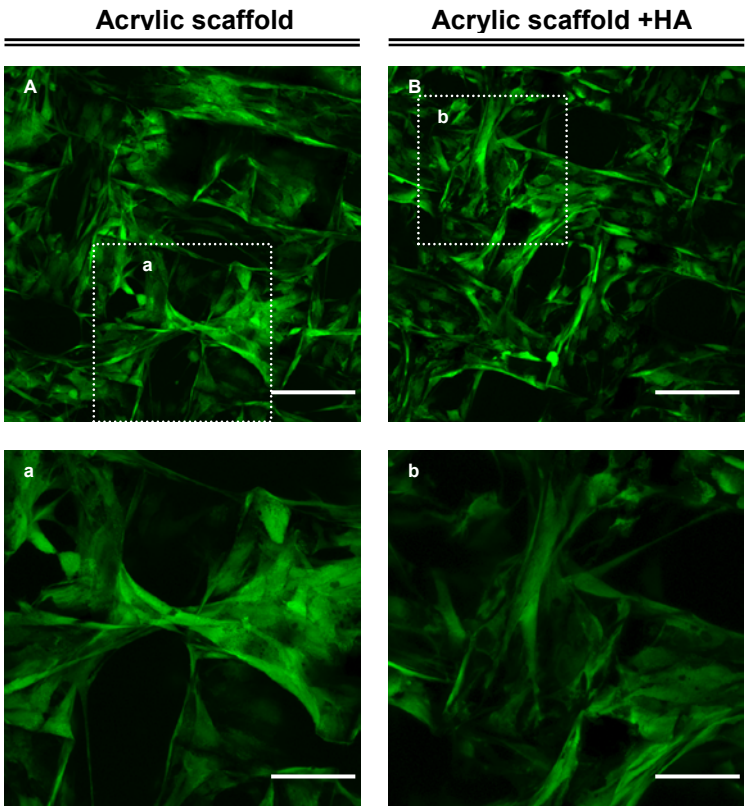

Figure 3.38. 8 days calcein stained U373 growing onto acrylic based biomaterials both without (left) and with HA-DVS (right) coating. The bar in images A and B corresponds to 150 microns; in a and b corresponds to 75 microns

Inflammatory effects

The E-selectin endothelial-specific expression by ECs was examined on acrylic scaffolds containing or lacking hyaluronan coating. ECs did not express their specific inflammation marker in culture with biomaterials while cells maintained their phenotypic characteristics growing on acrylic scaffolds either with or without hyaluronan coating expressing the protein upon LPS stimulation. The images corresponding to the inmunostaining of this protein are shown in Figure 3.39

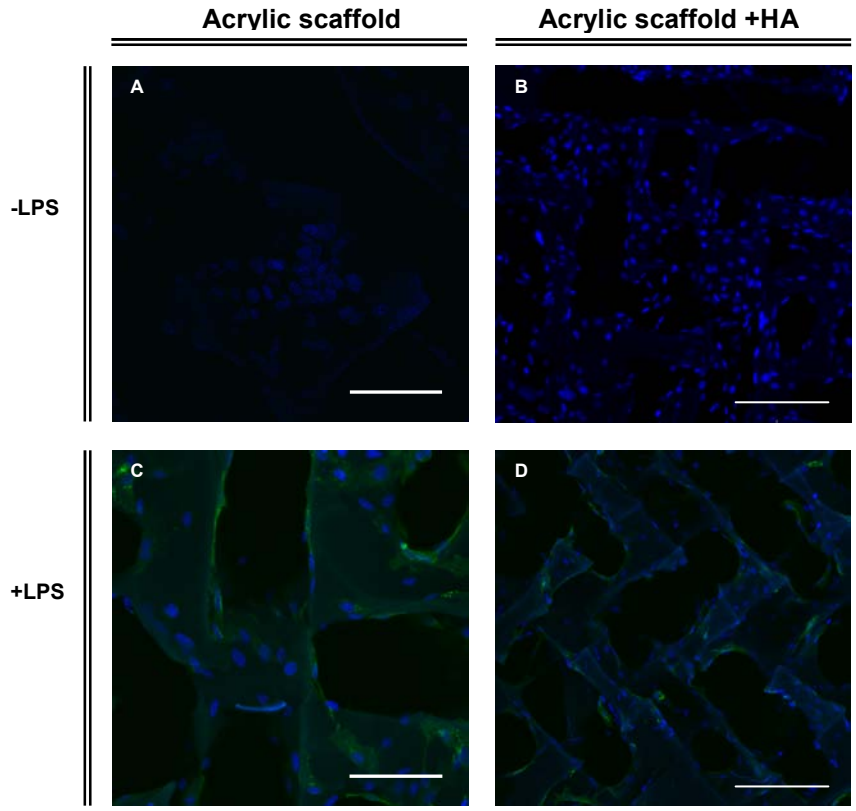

Figure 3.39. E-selectin was stained in green fluorescence in hCMEC growing on acrylic based scaffolds biomaterials without (left) or with (right) hyaluronan coating. Cells were cultured in presence (top) or absence (bottom) of LPS. Cell nuclei were stained with DAPI (blue fluorescence). Scale bar corresponds to 75 microns in A and C and to 150 microns in B and D.

Immunocytochemistry

The phenotype of hCMEC/D3 or U373 on acrylic scaffolds HA-DVS coated was observed by immunochemistry. PECAM-1 and vWF expression were assessed up to 21 days in culture. Cells were found in high densities both in non-coated and in hyaluronan coated biomaterials. Cells attached to the walls of the scaffold filling also the channels as can be appreciated with the transmitted photographs which have been merged with nuclei staining in Figure 3.40. In images A and B the background of the scaffold was highlighted to distinguish better the structure defined by the scaffold and the paths were cells spanned.

U373 were found in high density throughout the scaffolds displaying GFAP positive expression. In short times of culture (14 days) acrylic scaffolds lacking hyaluronan demonstrated higher expression of GFAP while those containing hyaluronan coating displayed a moderate expression. At longer times (21 days), considerably higher rate of reactive astrocytes (high expression of GFAP) were found in the case of acrylic scaffold which did not contain hyaluronan while the ones who contained HA displayed moderate expression. Figure 3.42 contains the confocal photographs obtained from the GFAP immunostaining on acrylic biomaterials.

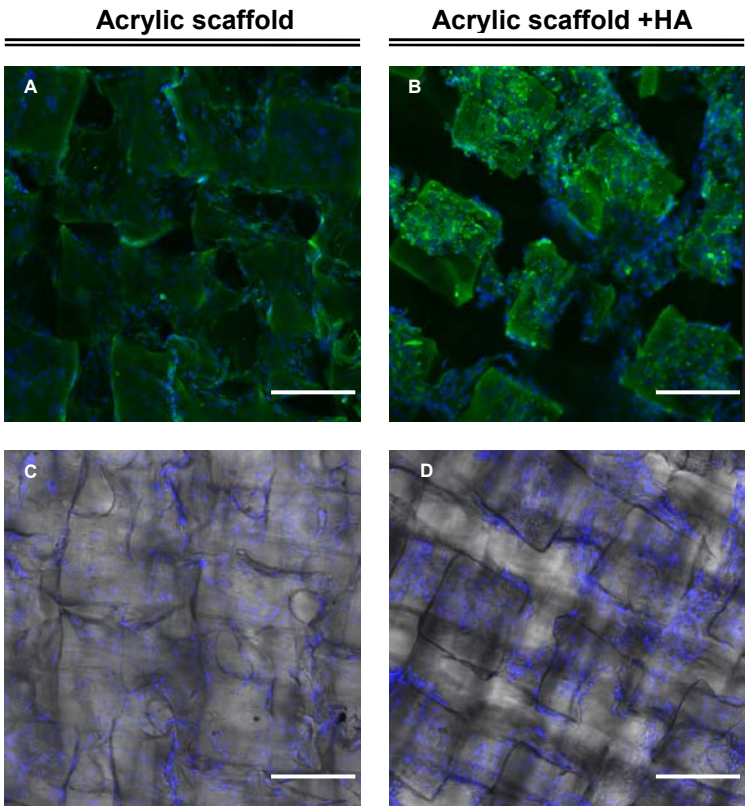

Figure 3.40. Immunofluorescent images of PECAM-1 expression (green fluorescence) by hCMEC/D3 growing during 21 days onto acrylic based scaffolds with cylindrical interconnected inner structure both without (left) and with HA-DVS (right) coating. Scaffolds were LN coated prior to cell seeding. Cell nuclei were stained with DAPI (blue fluorescence). The bar corresponds to 150 microns.

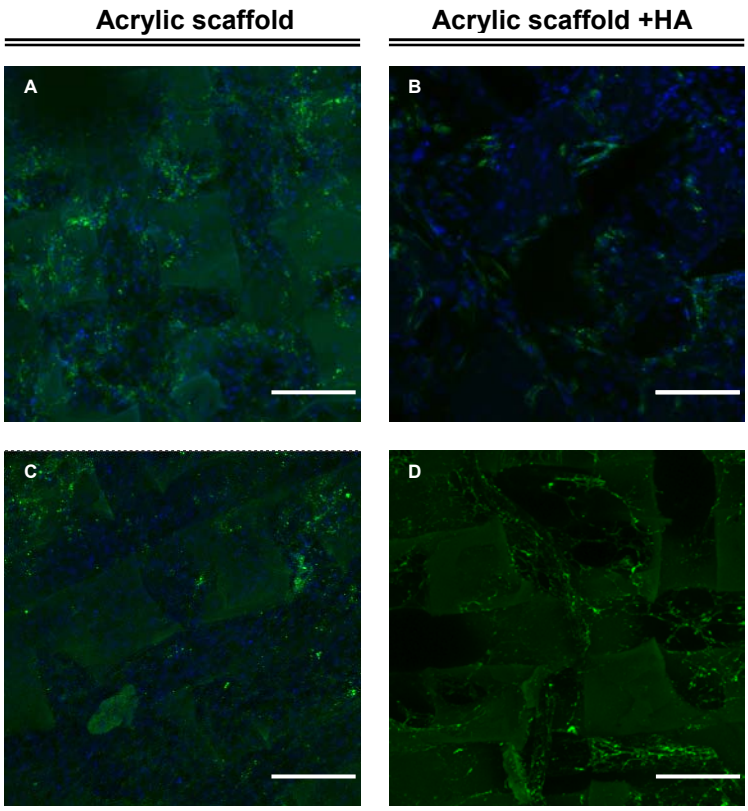

Figure 3.41. Immunofluorescent images of vWF expression (green fluorescence) by hCMEC/D3 growing on acrylic based scaffolds with cylindrical interconnected inner structure both without (left) and with (right) HA-DVS coating. Scaffolds were LN coated prior to cell seeding. Cell nuclei were stained with DAPI (blue fluorescence). Bar corresponds to 150 microns

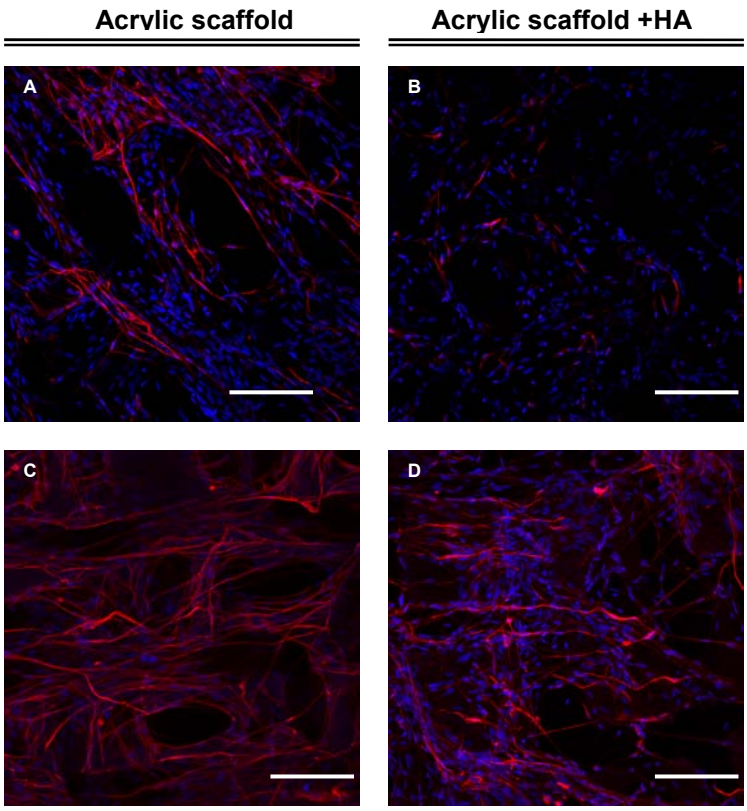

Figure 3.42. Immunofluorescent images of GFAP expression (red fluorescence) by U373 growing on acrylic based scaffolds with cylindrical interconnected inner structure both without (left) and with (right) HA-DVS coating. Scaffolds were LN coated prior to cell seeding. Cell nuclei were stained with DAPI (blue fluorescence). A and B correspond to 14 days of culture; C and D correspond to 21 days of culture.

Cytokine release

Angiopoietin-1 (Ang-1), Angiopoietin-2 (Ang-2) and vascular endothelial growth factor (VEGF) released by hCMEC/D3 or U373 into the supernatants of acrylic scaffolds were examined up to 21 days in culture.

The concentration of Ang-1 found into the supenatants was low in every case of controls while higher concentration was registered in the biomaterials supernatants. Slightly higher concentration of Ang-1 was found in the supernatants of biomaterials which contained hyaluronan. The concentration increased with time in culture.

The values resgistered for Ang-2 were lower in biomaterials compared with controls, which had high concentrations of the cytokine during the period evaluated. Biomaterials which did not contain hyaluronan displayed higher concentration of the cytokine compared with the ones with an HA coating. The release of VEGF by ECs was nil or very low in day 17 and 21 and both biomaterials nd controls displayed the same pattern.

In the case of the cytokines released by astrocytes, Ang-1 was secreted in higher concentrations compared with controls and HA-coated acrylates displayed higher concentrations compared with the ones lacking HA. Ang-2 was found in low concentrations in general and similar values were recorded in both biomaterials and controls. VEGF expression was high during the period of culture increasing the concentration with time. The concentrations of cytokines measured are graphed in Figure 3.43.

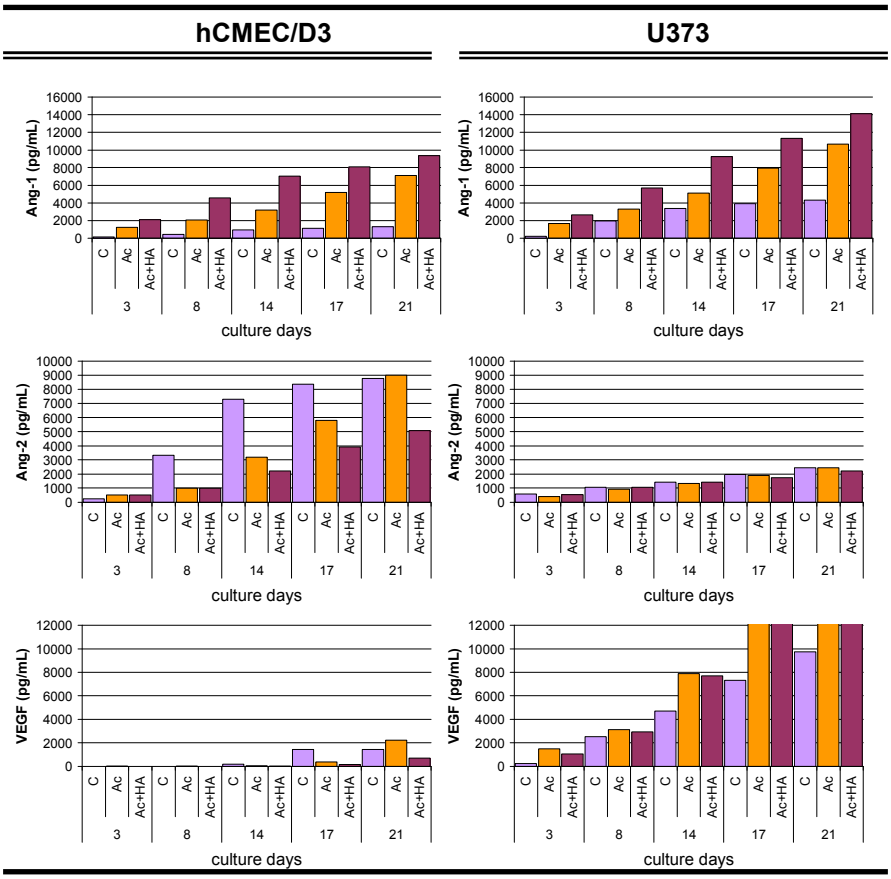

Figure 3.43. Angiogenic growth factors (Ang-1, Ang-2 and VEGF) released by hCMEC/D3 (left column) and U373 (right column) into the supernatants growing in monoculture onto acrylic based scaffolds . The release was evaluated during 21 days of culture and detected by enzyme-linked inmunosorbent assay (ELISA). Control (■), LN coated hyaluronan scaffolds (■) and fb coated hyaluronan scaffolds (■).

3.5. hCMEC/D3 and U373 co-cultures on biomaterials

Microvascular endothelial cells have been described to reorganize themselves into microcapillary-like structures when cultured in angiogenic-stimulating conditions *in vitro* (Montesano et al., 1983). In a propitious environment, as response to ECs activation by cytokines or growth factors secreted in the medium, the formation of those structures have been reported as a sign of their angiogenic potential.

The co-culture of hCMEC/D3 and U373 is thought to be a good model to mimic de BBB *in vitro* and this system together with biomaterials may provide a viable and permissive environment to recapitulate some aspects of the physiological conditions. The study of the co-culture of both cell lines in our biomaterials will provide us with more information about the interaction between those cells with the substrate when growing together. The medium of culture was provided with a promoter of angiogenesis, the basic fibroblast growth factor (bFGF) which activates the angiogenic cascade. The immunocytochemistry of specific proteins of the selected cell lines as well as released cytokines and growth factors by cells were evaluated and compared with the results obtained in controls.

The cell seeding was performed by two different mechanisms. On one hand, to favour adhesion of the the endothelial cell line both cell lines were seeded in different time points, first the hCMEC/D3 followed by the U373 after 24h of culture (successive seeding). Considering their different division rate ECs were seeded in a ten fold ratio respecting the astrocytic cell line. On the other hand, both cell lines were seeded together and in same ratio (simultaneous seeding). The successive cell seeding was studied following PECAM-1 expression by ECs and the simultaneous cell seeding both by vWF and GFAP expression by ECs and astrocytes respectively.

Control

To establish the interaction of both cell lines and the organization of ECs in culture, controls were performed in cover slides following the same conditions as performed with biomaterials.

The immunostaining results showed the distribution of both cell lines throughout the surface with periferic distribution of ECs with respect the astrocytes populations. Cells were viable and the conditions of co-culture were permissive for both cell lines.

Astrocytes were stained against GFAP expression in red fluorescence and endothelial cells were stained against PECAM-1 expression in green fluorescence or vWF expression for the successive or simultaneous seeding respectively.

Both protocols displayed random distribution of circular shaped structures delimited by ECs. As result of the successive cell seeding protocol, the size of the microcapillary-like structures formed by the ECs were smaller than in the case of simultaneous seeding displaying the latter a wide range of sizes from around 150 microns the smaller one. In the case of successive seeding those structures displayed sizes around 75 microns. In both cases astrocytes filled the areas delimited by the ECs thus demonstrating a propitious environment for cells to grow.

The expression of vWF was randomly distributed within ECs (Figure 3.45) and they were surrounded by astrocytes, stained in red fluorescence by their GFAP expression.

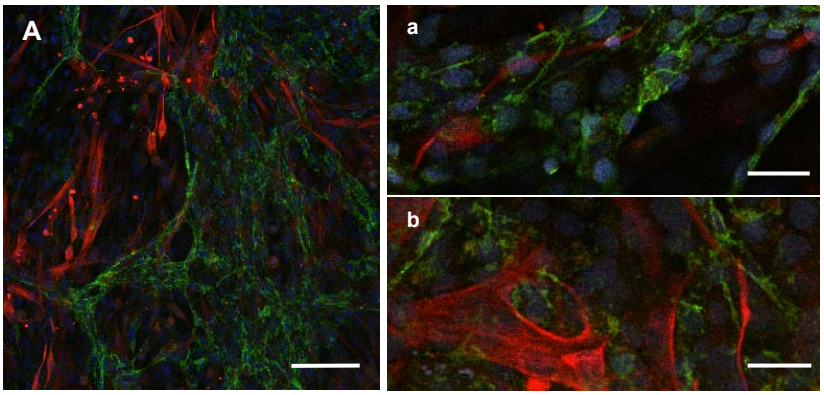

Figure 3.44. Immunofluorescent analysis of co-culture control of hCMEC/D3 and U373 by successive cell seeding. Samples were fixed after 14 days of co-culture. Green fluorescence corresponded to PECAM-1 expression by ECs. Red fluorescence corresponds to GFAP expression by astrocytes. Nuclei were stained in blue fluorescence with DAPI. A: scale bar corresponds to 150 microns; a and b: scale bar corresponds to 25 microns.

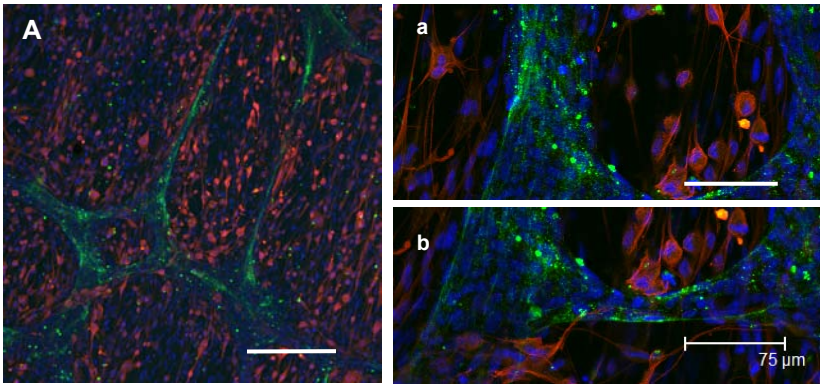

Figure 3.45. Expression of vWF and GFAP in co-cultured hCMEC/D3 by simultaneous cell seeding. Samples were fixed after 14 days of co-culture. Green fluorescence corresponds to vWF expression by ECs. Red fluorescence corresponded to GFAP expression by astrocytes. Nuclei were stained in blue with DAPI. Scale bar corresponds to 300 microns in A and to 75 microns in a and b.

3.5.1. HA based biomaterials

Endothelial and astrocytic cell lines were co-cultured onto either LN or fb coated hyaluronan based scaffolds. Because of the apical view of cells grown into biomaterials in which confocal micrographs were taken, and the spatial distribution of cells within the scaffold, it was not expected to find on the latter the same clear circular shapes that those found in 2D controls.

On the one hand, the results from the sucessive cell seeding demonstrated that ECs reorganized into cord-like structures and stablized contacts with each other. In day 14 of co-culture, the distribution of cells within the scaffold and the PECAM-1 expression by ECs made their junctions noticeable as well as their different reorganization in the 3D structure. The irregular pattern of the porous structure makes it difficult to determine whether the cells are following the scaffold pattern or if they reassemble into different shapes. Higher magnification gives a bit more information about the ECs distribution showing what seemed microcapillary-like structures both in LN or fb coated scaffolds (see details a and b in Figure 3.46). In this case, fibrin coated displayed similar shapes to the ones found in controls. In day 21 of culture, scaffolds precoated with fb showed higher organization of ECs into microcapillary-like structures followed by their PECAM-1 expression. Besides, LN coated biomaterials presented similar results to the ones found in 14 days. Confocal photographs collected for hyaluronan biomaterials are showed in Figure 3.46 in which detail of different areas are included.

On the other hand, the simultaneous cell seeding protocol was followed by vWF and GFAP expression by endothelial cells and astrocytes respectively. Both endothelial and astrocytes survived in co-culture during the period evaluated and expressed specific phenotypic proteins at the times evaluated. In day 14, those scaffolds pre-coated with fibrin showed higher rate of vWF positive cells compared with LN coated ones. In both cases astrocytes were found all around the structure (recognized by their GFAP expression) while the endothelial cells showed random aggregations as was

followed by their expression of vWF. In 21 days of culture the density of cells within the scaffolds was high in both cases. The distribution of cells were different and while rounded shaped endothelial cells were described in LN coated scaffolds, in fb coated ones there were clear and wider aggregations of cells describing shapes different to the pattern of the scaffold. In the latter, higher rate of apoptotic astrocytes (as suggest the rounded red shapes of several cells in image D in Figure 3.48) were found in contrast with none or very low rates in LN coated ones.

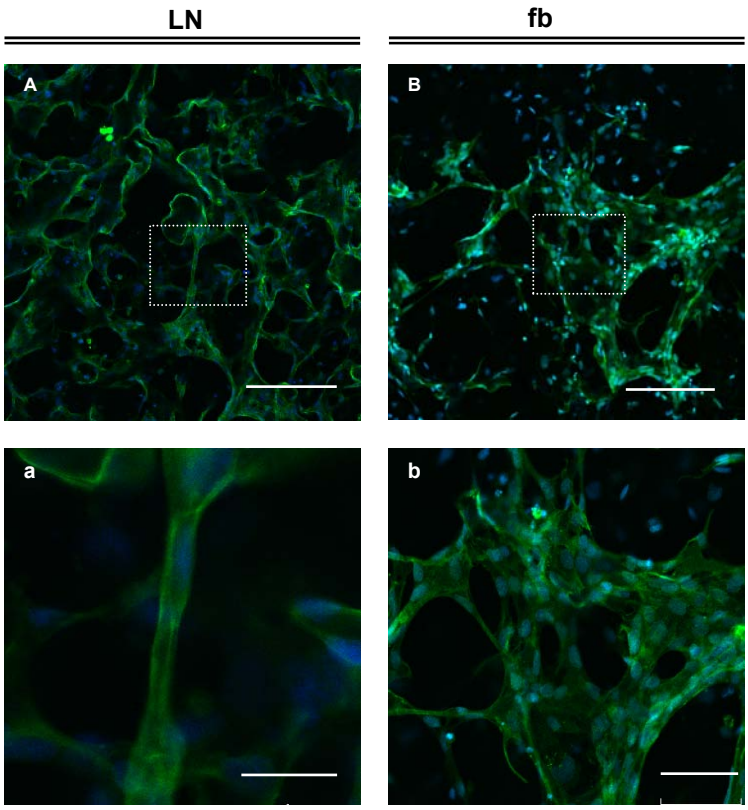

Figure 3.46. Immunofluorescent analysis of co-culture of hCMEC/D3 and U373 by successive cell seeding. A: HA-DVS scaffolds LN coated; B: HA-DVS scaffolds fb coated. Cells were fixed after 14 days of co-culture. Endothelial cells were stained against PECAM-1 expression in green fluorescence. Cell nuclei were stained with DAPI (blue). Scale bar corresponds to 150 microns in A and B, to 25 microns in a and to 75 microns in b.

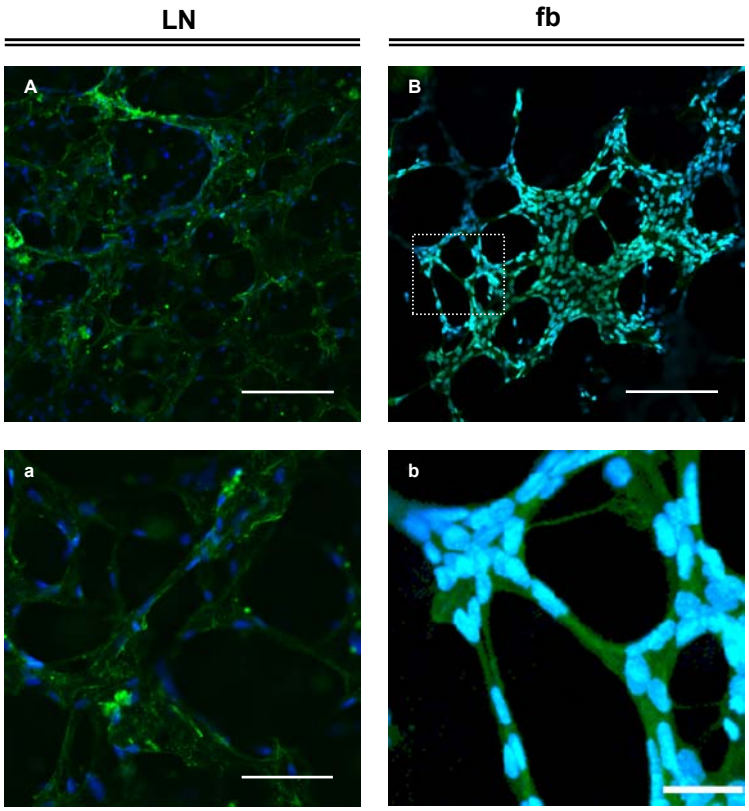

Figure 3.47. Immunofluorescent analysis of co-culture of hCMEC/D3 and U373 by successive cell seeding. A: HA-DVS scaffolds LN coated; B: HA-DVS scaffolds fb coated. Cells were fixed after 21 days of co-culture. Endothelial cells were stained against PECAM-1 expression in green fluorescence. Cell nuclei were stained with DAPI (blue). Scale bar corresponds to 150 microns in A and B, to 75 microns in a and to 30 microns in b.

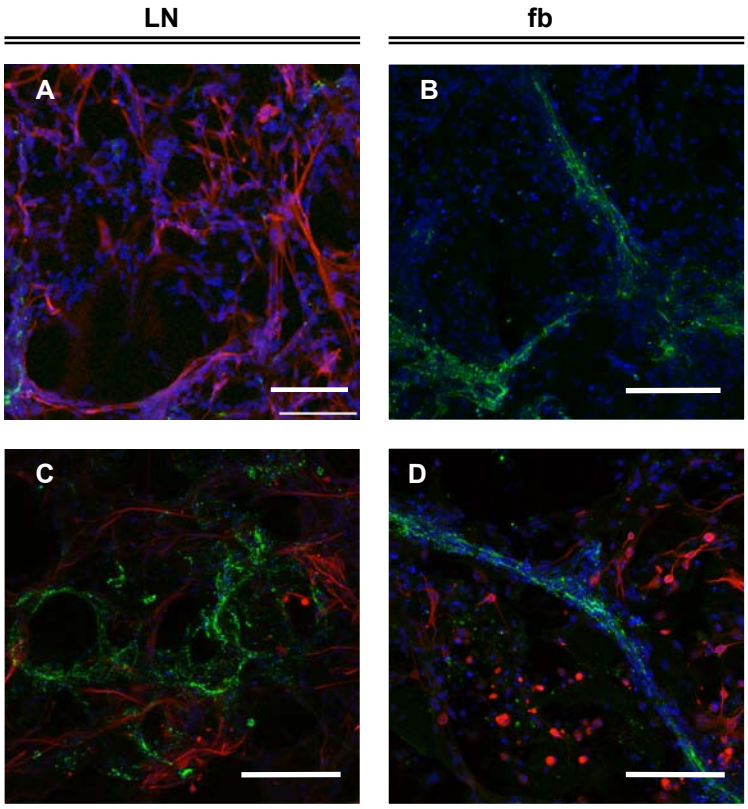

Figure 3.48. Immunofluorescent analysis of co-culture of hCMEC/D3 and U373 by simultaneous cell seeding. A: HA-DVS scaffolds LN coated; B: HA-DVS scaffolds fb coated. Cells were fixed after 14 days (top) and 21 days (bottom) of co-culture. Endothelial cells were stained against vWF expression in green fluorescence. Astrocytes were stained in red fluoresce against GFAP expression. Cell nuclei were stained with DAPI (blue). Scale bar corresponds to 150 microns.

In order to evaluate the structure of the scaffold after the culture periods and to have a little description of the morphology of cells adhered to the scaffold, scanning electron microscopy was performed in fibrin coated biomaterials. The structure of the scaffold was well defined after 21 days of culture showing the pores and their interconnections clearly defined. The porous structure maintained its integrity in the period evaluated displaying the pores similar diameter after the cell culture. Furthermore, it was possible to appreciate the invasion of cells within the pores and cells irregularly distributed filling the pores in a non aggregated disposition and establishing

contacts cell-biomaterial through cell filopodia. In samples fixed at day 14, layers of endothelial cells were found in the outer surface of the scaffold and high density of cells sourronding them. There were found throughout the porous structure areas filled with matrices which are similar to those observed for fibrin matrix, both in 14 and 21 days of culture. The formation of new extracellular matrix was appreciated. Figure 3.49 shows the SEM photographs of those biomaterials.

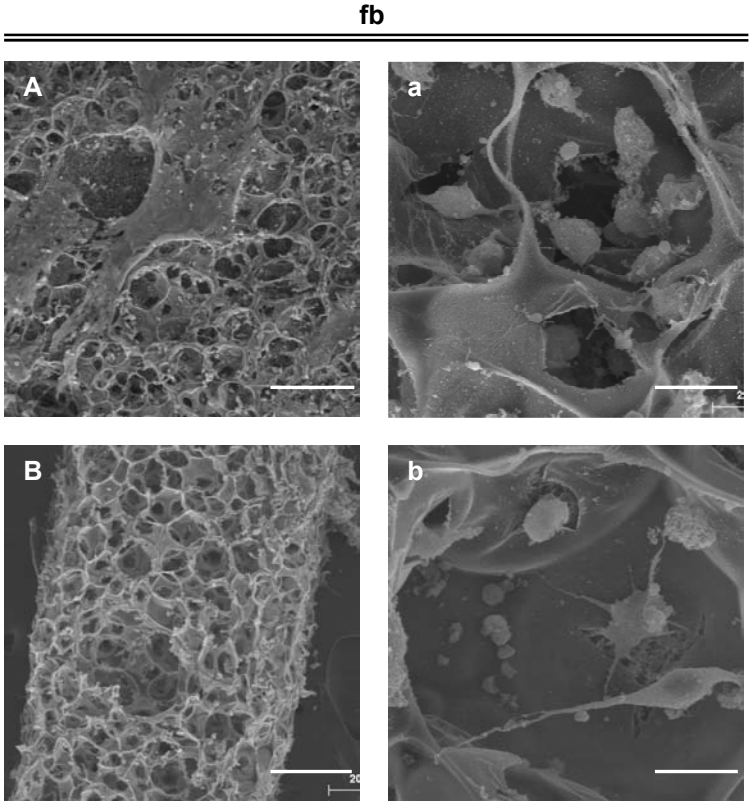

Figure 3.49. SEM images of co-culture of hCMEC/D3 and U373 growing on hyaluronan based scaffolds. Cell seeding was performed successively. Images correspond to interconnected spherical porous HA-DVS scaffolds coated with fibrin prior to cell co-culture and fixed at day 14 (A) and 21 (B) of culture. Scale bar corresponds to 200 microns in A and B and to 20 microns in a and b.

Cytokine release

Cytokines and growth factors released by cells in co-culture were analized by enzyme-linked inmunosorbent assay (ELISA). Supernatants of biomaterials co-cultured with ECs and astrocytes presented different releases depending on the coating employed. LN coated biomaterials had lower concentrations of Ang-1 compared with fibrin coated biomaterials which displayed similar or even higher concentrations than controls did. The release increased in time with culture.

Ang-2 was found in very low concentrations in both LN and fb coated biomaterials while high concentrations were observed in control release. The release of VEGF was high in every case and it increased in time with culture. LN coated biomaterials displayed concentrations similar to those recorded in controls while in fb coated ones the concentration was still higher.

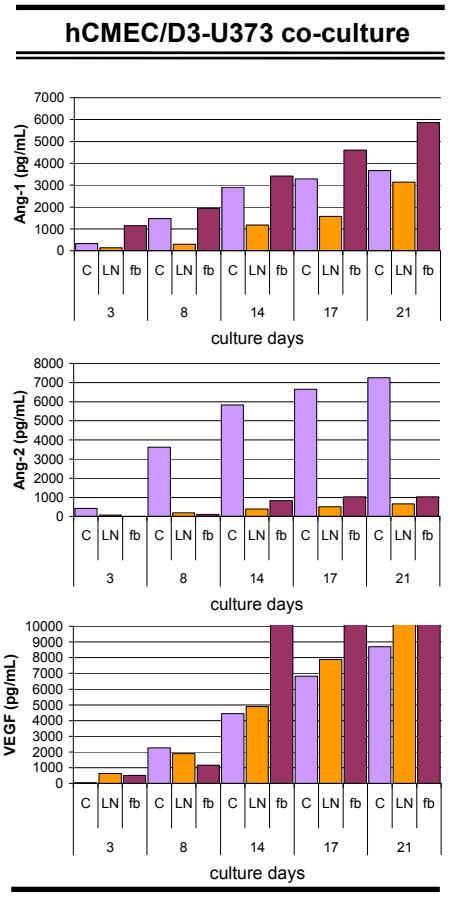

Figure 3.50. Angiogenic growth factors (Ang-1, Ang-2 and VEGF) released into the supernatants of co-cultured hCMEC/D3 and U373 growing in hyaluronan based scaffolds. The release was evaluated during 21 days of culture and detected by enzyme-linked inmunosorbent assay (ELISA). Control (■), LN coated hyaluronan scaffolds (■) and fb coated hyaluronan scaffolds (■).

3.5.2. Acrylic based biomaterials.

Immunocytochemistry

Co-culture of endothelial cells and astrocytes was performed in acrylic based scaffolds as well. Different results were obtained by the successive and the simultaneous cell seeding. Acrylate based scaffolds which were seeded by the successive cell seeding demonstrated a high density of cells attached to the scaffold. Hyaluronan coated acrylic scaffolds showed noticeable differences in the distribution of the endothelial cells with respect to the non-coated ones. Non-coated scaffolds displayed very low expression of PECAM-1 by ECs while the coated ones showed not only higher expression but different organization of the cells. In this case, cells were organized into cord-like structures following different paths to the one dictated by the scaffold architecture. This can be better appreciated by photos in Figure 3.51 where the nuclei have been merged with the transmitted photographs of the scaffold. In the case of hyaluronan coated acrylic scaffolds there was an aligned disposition of endothelial cells out of the walls of the channels while in non-coated ones, cells were clearly attached to the walls. Detail of the organization of ECs with higher magnification can be seen by images in Figure 3.52. Although it was not possible to perform a double immunostaining to differentiate both cell lines due to biomaterial-antibody crossreactions, it can be appreciated that different areas whith high PECAM-1 expression drawing different shapes and areas with no expression of the protein which can be interpreted as the presence of astrocytes in the surroundings. The PECAM-1 expression of the cell to cell junctions and the organization of the ECs can be appreciated in detail in Figure 3.52-a.1 (white arrows).

Simultaneous cell seeding gave completely different results. This procedure favored the growth of astrocytes in the scaffolds in detriment of the endothelial cell line. Results were similar for acrylic scaffolds containing or not containing hyaluronan. Generally, scaffolds were invaded

predominantly by astrocytes and the presence of vWF positive endothelial cells was limited to some areas (white arrows in Figure 3.53). Furthermore, samples displayed zones that were not populated by cells.

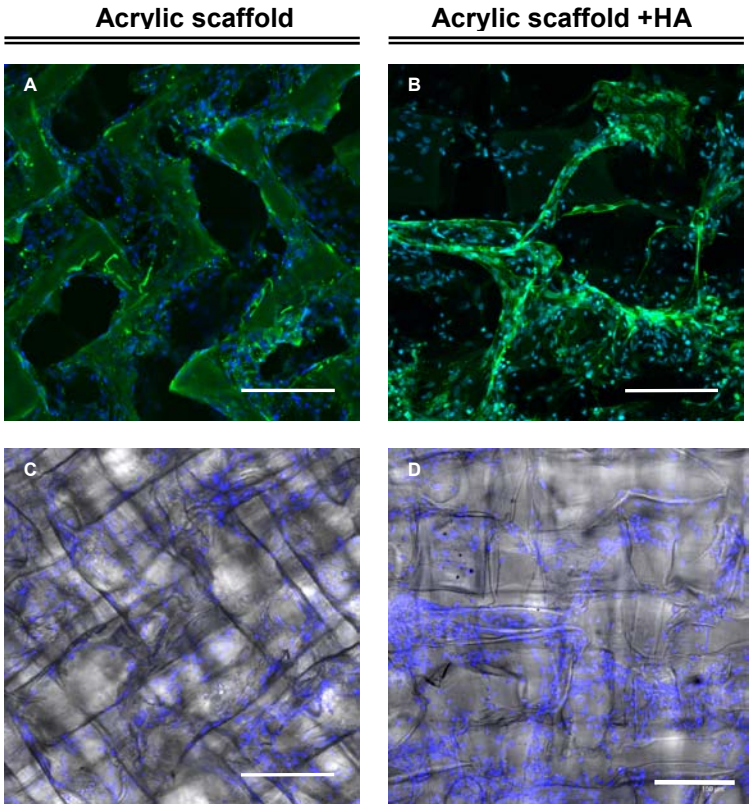

Figure 3.51. Immunofluorescent analysis of co-culture of hCMEC/D3 and U373 by successive cell seeding. A) acrylic based scaffolds with interconnected cylindrical channels; B) acrylic based scaffolds with interconnected cylindrical channels coated with HA-DVS. Images C and D show transmitted photographs containing the nuclei (A and B respectively). Cells were fixed after 21 days of co-culture. Samples were LN coated prior to cell culture. Endothelial cells were stained against PECAM-1 expression in green fluorescence. Cell nuclei were stained with DAPI (blue). Scale bar corresponds to 150 microns.

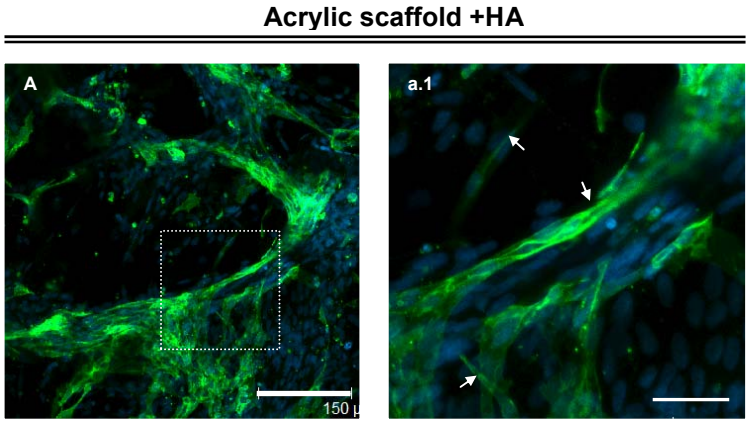

Figure 3.52. Immunofluorescent analysis of co-culture of hCMEC/D3 and U373 by successive cell seeding. A) Different areas found on acrylic based scaffolds with interconnected cylindrical channels coated with HA-DVS; a.1) Detail of A. Cells were fixed after 21 days of co-culture. Samples were LN coated prior to cell culture. Endothelial cells were stained against PECAM-1 expression in green fluorescence. Cell nuclei were stained with DAPI (blue). Scale bar corresponds to 150 microns.

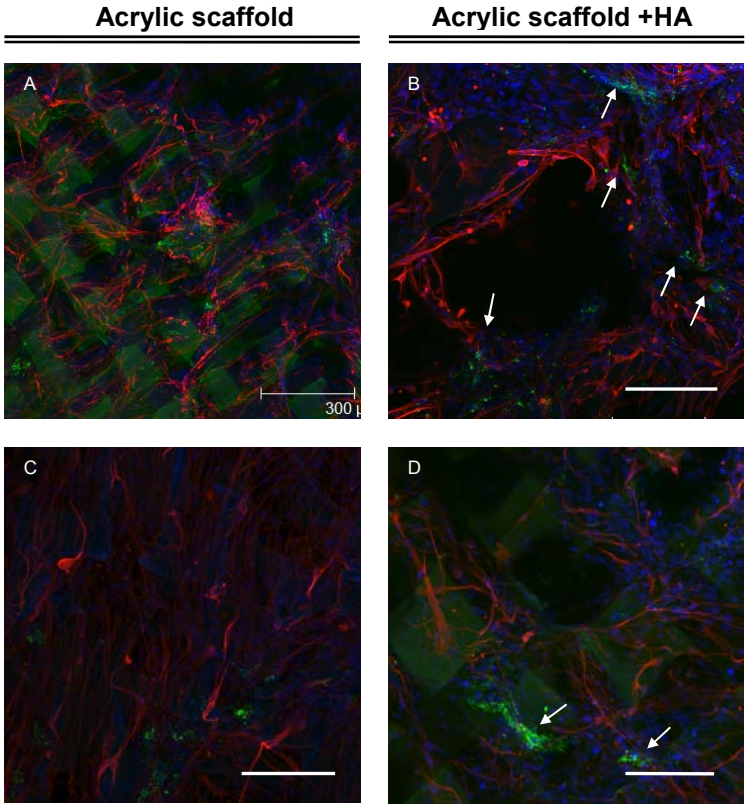

Figure 3.53. Immunofluorescent analysis of co-culture of hCMEC/D3 and U373 by simultaneous cell seeding. A) and C): Acrylic based scaffolds with interconnected cylindrical channels; B) and D): Acrylic based scaffolds with interconnected cylindrical channels coated with HA-DVS. Cells were fixed after 14 (images A and B) and 21 (images C and D) days of co-culture. Samples were LN coated prior to cell culture. Endothelial cells were stained against vWF expression in green fluorescence. Cell nuclei were stained with DAPI (blue). Scale bar corresponds to 150 microns. White arrows point to the areas with vWF expression.

SEM photographs of acrylic based scaffolds co-cultured with endothelial and astrocityc cells during 14 and 21 days yield some more information about the interaction of both cell lines and the invasion of the scaffold. Cells were completely covering the surface of the structure and filled their channels as can be appreciated in Figure 3.55.

Acrylic based scaffolds, with or without hyaluronan coating, were completely covered by cells since the early times of culture. Cells attached and expanded through the surface walls of the channels within the scaffold.

Extended morphologies with cell-cell and cell-biomaterial connections are noticeable. The observation of the inner structure of the scaffold showed that cells reached inner space of the scaffold.

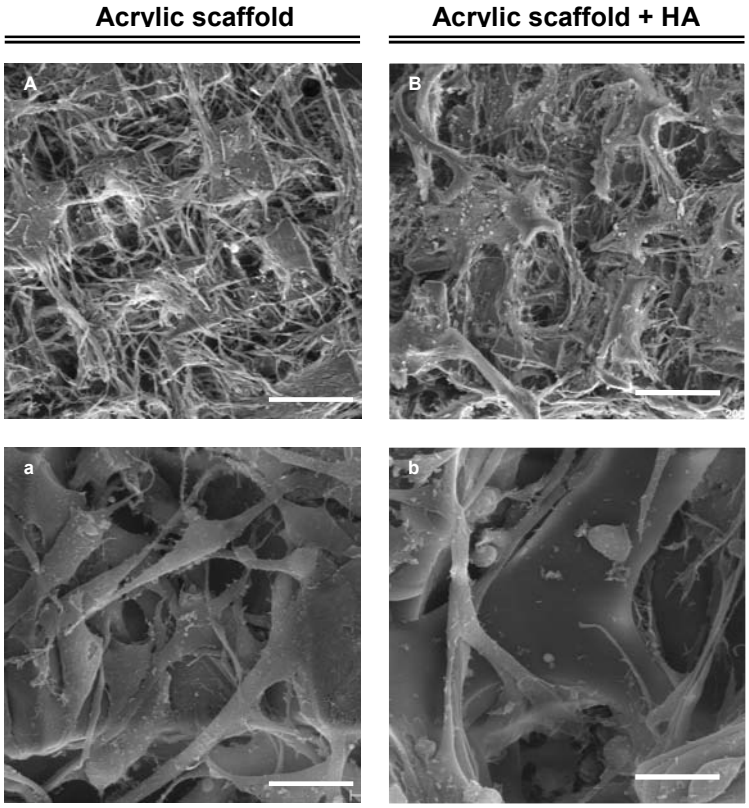

Figure 3.54. SEM micrographs of hCMEC/D3 and U373 growing in co-culture on acrylic based scaffolds with interconnected cylindrical channels during 14 days. A: without HA coating; B: with HA coating. a and b are details of A and B respectively. Samples were LN coated prior to cell seeding. Scale bar in images A and B correspond to 200 microns and to 20 microns in a and b.

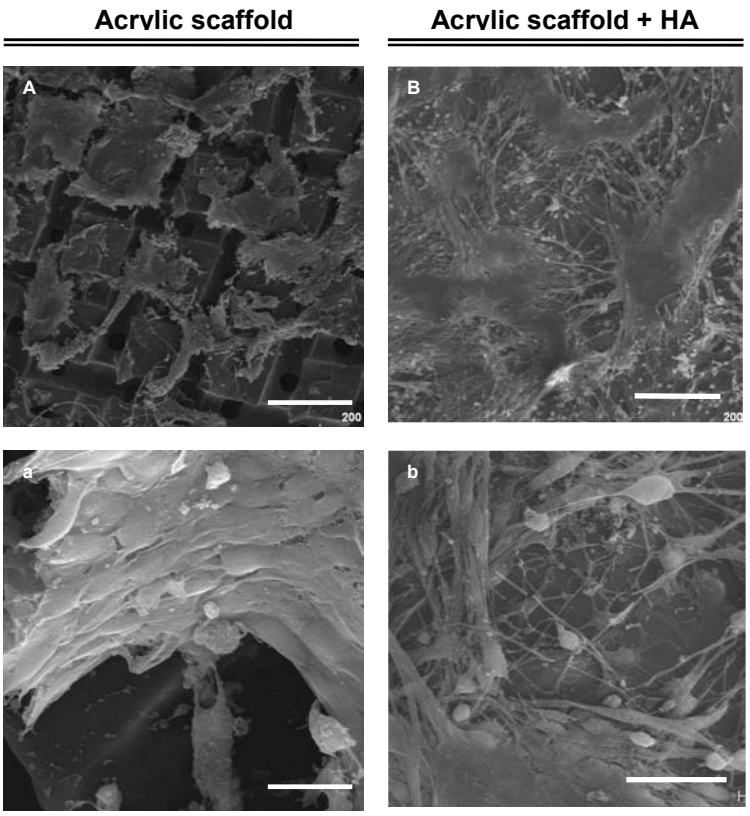

Figure 3.55. SEM micrographs of hCMEC/D3 and U373 growing in co-culture on acrylic based scaffolds with interconnected cylindrical channels during 21 days. A: without HA coating; B: with HA coating. a and b show detail of A and B respectively. Samples were LN coated prior to cell seeding. Scale bar in images A and B correspond to 200 microns, 20 microns in a and to 50 in b.

Cytokine release

The release of Ang-1, Ang-2 and VEGF by cells in co-culture was assessed. Ang-1 was found in biomaterials supernatants in higher concentration than controls did. Within the acrylic scaffolds, those containing hyaluronan had higher concentrations of the cytokine. Ang-2 was secreted moderately by cells growing into acrylic scaffolds with similar concentrations in the case of scaffolds with and without hyaluronan. The cytokine was found in higher concentrations in controls. The release of VEGF was very high since day 14 both in biomaterials and in controls.

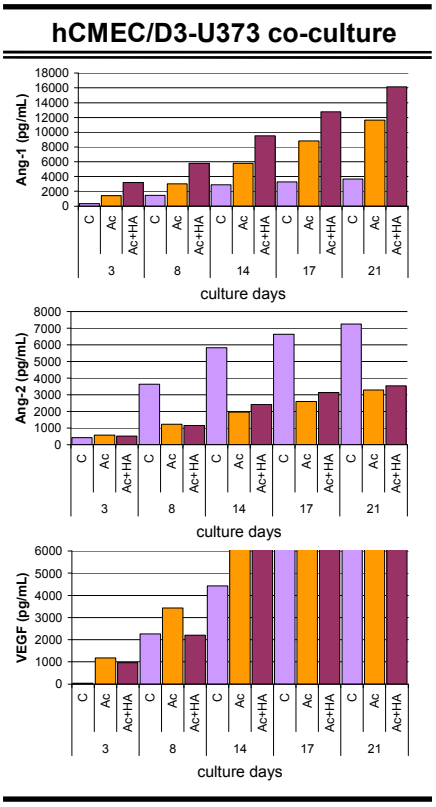

Figure 3.56. Angiogenic growth factors (Ang-1, Ang-2 and VEGF) released into the supernatants of co-cultured hCMEC/D3 and U373 growing in acrylic based scaffolds. The release was evaluated during 21 days of culture and detected by enzyme-linked inmunosorbent assay (ELISA). Control (■), acrylic scaffold (■) Hyaluronan coated acrylic scaffold (■).

CHAPTER 4

DISCUSSION

Development of hyaluronan insoluble materials for tissue engineering applications.

Hyaluronan insoluble structures have been widely synthesized by different crosslinking strategies, obtaining hydrogels with tuneable swelling properties (Collins & Birkinshaw, 2007). In this work, HA was crosslinked with either DEO or DVS obtaining hydrogels with different properties in terms of EWC, elasticity (Young modulus) and degradation rate. Each crosslinker is thought to react through different functional groups on the molecule, the carboxylic or hydroxyl group respectively. A discussion of the crosslinking chemistry will be outlined below.

Crosslinking with 1,2,7,8-diepoxioctane

Due to its high reactivity, epoxides are commonly used crosslinkers for biopolymers. In the hyaluronan molecule, carboxyl and hydroxyl groups are the functional groups available to react with the epoxide. When the reaction takes place in acidic conditions or very slightly basic conditions (pH lower than 8) it will react through available carboxyl groups, forming an ester bond (Collins & Birkinshaw, 2007; Zhao, 2006). The HA-DEO infrared spectra did not give much information about the crosslinking because the new formed bond, an ester bond, is already present in the molecule.

The pK of the carboxyl groups on the glucuronic acid residues is 3-4, depending on ion conditions (Hascall & T. C. Laurent, n d). In the pH in which reaction is taking place, the crosslinking is thought to occur via the carboxylic group of the hyaluronan. This acidic medium is catalyzing the opening of the epoxide leading to the formation of a diol in each end of the molecule. Then, the reaction between the carboxyl groups of hyaluronan and the hydroxyl groups from the diepoxi is giving the crosslinked hyaluronan polymer. Figure 4.1 shows a proposed scheme of reaction between hyaluronan and crosslinker to obtain the final product.

The new bond formed, an ester, is easily hydrolyzed in slightly basic pH resulting in the formation of carboxylic acid and hydroxyl groups newly. Thus, the obtained crosslinked material dissolves in pH values higher than 7.5. Cellular activity growing in culture may provoke changes in the pH of the medium. Thought to be used in biological applications, the solubility of HA-DEO hydrogels was assessed by immersing samples in cellular medium with different pH tuned adding either 0.1M HCl or 0.1M NaOH to acidify or basify respectively. There were prepared 5 different pH media: 7, 7.6, 8, 8.5 and 9. After 72h at 37ºC, hydrogels were found to dissolve completely at pH higher than 8 and were highly swollen at pH=7.6. Hydrogels immersed in pH=7 medium kept their initial shapes. Figure 4.1 details the hydrolysis of the ester bond under such conditions

The crosslinking reaction is really sensitive to the medium conditions and it is a complex function of several factors. The water present in the reaction medium (provided on the one hand by the ratio of acetone-hydrochloride aqueous solution and on the other hand by the amount of solvent employed to carry out the reaction) was not as relevant at long reaction times as for shorter. Thus, R_70 and R_100 conditions displayed almost similar EWC when reacted for 72h. At shorter times, the effect of the amount of water was higher and differences were found when comparing R_50 condition compared with R_70 and R_100 conditions (Figure 3.7).

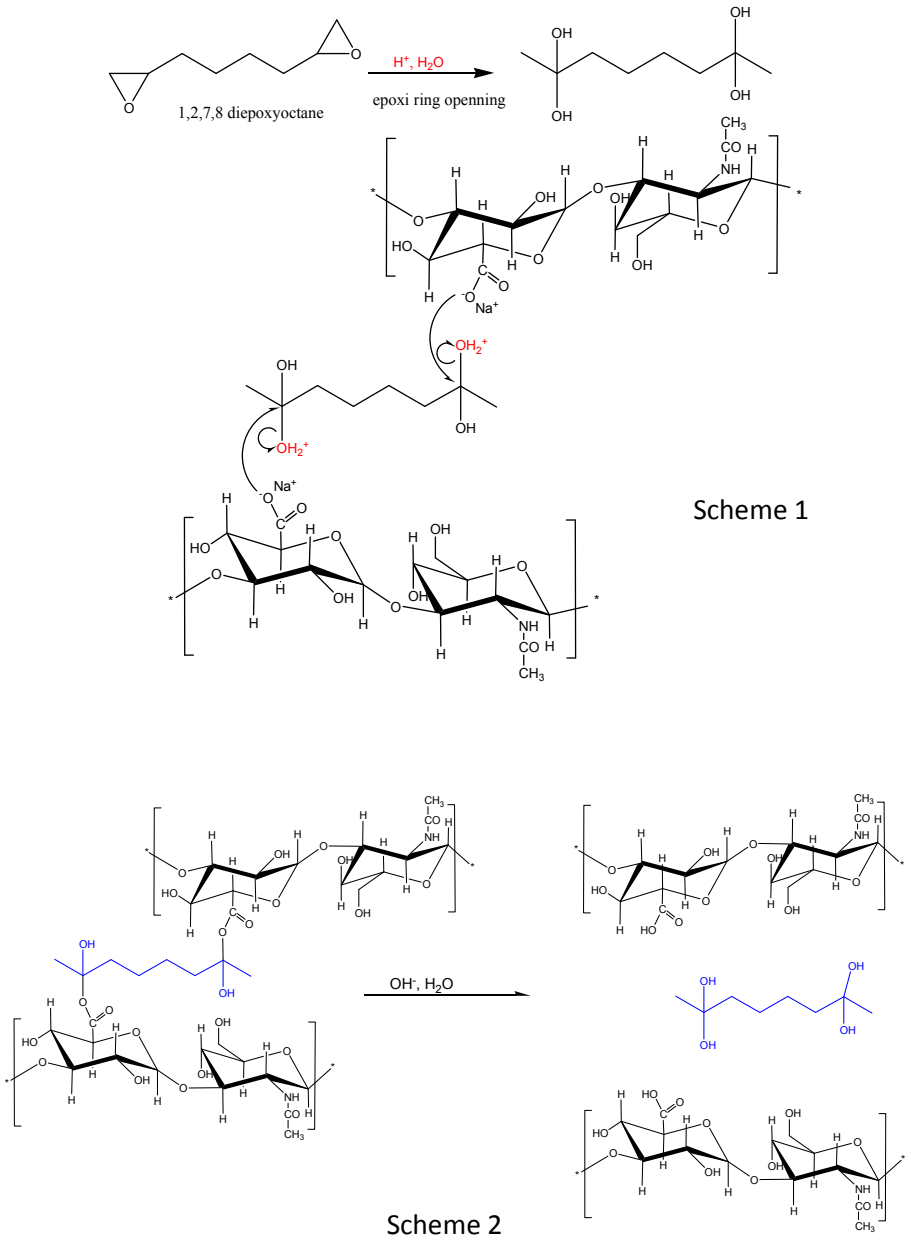

Figure 4.1. Reactions of hyaluronan. Scheme 1: reaction of hyaluronan crosslinking with 1,2,7,8-diepoxioctane; Scheme 2: reaction of ester bond hydrolysis in the HA macromolecule.

Crosslinking with divinyl sulfone

In contrast with the infrared spectra of HA-DEO, HA-DVS crosslinked hydrogels give some more information about the crosslinking showing a characteristic band in 1466 cm^{-1}. This band, which corresponds to the asymmetric stretching of the sulphur and oxygen bond (S=O), demonstrates the incorporation of the bisulphide to the hyaluronan polymer chains.

The DVS crosslinking was carried out in basic medium. Under alkaline conditions, the crosslink takes place through the secondary hydroxyl groups on the hyaluronan molecule [3] reacting with the vinyl groups of the DVS to bind through sulfonyl bisethyl crosslinks two chains of the macromolecule. A proposed structure and scheme of reaction for DVS crosslinked hyaluronan is showed in Figure 4.2.

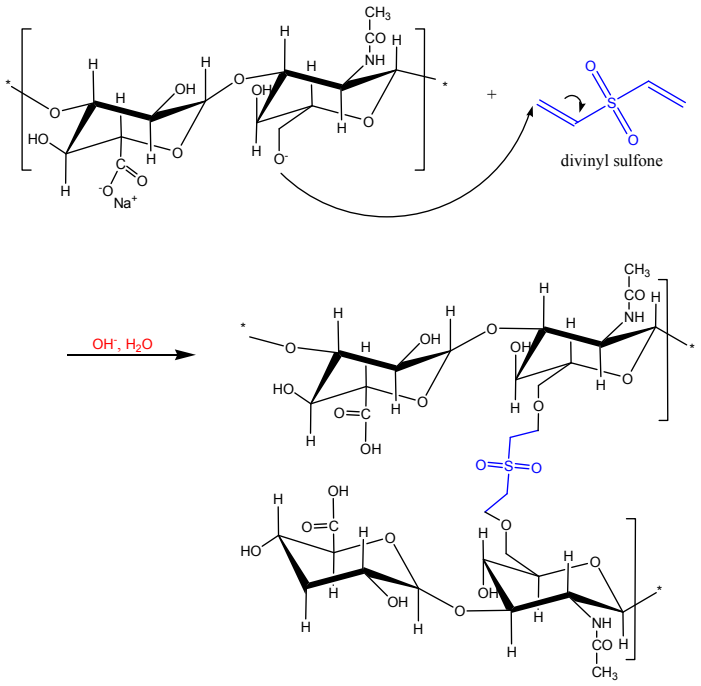

Figure 4.2. Scheme for hyaluronan divinylsulfone crosslinking reaction.

Washing solvent used at the end of the crosslinking reaction was demonstrated to influence the final product. Samples crosslinked in equal conditions showed lower rates of EWC when washed with solvent containing high concentrations of acetone, or only acetone. Besides, samples rinsed with solvents containing 20% or more water showed similar behaviour in terms of swelling. It is proposed that the high capacity of dehydration of the acetone may produce irreversible additional physical crosslinkings in the matrix thus affecting the final EWC. The acetone may dehydrate suddenly the hydrogel faster than the structure needs to shrink du to loss of the absorbed water so that structure collapses. It is also possible that the dehydration of the hydrogel itself exposes non reacted hydroxyl groups still available for crosslinking and non-reacted DVS molecules trapped in the bulk of the hydrogel. This fact may produce an enhancement in the number of chemical crosslinkings within the molecule due to the higher proximity of the groups to react. Samples washed in solvent containing high ratios of water, did not display such swelling response. In this case, the structure is allowed to contract its chains in equilibrium rates, while water and non-reacted DVS is washed out from the matrix. The matrix is no longer collapsed neither “overcrosslinked” by the solvent employed due to the content in water is so much higher, so the hydrogel does not deflate in response of the medium but swells during the washing, what maintains the properties of the matrix.

To better understand the suggested mechanisms underlying the collapse of the hydrogel crosslinked matrix two pieces, two pieces of the same hydrogel were submitted to different and contrary treatments (complete hydration and complete dehydration, Figure 4.3). Directly after crosslinking, one sample was immersed in 100% acetone (A) while another was immersed in 100% distilled water (W). Samples were kept immersed during 30 minutes. In the first case, the sample became completely white while reducing its size considerably. In the second case, the sample swelled and displayed complete transparency. The latter same sample was then

immersed in acetone to dehydrate its matrix and the sample became white and opaque. Afterwards, both samples (A and W) were rehydrated in water re-swelling in a different way. Sample "A" swelled displaying some translucent behaviour and did not recover its initial size. Besides, sample "W" swelled until it recovered its initial size and resulted in a colourless and transparent hydrogel.

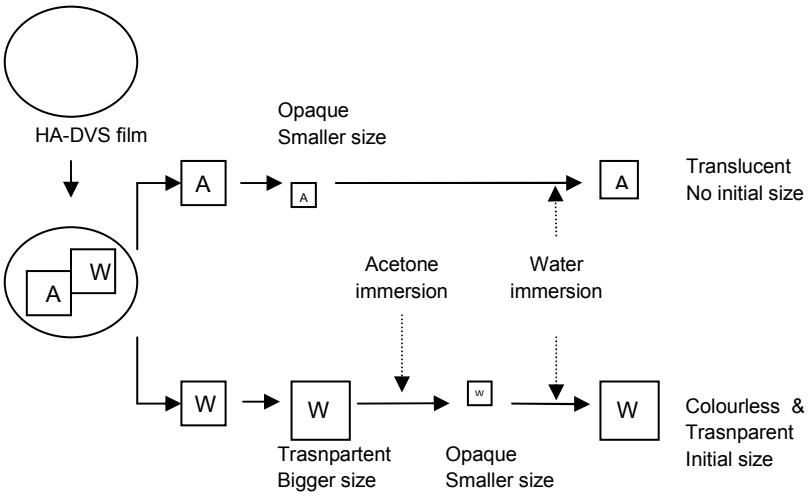

Figure 4.3. Schematic procedure to assess the influence of the solution employed for rinsing the HA-DVS hydrogels after crosslinking.

The effect of the solvent employed to work out the reaction made it possible to tune the swelling of the crosslinked matrix obtaining different behaviour with apparently same chemical degree of crosslinking within the structure.

Hyaluronan hydrogels crosslinked with either with epoxides or divinylsulfone have been reported to display EWC values in the range of 170-250% (Collins & Birkinshaw, 2007). Taking into account the final application of the synthesized hydrogels, results will be analyzed from the point of view of neural tissue. Brain is a soft and high water content tissue. It is known to be strongly inhomogeneous and anisotropic, with mechanical properties differing significantly from one region to another (Franze,

Reichenbach, & Käs, 2009). The water content in brain tissue of adult rats is in the range of 80% (Shulyakov, Cenkowski, Buist, & Del Bigio, 2011).

Besides, it has been reported that different cell types prefer diverse substrate elasticities, behaving in a different way in soft and stiff environments (Franze et al., 2009). Synthesized hydrogels, HA-DVS and HA-DEO, had different swelling capacities as well as Young moduli. In terms of water absorption, both hydrogels had higher rates of water compared with adult rat brains (140% of EWC for HA-DEO and 600% for HA-DVS) while displaying different mechanical properties. The Young modulus of the native brain tissue is one of the softest tissues in the body (E=0.5-1 kPa) (Gefen & Margulies, 2004; Taylor & K. Miller, 2004). The value of the modulus measured for the different hyaluronan matrices was 1.5 and 3 times higher ($E_{HA\text{-}DEO}$ and $E_{HA\text{-}DVS}$ respectively) than the maximum E for native brain tissue. According to Georges and co-workers the distribution and population sorting of CNS cells occurs based on the mechanical properties of the substrate (Georges, W. J. Miller, Meaney, Sawyer, & Janmey, 2006). This makes interesting to have a wide range of biomaterials with different elastic modulus and EWC. The substrate deformability is strongly affecting the behaviour of the different cell types. Georges and co-workers (Georges et al., 2006) report that the branching frequency of neurons on gels of 550 Pa is similar to those cultured on glass (whose elastic modulus is in the order of tens of GPa). Then, it can be assumed that for neurons composing the brain tissue, both of our synthetized hydrogels, HA-DEO and HA-DVS, will be the same substrate in terms of its stiffness. Furthermore, the response of neural support cells (astrocytes) to the stiff of the substrate is different to neurons preferring the first stiff substrates (Leipzig & Shoichet, 2009).

The degradation rates of hydrogels depend mainly on the matrix composition and hyaluronidase (Hase) concentration which makes very difficult to compare different composition in the reported data. Additionally, enzymatic *in vitro* degradability only represents an approximate view because in the end, the concentration of the enzyme *in vivo* depends on the

tissue and the availability in the area. Generally, hyaluronan crosslinked hydrogels have been described to degrade almost completely in short times within hours (Bulpitt & Aeschlimann, 1999; Ibrahim, Q. K. Kang, & Ramamurthi, 2010) until few days (Hahn, J. K. Park, Tomimatsu, & Shimoboji, 2007; Y. Liu, Shu, & Prestwich, 2005). This highlights the long degradation rates found for the hydrogels synthesized in this work. HA-DVS hydrogels were found to degrade 60% in 8 days and almost completely at day 21 while HA-DEO degraded at slower rates.

Different chain lengths obtained as a result of *in vivo* degradation trigger the activation of different processes related to angiogenic cascade. Hyaluronan polymers chains found in the ECM of most mature tissues have high molecular weight hyaluronan (HMW-HA) (Garg & Hales, 2004). The biodegradation of natural hyaluronan is reported to be a step-wise process (Rodén et al., 1989). Hyaluronidases are considered responsible for most of the HA catabolism taking place in the organisms. Hyaluronidases have different mechanisms of action and cleave the hyaluronan chains at different sites, yielding diverse molecules of lower molecular weight. The type of hyaluronidase employed (testis type, E.C. 3.2.1.35) is reported to cleave HA yielding tetra and hexa oligosaccharides as the major end products (Girish & Kemparaju, 2007). In any case, it can be predicted that chains with higher molecular weights will be released during *in vitro* degradation due to crosslink of the polymer chains of HA by covalent bonds. In fact, diverses MWs were recorded in the degradation supernatants. Higher MWs were found in HA-DVS than in HA-DEO hydrogels as can be expected from a less crosslinked matrix.

DEVELOPMENT OF 3D STRUCTURES

Scaffolds designed to be used in brain implantation should promote neural cells survival while reducing the inflammatory response to prevent glial scarring. The architecture of the tissue must be taken in account in order to adequate the scaffold to the tissue to be regenerated. Scaffolds should be designed considering the permeability of nutrients, thus, containing inner microporosity allowing the access of oxygen and nutrients as well as permitting the removal of debris from cell activity. Additionally, the scaffold should provide enough space to allow cell growth and colonization of the porous structure.

Different architectures are required depending on the final application. One possible application of the designed scaffolds is their use as **cell carriers** to provide cell supply in cell lacking areas. Mesenchymal cells or dopaminergic neurons can be seeded into soft highly porous scaffolds and implanted in damaged tissue with cells capable to proliferte into a damage area differentiate into the cells can then proliferate and mature reaching connectivity with the host tissue. To this end, highly porous structures were manufactured. Those structures were fabricated with porogen leaching techniques resulting in scaffolds with high pore size. The sizes of the pores correlated with the sizes of porogen examined by SEM, ranging from 50 microns (or even smaller) to 150 microns (Figure 3.19-A, black arrows). Lower ratios of porogen to HA were tested giving structures with less or lack of interconnectivity as can be seen in Figure 4.4.

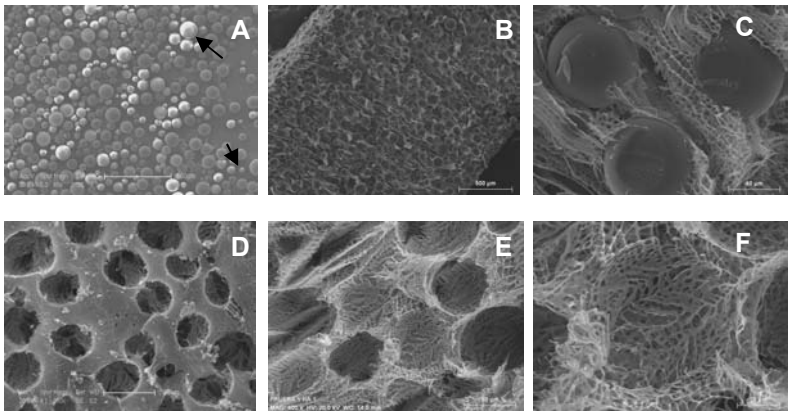

Figure 4.4. SEM photographs of hyaluronan scaffold. A) Porogen beads of polymethylmethacrylate showing dispersion in bead size. B and C) inner structure of the scaffolds prior to removal the porogen; D) Lyophilized hyaluronan scaffold once the porogen was removed from the structure. E and F show details of the porosity and their walls.

Another interesting application is the use of scaffolds as a guiding **support for repopulation** of damaged areas. After injury, NSC can theoretically migrate from the SVZ to the damage area to repopulate the area although they usually fail in their duty because in absence of mechanical support in the damage tissue they are likely to die. Scaffolds both with regular interconnected porous inner structures or with randomly disposition of the pores with high interconnection between them are thought to provide a good environment for those cells to grow and differenciate. In this sense, acrylic scaffolds with a regular pattern of interconnected channels were developed. Those non-biodegradable structures were coated with hyaluronan to provide the scaffold with different environment in which cells may better attach and proliferate due to its biological properties. The regular channels may give support to accommodate those cells successfully and guide the growing of axons.

Another application of scaffolds for neural tissue regeneration may lie in the **reconstruction of axonal pathways** within the nervous system. Hollow tubes are of interest for applications in nerve guides or vascular grafts (Dalton & Shoichet, 2001) (Freier et al., 2005). Hyaluronan crosslinked

porous bulk cylinders and tubes of highly porosity were fabricated. The employed technique allowed preparing small samples with highly porous walls. The design permitted to obtain samples in the order of 1mm and 2mm outer diameter. The microporosity (with an average size of 30 microns) was obtained by freeze drying; channels were achieved by fiber moulding being possible to tune the diameter of the channel. Channelled scaffolds may help axons to grow and reconnect with their specific sites thus helping to recover lost functionalities. The necessity of axon guidance for successful axon regrowth is widely reported (Francisco, Yellenb, Halversonc, Friedmanc, & Gallo, 2007; SMEAL, RABBITT, BIRAN, & TRESCO, 2005; Stokols et al., 2006). Hyaluronan channelled scaffolds with different inner porosity and wall sizes were fabricated with both crosslinkers employed in this work. HA-DEO multichanneled scaffolds were fabricated with channels of 100 or 200 microns in diameter. The channels, obtained by employing different filaments (heat conductive or non-conductive) resulted in different structures. Conductive filaments (Copper, 100 microns) lead to characteristic lamellar structures in samples due to the appearance of temperature gradients. Those structures were not visible in structures fabricated with non-conductive filaments (polymeric filament, 100 microns) or with lower conductivity (stainless steal, 200 microns). HA-DVS multichanneled scaffolds were fabricated with polymeric filaments of 100 microns in diameter. After the process of crosslinking samples were swollen in water and then lyophilized. The channels displayed smooth walls in those surfaces which were in contact with the filaments. Besides, the bulk hyaluronan within the walls displayed two different structures. In contact with the filaments there were between 3 to 4 microns thick of polymer within any visible porosity defining perfectly the channels followed by a microporous structure displaying pores in the range between 8 to 25 microns. The microporosity is forced by the process of freeze-drying which evidences the structure of the swollen scaffold.

The nigrostrialtal pathway, which connects the *substantia nigra* and the *striatum* is known to be degenerated in neural diseases as Parkinson's disease. Those channelled natural scaffolds with mechanical properties close to brain tissue and high permeability may be used for the reestablishment of dopaminergic pathways with the recovering of lost functionailities.

Furthermore, acrylic based non-degradable scaffolds, with inner structures mimicking the region of cortex in the brain, were coated with a thin layer of HA though to take advantage of the hyaluronan properties. Hyaluronan content referred to the total volume of the scaffold was estimated to be around 7% in weight which was sufficient to be noticed by cells while leaving enough remaining space within the channels for cells to grow. The Alcian Blue assay which stains GAGs was employed to confirm complete distribution of the coating throughout the porous structure giving regular staining (figure 3.20).

Biological in vitro characterization of biomaterials

Hyaluronan-based materials

Only HA-DVS hydrogels were selected for further biological characterization due to their longer stability in culture media.

It is established that the first mechanism of adhesion between cell-cell and cell-surfaces is integrin mediated. Intengrins are a family of transmembrane receptors that recognize proteins from the extracellular matrix such as fibronectin (FN), laminin (LN) and type I collagen (COL-I) (García, 2006). Therefore, to improve cell-biomaterial interactions, such proteins have been employed for improving cell adhesion on biomaterials with proper signals for cell adhesion. Different ways to incorporate such proteins in biomaterials have been employed such as absorption from protein solutions or surface engineered by grafting of bioadhesive motifs.

Hyaluronan hydrogels have been modified with laminin (Shaoping Hou et al., 2005), poly-D-lysine (Wm Tian et al., 2005) or grafted with protein sequences of known relevancy in cell adhesion (I.S.Lee, 2006; Y. T. Wei et al., 2007). In all cases authors reported that hyaluronan modified with those adhesion sequences provide the HA hydrogel with an environment conductive to CNS regeneration. Modified surfaces with fibrin-HA coating have been as well developed for use in bone regeneration and improved cell adhesion and tissue regeneration were reported (S.-woong Kang et al., 2011). Hyaluronan hydrogels have been shown to support viable neural precursors cells (NPCs) and their differentiation into neurons and glial cells (Pan et al., 2009). Human astrocytes have been cultured in sulphated hyaluronan and results suggested that sulphate hyaluronan may be involved in the astrocyte activity (Yamada, Sawada, & Tsuchiya, 2008).

In this work, we prepared DVS crosslinked hyaluronan based biomaterials which were coated with two different proteins prior to cell seeding: Laminin (LN) and fibrin (fb). Laminin is widely used as a coating to improve nerve cell adhesion and growth (Liesi, Dahl, & Vaheri, 1984) since it has been reported to play an important role in neural cell migration, differentiation and neurite growth (W. He & Bellamkonda, 2005; Heiduschka, 2001). Fb has been demonstrated to be involved in repair associated angiogenesis providing cells with a temporary matrix which may act as scaffold for invading ECs (van Hinsbergh, Collen, & Koolwijk, 2001). In our biomaterials, the coating was not covalently bonded to the matrix but deposited by protein adsorption on the surface.

An endothelial and an astrocytic cell line were cultured individually onto HA-DVS hydrogels. Cells were viable in both LN or fb coated hyaluronan. ECs seeded onto fibrin coated 2D HA-DVS hydrogels demonstrate poor adhesion to the surface at early times while similar viability was found in longer times of culture (8 days). LN seemed to promote cell adhesion also at early times, being the cells homogeneously distributed on the surface of the hydrogel. This observation evidenced different behaviour of ECs depending

on the protein coating employed prior to cell seeding. A non-homogeneous distribution of the protein coating on the biomaterial surface may explain those differences. The areas where the protein has deposited properly would induce the adhesion of cells in clusters. Those cells can start secreting afterwards their own extracellular matrix providing signals to other cells to adhere and proliferate throughout the whole surface. Astrocytes showed better viability on LN coated biomaterials although fibrin coated ones displayed high density of viable cells as well. In any case, both cell lines demonstrated good viability growing onto HA-DVS hydrogels in monoculture.

Hydrogels, in general, are known to have good biocompatibility and to cause minimal inflammatory responses. Nevertheless, the chemicals employed to obtain insoluble structures from hydrogels by i.e. crosslinking hyaluronan hydrogels, may elicit toxic reactions in the body. To assure the biocompatibility of synthesized biomaterials with cells *in vitro*, the expression of E-selectin by ECs was evaluated. This cell adhesion molecule is expressed by endothelial cells after their activation by cytokines in response of inflammation. Because different procedures were followed to obtain the 2D and 3D structures, both hydrogels were assessed. None of the biomaterials elicited any expression of E-selectin in ECs; whereas in positive inflammation controls using LPS activation cells grown onto HA-DVS hydrogels expressed their inflammatory phenotype. The phenotype of cells growing on hyaluronan hydrogels was followed by expression of specific proteins for each cell line. ECs were immunoassayed against von Willebrand factor (vWF) and the platelet/endothelial cell adhesion molecule-1 (PECAM) while astrocytes were followed by their glial fibrillary acidic protein (GFAP) expression.

ECs cultured alone onto HA-DVS hydrogels demonstrated typical phenotypic characteristics expressing PECAM-1 at cell-cell junctions or aggregates of vWF. Astrocytes expressed highly the intermediate filament GFAP; higher expression was observed in the cells cultured onto HA-DVS hydrogels LN coated. Cells grown onto fibrin coated hydrogels showed less

GFAP positive cells at long times of culture. GFAP is a marker of mature astrocytes. The lower GFAP expression on fibrin coated biomaterials may demonstrate either a lower gliotic response or permanence of astrocytes proliferative phase, as it is known that proliferative immature astrocytes do not secrete GFAP.

A proper integration of the biomaterial requires a good connectivity with the host tissue to supply cells with nutrients and oxygen and to allow the removal of cell waste. To this end, a good vascularisation of the scaffold is needed. The formation of new vascular sprouts requires the interaction between several factors and cell types. Released cytokines and growth factors activate endothelial cells to start the angiogenesis process.

Studies focused on the interaction of angiopoietins and VEGF have elicited information about the interaction of cytokines and ECs. Risau and co-workers described the angiopoietin-1 (Ang-1) as a potent inducer of sprouting angiogenesis and found that its depletion inhibited completely sprout formation (Koblizek, C. Weiss, Yancopoulos, Deutsch, & W Risau, 1998). Hyaluronan has been found either to inhibit cell adhesion (M. K. Cho, G. H. Lee, E. Y. Park, & S. G. Kim, 2004) or to promote proliferation and production of Col II [28]. The molecular weight of hyaluronan was determined to be the ultimate responsible in being pro- or antiangiogenic (Struve et al., 2005). Riley and co-workers (Rilley et al., 2006) tried to better understand the molecular mechanisms by which HA induce angiogenesis and the mechanisms of interaction between HA, VEGF and Ang-1. To do that, they prepared HA crosslinked hydrogels containing delivering VEGF, Ang-1 or co-delivering of both of them. They found that *in vivo*, HA hydrogels combined with those three factors together produced the greatest angiogenic response compared with hydrogels with single delivery or lacking both of them. Besides, Hsu Ma and co-workers (Perng, Y.-J. Wang, Tsi, & H. Ma, 2009), studied the effect of the molecular weight of HA in angiogenesis with collagen/HA scaffolds. They reported that the potential of hyaluronan to induce angiogenesis processes depended on the molecular weight of the

hyaluronan getting faster revascularization those with lower molecular weights (Rilley et al., 2006).

The study of cells in co-culture has been employed widely in literature with different purposes, one of them for vascularization studies where endothelial cells are the main focus. ECs have been cultured with osteoblasts (M. I. Santos, Ronald E Unger, Sousa, Rui L Reis, & C James Kirkpatrick, 2009; Ronald E Unger et al., 2007), mesenchymal stem cells (Kolbe, Xiang, Dohle, Tonak, & Fuchs, 2011) or nervous cells (Lefranc et al., 2004) among others. Studies intended to mimic the BBB in vitro are focused on the culture of cerebral endothelial cells and it is desirable to grow them in co-culture with astrocytes and/or pericytes (Garberg et al., 2005) .

To achieve better knowledge about the response of cells growing on our HA-DVS scaffolds, as first approaching to physiological conditions we co-cultured a microvascular endothelial cell line (hCMEC/D3) and a glioma cell line (U373). To induce angiogenesis *in vitro*, basic fibroblast growth factor (bFGF) was employed as it was identified as the first EC mitogen and chemotactic factor for EC and it is described as highly angiogenic (J. Abraham et al., 1986).

Due to the different division rate of both cell lines, we followed two different protocols for cell seeding. On the one hand, in order to favour the endothelial cell line they were seeded first and in a ten fold ratio to U373. 24h later, astrocytes were seeded (successive cell seeding). In another experiment cells were seeded simultaneously and at a 1:1 ratio.

Controls of both methods showed differences in the organization of the cells in culture. Simultaneous cell seeding gave a clear organization of the endothelial cells into ring-like fashion and forming a network throughout the surface of the 2D cultures in which the space between such string-like formations were completely occupied by astrocytes. However, the successive cell seeding did not result in that clear organization of the endothelial cells, which appeared mixed with astrocytes in the co-culture and as spontaneous ring-like distributions along the surface of culture.

Nonetheless, controls demonstrated that both the simultaneous and the successive cell seeding conducted to the formation of *in vitro* capillary-like structures.

Hyaluronan based scaffolds

It is thought that the biomaterial itself, which composes the primary scaffold structure, may favour the preferential adhesion and survival of one cell line over the other one.

The co-culture of hCMEC/D3 and U373 onto hyaluronan scaffolds gave different responses depending o the method employed for cell-seeding. The successive cell seeding, in which the endothelial cell line attachment to the biomaterial was favoured by being seeded first, ECs reorganized into capillary-like in fb coated scaffolds while in the LN coated did not. Results from the simultaneous cell seeding showed organization of ECs in both cases with different geometries. In this case, the structures on LN coated biomaterials seemed to be a better system for the co-culture as can be analyzed both by the vWF expression and GFAP.

The study of the cytokines released to the medium during the co-culture within hyaluronan scaffolds did not give further insights about the formation of the capillary-like structures. Ang-2 and Ang-1 are competitive ligands for the Tie-2 receptor of ECs. Ang-1 has been determined to be necessary for endothelial sprout formation in *in vitro* studies (Ronald E Unger et al., 2007). Furthermore, the presence of VEGF, the unique cytokine with mitogenic effect on endothelial cells, is required for sprouting angiogenesis. Only Ang-1 can activate the Tie-2 receptor to signal the recruitment of support cells in order to stabilize effect ECs in the new vascular sprout formed. It is proposed that Ang-2 function is binding Tie-2 to block Ang-1 effect thus, facilitating the migration of EC from the vessel to form a new capillary (Nomi et al., 2002). Studies of the biological activity of Ang-1 in vitro demonstrated that Ang-1 containing supernatants induced the formation of capillary sprouts, whereas they were not found in the control supernatants (Koblizek, C. Weiss, Yancopoulos, Deutsch, & W Risau, 1998). Ang-2 is expressed only at the sites of vascular remodeling and in the presence of VEGF, Ang-2 promotes vascular sprouting. The supernatants evaluated contained high concentrations of Ang-1 and VEGF while low concentration of Ang-2 in

contrast to control supernatants in which high concentrations of the latter were found. The study of these cytokines does not provide enough extra information to support the results of the immunohistochemistry assays were organization of ECs into different geometries reminding the capillary-like structures was observed in i*n vitro* assays.

Acrylic based scaffolds

Hyaluronan has been recently reported to improve the therapeutic effect of injected human umbilical vein ECs (HUVECs) into mouse ischemic hindlimbs by promoting angiogenesis (Z. C. W. Tang, Liao, A. C. L. Tang, Tsai, & P. C. H. Hsieh, 2011). Evidences of high organization of ECs were found in acrylic scaffolds containing hyaluronan coating (Figure 3.51). Cord-like distribution of ECs that was clearly not governed by the geometry of the scaffold were appreciated in hyaluronan coated acrylic scaffolds. Those structures were not found in acrylic scaffolds alone. Detail in Figure 3.52 shows the PECAM-1 expression at cell-cell junctions. However, the simultaneous cell seeding did not seem to be favourable in acrylic scaffolds in which low populations were found both of endothelial and astrocytic cell lines.

The cytokines analyzed in the supernatants did not contribute to elucidate the promotion or not of angiogenesis within those biomaterials.

In general, both mechanisms of cell seeding resulted in different structures in both kinds of scaffolds. Not only the method of cell seeding may influence in the results but elements such as scaffold pore size and density play a key role. The succesive cell seeding gave best results for hyaluronan scaffolds and in acrylates scaffolds that seemed to be better invaded by cells through the successive cell seeding with the subsequent formation of string-like structures by ECs.

1. Two different crosslinkers have been employed to obtain insoluble hyaluronan hydrogels. With this aim, 1,2,7,8-diepoxyoctane and divinylsulfone were employed crosslinking the hyaluronan polymer through different functional groups in the sugar. Both crosslinkers gave hydrogels with different mechanical properties, degradation rates and swelling in water.

2. The two methods to crosslink hyaluronan permitted the obtaining of tridimensional structures with different geometries and porosities. It was possible to fabricate cylinders, channelled scaffolds and interconnected spherical porosus structures all of them thought to be useful for different applications of neural tissue regeneration.

3. It was possible to obtain hybrid samples by performing a coating of hyaluronan hydrogel into acrylic samples, thus combining the advantages of non-degradable structures giving mechanical support and biodegradable polymer as hyaluronan which is expected to improve the biological interaction of the construct in physiologic conditions.

4. The synthetized hyaluronan DVS crosslinked hydrogels demonstrated to permit optimal viabilities of the cells evaluated, a human microvascular endothelial cell line (hCMEC/D3) and a human gliobastoma cell line (U373). Those cells expressed their phenotypic markers during the period evaluated in monoculture with the biomaterials.

5. The HA-DVS scaffolds fabricated did not provoke any toxic response in the endothelial cells as evaluated by their E-selectin expression. Furthermore, cells expressed their inflammatory marker upon activation with LPS, thus showing a normal phenotype when growing on the designed scaffolds.

6. The use of different protein coating, LN or fb, prior to cell seeding did not influence the expression cell phenotypic markers when growing on biomaterials. However, the viability assays of cells growing on 2D hydrogels showed a preference of LN for astrocytes and fb for ECs.

7. Cells cultured on LN and fb coated biomaterials showed a distinct release of cytokines to the culture medium.

8. The co-culture ECs and astrocytes gave different results depending on the protocol used for cell seeding. The co-culture by simultaneous cell seeding on hyaluronan based biomaterials led to the formation of cord-like structures thus demonstrating a kind of organization of the ECs within the scaffolds. However, the cell seeding by this protocol in acrylic samples resulted in a low survival of ECs in the co-culture. The successive cell seeding led to the organization of ECs in acrylic samples.

9. The cytokine analysis was not consistent with the formation of capillary-like structures *in vitro* by controls and biomaterials.

REFERENCES

[1] R. Langer and J.P. Vacanti, "Tissue Engineering," *Science*, vol. 260, 1993, pp. 920-926.

[2] R. Lanza, R. Langer, and J. Vacanti, *Principles of Tissue Engineering*, 2007.

[3] A. Atala, "Tissue Engineering and Regenerative Medicine: Concepts for Clinical Application," *Rejuvenation Research*, vol. 7, 2004.

[4] A. Magnani, A. Priamo, D. Pasqui, and R. Barbucci, "Cell behaviour on chemically microstructured surfaces," *Materials Science and Engineering C*, vol. 23, 2003, pp. 315 - 328.

[5] A. Mikos and J. Temenoff, "Formation of highly porous biodegradable scaffolds for tissue engineering," *Electronic Journal of Biotechnology*, vol. 3, 2000, pp. 114-119.

[6] M. Monleón Pradas, J.L. Gómez Ribelles, A. Serrano Aroca, G. Gallego Ferrer, J. Suay Antón, and P. Pissis, "Porous poly(2-hydroxyethyl acrylate) hydrogels," *Polymer*, vol. 42, Feb. 2001, pp. 4667-4674.

[7] A. Spanoudaki, D. Fragiadakis, K. Vartzeli-Nikaki, P. Pissis, J. Rodríguez Hernandez, and M. Monleón Pradas, "Nanostructured and nanocomposite hydrogels for biomedical applications," *Surface Chemistry in Biomedical and Environmental Science*, 2006, pp. 229-240.

[8] D.J. Mooney, D.F. Baldwin, N.P. Suh, J.P. Vacanti, and R. Langer, "Novel approach to fabricate porous sponges of poly(D,L-lactic-co-glycolic acid) without the use of organic solvents.," *Biomaterials*, vol. 17, Jul. 1996, pp. 1417-22.

[9] M.-H. Ho, P.-Y. Kuo, H.-J. Hsieh, T.-Y. Hsien, L.-T. Hou, J.-Y. Lai, and D.-M. Wang, "Preparation of porous scaffolds by

using freeze-extraction and freeze-gelation methods," *Biomaterials*, vol. 25, 2004, pp. 129-138.

[10] M.J. Moore, J.A. Friedman, E.B. Lewellyn, S.M. Mantila, A.J. Krych, S. Ameenuddin, A.M. Knight, L. Lu, B.L. Currier, R.J. Spinner, R.W. Marsh, A.J. Windebank, and M.J. Yaszemski, "Multiple-channel scaffolds to promote spinal cord axon regeneration," *Biomaterials*, vol. 27, 2006, pp. 419-429.

[11] D. Williams, *The Williams dictionary of biomaterials*, Liverpool University Press, 1999.

[12] L. Nair and C.T. Laurencin, "Biodegradable polymers as biomaterials," *Progress in Polymer Science*, vol. 32, 2007, pp. 762-798.

[13] M.S. Dhillon, S. Prabhakar, and C. Prasanna, "Preliminary experience with biodegradable implants for fracture fixation," *Indian Journal of Orthopaedics*, vol. 42, 2008, pp. 319-322.

[14] S. Tredwell, J.K. Jackson, D. Hamilton, V. Lee, and H.M. Burt, "Use of fibrin sealants for the localized , controlled release of cefazolin," *Canadian journal of surgery*, vol. 49, 2006, pp. 347-352.

[15] T.A. Donato, L.H. de Almeida, R.A. Noguiera, T.C. Niemeyer, C.R. Grandini, R. Caram, S.G. Schneider, and A.R.J. Santos, "Cytotoxicity study of some Ti alloys used as biomaterial," *Materials Science and Engineering: C*, vol. 29, 2009, pp. 1365-1369.

[16] C.E. Wilson, C.A. van Blitterswijk, A.J. Verbout, W.J.A. Dhert, and J.D. de Bruijn, "Scaffolds with a standardized macro-architecture fabricated from several calcium phosphate ceramics using an indirect rapid prototyping technique," *Journal of Material Science: Materials in Medicine*, vol. 22, 2011, pp. 97-105.

[17] V. Janakiraman, B.L. Kienitz, and H. Baskaran, “Lithography Technique for Topographical Micropatterning of Collagen-Glycosaminoglycan Membranes for Tissue Engineering Applications,” *Journal of Medical Devices*, vol. 1, 2007, pp. 233-237.

[18] R.E. Unger, K. Peters, M. Wolf, A. Motta, C. Migliaresi, and C.J. Kirkpatrick, “Endothelialization of a non-woven silk fibroin net for use in tissue engineering : growth and gene regulation of human endothelial cells,” *Biomaterials*, vol. 25, 2004, pp. 5137-5146.

[19] E.K. Purcell, A. Singh, B. Tech, and D.R. Kipke, “Alginate Composition Effects on a Neural Stem Cell – Seeded Scaffold,” *Tissue Engineering: Part C*, vol. 15, 2009.

[20] T. Freier, R. Montenegro, H.S. Koh, and M.S. Shoichet, “Chitin-based tubes for tissue engineering in the nervous system,” *Biomaterials*, vol. 26, 2005, pp. 4624-4632.

[21] S. Ibrahim, Q.K. Kang, and A. Ramamurthi, “The impact of hyaluronic acid oligomer content on physical, mechanical, and biologic properties of divinyl sulfone-crosslinked hyaluronic acid hydrogels,” *Journal of Biomedical Materials Research Part A*, vol. 94A, 2010, pp. 355-370.

[22] J.C. Antunes, J.M. Oliveira, R.L. Reis, J.M. Soria, J.L. Gomez Ribelles, and J.F. Mano, “Novel poly (L -lactic acid)/ hyaluronic acid macroporous hybrid scaffolds : Characterization and assessment of cytotoxicity,” *Journal of Biomedical Materials Research A*, vol. 94, 2010, pp. 856-869.

[23] Y. Liu, X.Z. Shu, S.D. Gray, and G.D. Prestwich, “Disulfide-crosslinked hyaluronan – gelatin sponge : growth of fibrous tissue in vivo,” *Journal of Biomedical Materials Research A*, vol. 68, 2004, pp. 142-149.

[24] C.E. Schmidt and J.B. Leach, “Neural Tissue Engineering: Strategies for Repair and Regeneration,” *Annual Review of Biomedical Engineering*, vol. 5, 2003, pp. 293-347.

[25] I. Markiewicz and B. Lukomska, “The role of astrocytes in the physiology and pathology of the central nervous system.,” *Acta neurobiologiae experimentalis*, vol. 66, Jan. 2006, pp. 343-58.

[26] B. Briefings, *September* 2010.

[27] L.F. Eng, R.S. Ghirnikar, and Y.L. Lee, “Glial fibrillary acidic protein: GFAP-thirty-one years (1969-2000).,” *Neurochemical research*, vol. 25, Oct. 2000, pp. 1439-51.

[28] N.J. Abbott, “Astrocyte–endothelial interactions and blood–brain barrier permeability,” *Journal of Anatomy*, 2002, pp. 629-638.

[29] R. Balabanov and P. Dore-Duffy, “Mini-Review Role of the CNS Microvascular Pericyte in the Blood-Brain Barrier,” *Journal of Neuroscience Research*, vol. 53, 1998, pp. 637-644.

[30] H. Wolburg, A. Lippoldt, and K. Ebnet, *Neural Membranes and Barriers. Tight Junctions in the Blood-Brain Barrier*, Springer-Verlag Berlin Heidelberg, 2007.

[31] I. Wilhelm, C. Fazakas, and I. a Krizbai, “In vitro models of the blood-brain barrier.,” *Acta neurobiologiae experimentalis*, vol. 71, Jan. 2011, pp. 113-28.

[32] N.M. Nakagawa S, Deli MA, Kawaguchi H, Shimizudani T, Shimono T, Kittel A, Tanaka K, “A new blood-brain barrier model using primary rat brain endothelial cells, pericytes and astrocytes,” *Neurochemistry International*, vol. 54, 2009, pp. 253-263.

[33] B.B. Weksler, E. a Subileau, N. Perrière, P. Charneau, K. Holloway, M. Leveque, H. Tricoire-Leignel, A. Nicotra, S. Bourdoulous, P. Turowski, D.K. Male, F. Roux, J. Greenwood,

I. a Romero, and P.O. Couraud, “Blood-brain barrier-specific properties of a human adult brain endothelial cell line.,” *The FASEB journal*, vol. 19, Nov. 2005, pp. 1872-4.

[34] K.-kai Wang, I.R. Nemeth, B.R. Seckel, D.P. Chakalis-Haley, D.A. Swann, J.-W. Kuo, D.J. Bryan, and C.L. Cetrulo, “Hyaluronic acid enhances peripheral nerve regeneration in vivo,” *Microsurgery*, vol. 18, 1998, pp. 270-275.

[35] N. Zhang, H. Yan, and X. Wen, “Tissue-engineering approaches for axonal guidance,” *Brain Research Reviews*, vol. 49, 2005, pp. 48-65.

[36] A.K. Meyer, M. Maisel, A. Hermann, K. Stirl, and A. Storch, “Restorative approaches in Parkinson’s Disease: which cell type wins the race?,” *Journal of the neurological sciences*, vol. 289, Feb. 2010, pp. 93-103.

[37] J.N. Joyce, H.L. Ryoo, T.B. Beach, J.N. Caviness, M. Stacy, E.V. Gurevich, M. Reiser, and C.H. Adler, “Loss of response to levodopa in Parkinson ’ s disease and co-occurrence with dementia : role of D 3 and not D 2 receptors,” *Brain Research*, vol. 955, 2002, pp. 138-152.

[38] N. Naoyuki, K. Kakishita, and T. Itakura, “Protection of dopamine neurons by bone marrow stromal cells,” *Brain Research*, vol. 1186, 2007, pp. 48-55.

[39] P.M. Reeves, B. Bommarius, S. Lebeis, S. McNulty, J. Christensen, A. Swimm, A. Chahroudi, R. Chavan, M.B. Feinberg, D. Veach, W. Bornmann, M. Sherman, and D. Kalman, “Disabling poxvirus pathogenesis by inhibition of Abl-family tyrosine kinases.,” *Nature medicine*, vol. 11, Jul. 2005, pp. 731-9.

[40] W. Palmer and K.M. John, “The polysaccharide of the vitreous humor,” *Ophthalmology*, pp. 629-634.

[41] B. Weissmann and K. Meyer, “The Structure of Hyalobiuronic Acid and of Hyaluronic Acid from Umbilical Cord.,” 1954, pp. 1753-1757.

[42] H.G. Garg and C.A. Hales, *Chemistry and Biology of Hyaluronan*, Elsevier, 2004.

[43] J.R.E. Fraser, T.C. Laurent, and U.B.G. Laurent, “Hyaluronan: its nature, distribution, functions and turnover,” *Journal of Internal Medicine*, vol. 242, 1997, pp. 27-33.

[44] D. Jiang, J. Liang, and P.W. Noble, “Hyaluronan in Tissue Injury and Repair,” *Annual Review of Cell and Developmental Biology*, vol. 23, 2007, pp. 435-461.

[45] L. Callegaro, “Coatings based on Hyaluronic Acid and the derivates thereof for the protection of electronic parts from external agents,” , 2002.

[46] K.S. Girish and K. Kemparaju, “The magic glue hyaluronan and its eraser hyaluronidase : A biological overview,” *Life Sciences*, vol. 80, 2007, pp. 1921 - 1943.

[47] K.P. Redbord, M. Busso, and C.W. Hanke, “Soft-tissue augmentation with hyaluronic acid and calcium hydroxyl apatite fillers,” *Dermatologic Therapy*, vol. 24, 2011, pp. 71-81.

[48] X. Zhao, “Synthesis and characterization of a novel hyaluronic acid hydrogel,” *Journal of Biomaterial Science: Polymer Edition*, vol. 17, 2006, pp. 419-33.

[49] K. Tomihata and Y. Ikada, “Crosslinking of hyaluronic acid with water-soluble carbodiimide,” *Journal of Biomedical Materials Research*, vol. 37, 1997, pp. 243-251.

[50] G. Pitarresi, E.F. Craparo, F.S. Palumbo, B. Carlisi, and G. Giammona, “Composite Nanoparticles Based on Hyaluronic

Acid Chemically Cross-Linked with Polyaspartylhydrazide," *Biomacromolecules*, vol. 8, 2007, pp. 1890-1898.

[51] V. Vindigni, R. Cortivo, L. Iacobellis, G. Abatangelo, and B. Zavan, "Hyaluronan Benzyl Ester as a Scaffold for Tissue Engineering," *International Journal of Molecular Science*, vol. 10, 2009, pp. 2972-2985.

[52] Y. Luo and G.D. Prestwich, "Synthesis and Selective Cytotoxicity of a Hyaluronic Acid-Antitumor Bioconjugate," *Bioconjugate Chemistry*, vol. 10, 1999, pp. 755-763.

[53] M. Mason, K.P. Vercruysse, K.R. Kirker, R. Frisch, D.M. Marecak, G.D. Prestwich, and W.G. Pitt, "Attachment of hyaluronic acid to polypropylene, polystyrene, and polytetrafluoroethylene," *Biomaterials*, vol. 21, 2000, pp. 31-36.

[54] J. Kim, I.S. Kim, T.H. Cho, B.K. Lee, S.J. Hwang, G. Tae, I. Noh, S.H. Lee, Y. Park, and K. Sun, "Bone regeneration using hyaluronic acid-based hydrogel with bone morphogenic protein-2 and human mesenchymal stem cells," *Biomaterials*, vol. 28, 2007, pp. 1830-1837.

[55] R. Barbucci, A. Magnani, R. Rappuoli, S. Lamponi, and M. Consumi, "Immobilisation of sulphated hyaluronan for improved biocompatibility," *Journal of Inorganic Biochemistry*, vol. 79, 2000, pp. 119-125.

[56] J. Patterson, R. Siew, S.W. Herring, A.S.P. Lin, R. Guldberg, and P.S. Stayton, "Biomaterials Hyaluronic acid hydrogels with controlled degradation properties for oriented bone regeneration," *Biomaterials*, vol. 31, 2010, pp. 6772-6781.

[57] X. Jia, Y. Yeo, R.J. Clifton, T. Jiao, D.S. Kohane, J.B. Kobler, S.M. Zeitels, and R. Langer, "Hyaluronic Acid-Based Microgels and Microgel Networks for Vocal Fold Regeneration," *Biomacromolecules*, vol. 7, 2006, pp. 3336-3344.

[58] C.-H. Chang, H.-C. Liu, C.-C. Lin, C.-H. Chou, and F.-H. Lin, “Gelatin–chondroitin–hyaluronan tri-copolymer scaffold for cartilage tissue engineering,” *Biomaterials*, vol. 24, Nov. 2003, pp. 4853-4858.

[59] Y. Sakai, Y. Matsuyama, K. Takahashi, T. Sato, T. Hattori, S. Nakashima, and N. Ishiguro, “New artificial nerve conduits made with photocrosslinked hyaluronic acid for peripheral nerve regeneration,” *Bio-medical Materials and Engineering*, vol. 17, 2007, pp. 191-197.

[60] S. Hou, Q. Xu, W. Tian, F. Cui, Q. Cai, and I.-soup Lee, “The repair of brain lesion by implantation of hyaluronic acid hydrogels modified with laminin,” *Journal of Neuroscience Methods*, vol. 148, 2005, pp. 60-70.

[61] W. Tian, S. Hou, J. Ma, C. Zhang, Q. Xu, I. Lee, H. Li, M. Spector, and F. Cui, “Hyaluronic acid-poly-D-lysine-based three-dimensional hydrogel for traumatic brain injury,” *Tissue Engineering*, vol. 11, 2005, pp. 513-525.

[62] I.S.Lee, “Hyaluronic acid hydrogel immobilized with RGD peptides for brain tissue engineering,” *Journal of materials science. Materials in medicine*, vol. 17, 2006, pp. 1393-1401.

[63] Y.T. Wei, W.M. Tian, X. Yu, F.Z. Cui, S.P. Hou, Q.Y. Xu, and I.-S. Lee, “Hyaluronic acid hydrogels with IKVAV peptides for tissue repair and axonal regeneration in an injured rat brain,” *Biomedical Materials*, vol. 2, 2007, p. S142-S146.

[64] K. Bergman, U. Wallenquist, S. Svahn, T. Bowden, and K. Bra, “Enhanced Neuronal Differentiation in a Three-Dimensional Collagen-Hyaluronan Matrix,” *Journal of Neuroscience Research*, vol. 85, 2007, pp. 2138-2146.

[65] J. Ma, W.-M. Tian, S.-P. Hou, Q.-Y. Xu, M. Spector, and F.-Z. Cui, “An experimental test of stroke recovery by implanting a hyaluronic acid hydrogel carrying a Nogo receptor antibody in

a rat model.," *Biomedical materials*, vol. 2, Dec. 2007, pp. 233-40.

[66] T.-wei Wang and M. Spector, "Development of hyaluronic acid-based scaffolds for brain tissue engineering," *Acta Biomaterialia*, vol. 5, 2009, pp. 2371-2384.

[67] L. Pan, Y. Ren, F. Cui, and Q. Xu, "Viability and Differentiation of Neural Precursors on Hyaluronic Acid Hydrogel Scaffold," *Journal of Neuroscience Research*, vol. 87, 2009, pp. 3207-3220.

[68] Y.-T. Wei, Y. He, C.-L. Xu, Y. Wang, B.-F. Liu, X.-M. Wang, X.-D. Sun, F.-Z. Cui, and Q.-Y. Xu, "Hyaluronic acid hydrogel modified with nogo-66 receptor antibody and poly-L-lysine to promote axon regrowth after spinal cord injury.," *Journal of biomedical materials research. Part B, Applied biomaterials*, vol. 95, Oct. 2010, pp. 110-7.

[69] J. Folkman and C. Haudenschild, "Angiogenesis in vitro," *Nature*, vol. 288, 1980, pp. 551-556.

[70] R. Montesano, L. Orci, and P. Vassalli, "In vitro rapid organization of endothelial cells into capillary-like networks is promoted by collagen matrices.," *The Journal of cell biology*, vol. 97, Nov. 1983, pp. 1648-1652.

[71] W. Risau, "mechanism of angiogenesis," *Nature*, vol. 386, 1997, pp. 671-674.

[72] S. Stromblad and D. Cheresh, "Cell adhesion and angiogenesis," *Trends in Cell Biology*, vol. 6, Dec. 1996, pp. 462-468.

[73] T.I. Koblizek, C. Weiss, G.D. Yancopoulos, U. Deutsch, and W. Risau, "Angiopoietin-1 induces sprouting angiogenesis in vitro.," *Current biology*, vol. 8, Apr. 1998, pp. 529-32.

[74] G. Breier and W. Risau, “The role of vascular endothelial growth factor in blood vessel formation.,” *Trends in cell biology*, vol. 6, Dec. 1996, pp. 454-6.

[75] J. Folkman and P. a D’Amore, “Blood vessel formation: what is its molecular basis?,” *Cell*, vol. 87, Dec. 1996, pp. 1153-5.

[76] G. Bunone, P. Vigneri, L. Mariani, S. Butó, P. Collini, S. Pilotti, M. a Pierotti, and I. Bongarzone, “Expression of angiogenesis stimulators and inhibitors in human thyroid tumors and correlation with clinical pathological features.,” *The American journal of pathology*, vol. 155, Dec. 1999, pp. 1967-76.

[77] M. Nomi, A. Atala, P.D. Coppi, and S. Soker, “Principals of neovascularization for tissue engineering.,” *Molecular aspects of medicine*, vol. 23, Dec. 2002, pp. 463-83.

[78] D. Hanahan and J. Folkman, “Patterns and emerging mechanisms of the angiogenic switch during tumorigenesis.,” *Cell*, vol. 86, Aug. 1996, pp. 353-64.

[79] K.M. Cook and W.D. Figg, “Angiogenesis inhibitors: current strategies and future prospects.,” *CA: a cancer journal for clinicians*, vol. 60, 2011, pp. 222-43.

[80] J.A. Abraham, A. Mergia, J.L. Whang, A. Tumolo, J. Friedman, G. Hjerrild, K.A., and J.C. D., Fiddes, “Nucleotide sequence of a bovine clone encoding the angiogenic protein, basic fibroblast growth factor,” *Science*, vol. 233, 1986, pp. 545-548.

[81] C. Basilico and D. Moscatelli, “The FGF family of growth factors and oncogenes,” *Advances in Cancer Research*, vol. 59, 1992, pp. 115-165.

[82] N. Ferrara, “Role of vascular endothelial growth factor in regulation of physiological angiogenesis,” *American Journal of*

Physiology -Cell Physiology, vol. 280, Jul. 2001, p. C1358-C1366.

[83] A. Carmeliet, P., Ferreira, V., Breier, G., Pollefeyt, S., Kieckens, L., Gertsenstein, M., Fahrig, M., Vandenhoeck, A., Harpal, K., Eberhardt, C., Declercq, C., Pawling, J., Moons, L., Collen, D., Risau, W., Nagy, "Abnormal blood vessel development and lethality in embryos lacking a single VEGF allele," *Nature*, vol. 380, pp. 435-439.

[84] T. Alon, I. Hemo, A. Itin, J. Peter, J. Stone, and E. Keshet, "Vascular endothelial growth factor acts as a survival factor for newly formed retinal vessels and has implications for retinopathy of prematurity," *Nature Medicine*, vol. 1, 1995, pp. 1024 -1028.

[85] C. Suri, P.F. Jones, S. Patan, S. Bartunkova, P.C. Maisonpierre, S. Davis, T.N. Sato, and G.D. Yancopoulos, "Requisite role of angiopoietin-1, a ligand for the TIE2 receptor, during embryonic angiogenesis.," *Cell*, vol. 87, Dec. 1996, pp. 1171-80.

[86] J. Oliner, H. Min, J. Leal, D. Yu, S. Rao, E. You, X. Tang, H. Kim, S. Meyer, S.J. Han, N. Hawkins, R. Rosenfeld, E. Davy, K. Graham, F. Jacobsen, S. Stevenson, J. Ho, Q. Chen, T. Hartmann, M. Michaels, M. Kelley, L. Li, K. Sitney, F. Martin, J.-R. Sun, N. Zhang, J. Lu, J. Estrada, R. Kumar, A. Coxon, S. Kaufman, J. Pretorius, S. Scully, R. Cattley, M. Payton, S. Coats, L. Nguyen, B. Desilva, A. Ndifor, I. Hayward, R. Radinsky, T. Boone, and R. Kendall, "Suppression of angiogenesis and tumor growth by selective inhibition of angiopoietin-2.," *Cancer cell*, vol. 6, Dec. 2004, pp. 507-16.

[87] A. Zacharek, J. Chen, X. Cui, A. Li, Y. Li, C. Roberts, Y. Feng, and M. Chopp, "Angiopoietin1/Tie2 and VEGF/Flk1 induced by MSC treatment amplifies angiogenesis and vascular stabilization after stroke," *Journal of Cerebral Blood Flow Metabolism*, vol. 27, 2007, pp. 1684-1691.

[88] J.C. Rodriguez Hernández, Á. Serrano Aroca, J.L. Gómez Ribelles, and M. Monleón Pradas, "Three-Dimensional Nanocomposite Scaffolds With Ordered Cylindrical Orthogonal Pores," *Journal of Biomedical Materials Research Part B Appl Biomater*, 2008, pp. 541-549.

[89] M.N. Collins and C. Birkinshaw, "Comparison of the Effectiveness of Four Different Crosslinking Agents with Hyaluronic Acid Hydrogel Films for Tissue-Culture Applications," *Journal of Applied Polymer Science*, vol. 104, 2007, pp. 3183-3191.

[90] V.C. Hascall and T.C. Laurent, "Hyaluronan: Structure and Physical properties," *Hyaluronan Today*, pp. 2-6.

[91] K. Franze, A. Reichenbach, and J. Käs, *Mechanosensitivity of the Nervous System.Biomechanics of the CNS*, 2009.

[92] A.V. Shulyakov, S.S. Cenkowski, R.J. Buist, and M.R. Del Bigio, "Age-dependence of intracranial viscoelastic properties in living rats," *Journal of the Mechanical Behavior of Biomedical Materials*, vol. 4, 2011, pp. 484-497.

[93] A. Gefen and S.S. Margulies, "Are in vivo and in situ brain tissues mechanically similar?," *Journal of Biomechanics*, vol. 37, Sep. 2004, pp. 1339-52.

[94] Z. Taylor and K. Miller, "Reassessment of brain elasticity for analysis of biomechanisms of hydrocephalus.," *Journal of Biomechanics*, vol. 37, Aug. 2004, pp. 1263-9.

[95] P.C. Georges, W.J. Miller, D.F. Meaney, E.S. Sawyer, and P.A. Janmey, "Matrices with Compliance Comparable to that of Brain Tissue Select Neuronal over Glial Growth in Mixed Cortical Cultures," *Biophysical Journal*, vol. 90, 2006, pp. 3012-3018.

[96] N.D. Leipzig and M.S. Shoichet, “The effect of substrate stiffness on adult neural stem cell behavior.,” *Biomaterials*, vol. 30, Dec. 2009, pp. 6867-78.

[97] P. Bulpitt and D. Aeschlimann, “New strategy for chemical modification of hyaluronic acid : Preparation of functionalized derivatives and their use in the formation of novel biocompatible hydrogels,” *Journal of Biomedical Materials Research*, vol. 47, 1999, pp. 152-169.

[98] S.K. Hahn, J.K. Park, T. Tomimatsu, and T. Shimoboji, “Synthesis and degradation test of hyaluronic acid hydrogels,” *International Journal of Biological Macromolecules*, vol. 40, 2007, pp. 374-380.

[99] Y. Liu, X.Z. Shu, and G.D. Prestwich, “Biocompatibility and stability of disulfide-crosslinked hyaluronan films,” *Biomaterials*, vol. 26, 2005, pp. 4737-4746.

[100] L. Rodén, P. Campbell, F. Fraser, T. Laurent, H. Pertoft, and J. Thompson, *Enzymic pathways of hyaluronan catabolism*, 1989.

[101] P.D. Dalton and M.S. Shoichet, “Creating porous tubes by centrifugal forces for soft tissue application,” *Biomaterials*, vol. 22, 2001, pp. 2661-2669.

[102] H. Francisco, B.B. Yellenb, D.S. Halversonc, G. Friedmanc, and G. Gallo, “Regulation of axon guidance and extension by three-dimensional constraints,” *Biomaterials*, vol. 28, 2007, pp. 3398-3407.

[103] R.M. SMEAL, R. RABBITT, R. BIRAN, and P.A. TRESCO, “Substrate Curvature Influences the Direction of Nerve Outgrowth,” *Annals of Biomedical Engineering*, vol. 33, 2005, pp. 376-382.

[104] S. Stokols, J. Sakamoto, C. Breckon, T. Holt, J. Weiss, and M.H. Tuszynski, “Templated Agarose Scaffolds Support Linear

Axonal Regeneration," *Tissue Engineering*, vol. 12, 2006, pp. 2777-2787.

[105] A.J. García, "Interfaces to Control Cell-Biomaterial Adhesive Interactions," *Advanced Computer Simulation Approaches For Soft Matter Sciences I*, vol. 203, 2006, pp. 171-190.

[106] S.-woong Kang, J.-su Kim, K.-sook Park, B.-hyun Cha, J.-hyung Shim, J. Young, D.-woo Cho, J.-won Rhie, and S.-hong Lee, "Surface modification with fibrin / hyaluronic acid hydrogel on solid-free form-based scaffolds followed by BMP-2 loading to enhance bone regeneration," *Bone*, vol. 48, 2011, pp. 298-306.

[107] T. Yamada, R. Sawada, and T. Tsuchiya, "The effect of sulfated hyaluronan on the morphological transformation and activity of cultured human astrocytes," *Health (San Francisco)*, vol. 29, 2008, pp. 3503-3513.

[108] P. Liesi, D. Dahl, and A. Vaheri, "Neurons cultured from developing rat brain attach and spread preferentially to laminin," *Journal of Neuroscience Research*, vol. 11, 1984, pp. 241-251.

[109] P. Heiduschka, "Defined adhesion and growth of neurones on artificial structured substrates," *Electrochimica Acta*, vol. 47, Sep. 2001, pp. 299-307.

[110] W. He and R.V. Bellamkonda, "Nanoscale neuro-integrative coatings for neural implants.," *Biomaterials*, vol. 26, Jun. 2005, pp. 2983-90.

[111] V.W. van Hinsbergh, a Collen, and P. Koolwijk, "Role of fibrin matrix in angiogenesis.," *Annals of the New York Academy of Sciences*, vol. 936, Jan. 2001, pp. 426-37.

[112] M.K. Cho, G.H. Lee, E.Y. Park, and S.G. Kim, "Hyaluronic acid inhibits adhesion of hepatic stellate cells in spite of its

stimulation of DNA synthesis," *Tissue & Cell*, vol. 36, 2004, pp. 293-305.

[113] E.M. Ehlers, P. Behrens, L. Wünsch, W. Kühnel, and M. Russlies, "Effects of hyaluronic acid on the morphology and proliferation of human chondrocytes in primary cell culture," *Annals of Anatomy*, 1998, pp. 13-17.

[114] J. Struve, P.C. Mahe, Y.-Q. Li, S. Kinney, M.G. Fehlings, C. Kuntz IV, and L.S. Sherman, "Disruption of the Hyaluronan-Based Extracellular Matrix in Spinal Cord Promotes Astrocyte Proliferation," *Glia*, vol. 52, 2005, pp. 16-24.

[115] C.M. Rilley, P.W. Fuegy, M.A. Firpo, X.Z. Shu, G.D. Prestwich, and R.A. Peattie, "Stimulation of In Vivo Angiogenesis Using Dual Growth Factor- loaded Crosslinked Glycosaminoglycan Hydrogels," *Biomaterials*, vol. 27, Jul. 2006, pp. 5935-5943.

[116] C.-K. Perng, Y.-J. Wang, C.-H. Tsi, and H. Ma, "In Vivo Angiogenesis Effect of Porous Collagen Scaffold with Hyaluronic Acid Oligosaccharides.," *The Journal of surgical research*, vol. 7, Oct. 2009, pp. 1-7.

[117] M.I. Santos, R.E. Unger, R. a Sousa, R.L. Reis, and C.J. Kirkpatrick, "Crosstalk between osteoblasts and endothelial cells co-cultured on a polycaprolactone-starch scaffold and the in vitro development of vascularization.," *Biomaterials*, vol. 30, Sep. 2009, pp. 4407-15.

[118] R.E. Unger, A. Sartoris, K. Peters, A. Motta, C. Migliaresi, M. Kunkel, U. Bulnheim, J. Rychly, and C.J. Kirkpatrick, "Tissue-like self-assembly in cocultures of endothelial cells and osteoblasts and the formation of microcapillary-like structures on three-dimensional porous biomaterials.," *Biomaterials*, vol. 28, Sep. 2007, pp. 3965-76.

[119] M. Kolbe, Z. Xiang, E. Dohle, M. Tonak, and C.J.K.S. Fuchs, "Paracrine Effects Influenced by Cell Culture Medium and

Consequences on Microvessel-Like Structures in Cocultures of Mesenchymal Stem Cells and Outgrowth Endothelial Cells," *Tissue Engineering Part A.*, vol. 17, 2011.

[120] F. Lefranc, T. Mijatovic, V. Mathieu, S. Rorive, C. Decaestecker, O. Debeir, J. Brotchi, P. Van Ham, I. Salmon, and R. Kiss, "Characterization of gastrin-induced proangiogenic effects in vivo in orthotopic U373 experimental human glioblastomas and in vitro in human umbilical vein endothelial cells.," *Clinical cancer research*, vol. 10, Dec. 2004, pp. 8250-65.

[121] P. Garberg, M. Ball, N. Borg, R. Cecchelli, L. Fenart, R.D. Hurst, T. Lindmark, A. Mabondzo, J.E. Nilsson, T.J. Raub, D. Stanimirovic, T. Terasaki, J.-O. Oberg, and T. Osterberg, "In vitro models for the blood-brain barrier.," *Toxicology in vitro*, vol. 19, Apr. 2005, pp. 299-334.

[122] J. Abraham, A. Mergia, J. Whang, A. Tumolo, J. Friedman, K. Hjerrild, D. Gospodarowicz, and J. Fiddes, "Nucleotide sequence of a bovine clone encoding the angiogenic protein, basic fibroblast growth factor," *Science*, vol. 4763, 1986, pp. 545-8.

[123] Z.C.W. Tang, W.-Y. Liao, A.C.L. Tang, S.-J. Tsai, and P.C.H. Hsieh, "The enhancement of endothelial cell therapy for angiogenesis in hindlimb ischemia using hyaluronan.," *Biomaterials*, vol. 32, Jan. 2011, pp. 75-86.

ACT	Autologous chondrocyte transplantation
ADH	Adipic acid DiHydrazide
AIBN	Azo Iso-butyronitrile
Ang-1	Angiopoietin 1
Ang-2	Angiopoietin 2
bFGF	basic fibroblast growth factor
CLSM	Confocal laser scanning microscopy
Da	Dalton
DEO	1,2,7,8-diepoxioctane
DMF	Dimethyl Formamide
DPBS	Dubelco's Phosphate Buffer Solution
DVS	Divinyl sulfone
EA	Ethyl Acrylate
EC	Endothelial cell
ECM	Extracellular Matrix
EGDMA	EtilenGlycolDiMethacrylate
EWC	Equilibrium Water Content
fb	Fibrine
FCS	Fetal Serum
FTIR-ATR	Fourier Transformed Infrared Spectra-
GAG	GlucosAminoGlicane
GFAP	Glial Fibrillar Acid Protein
Gpa	Giga Pascal
HA	Hyaluronic Acid
HA-GMA	Glycidyl methacrylate modified hyaluronic Acid
HASs	Hyaluronic Acid Synthases
HCl	Hydrochloride
HEA	HydroxyEthyl Acrylate
HEPES	4-(2-HydroxyEthyl)-1-PiperazineEthaneSulfonic acid
hMSC	human Mesenchimal Stem Cell
HOBt	HydrOxyBenzoTriazole
HYAFF®	benzyl ester derivates of hyaluronic acid
IKVAV	Isoleucine-Lysine-Valine-Alanine-Valine
LN	Laminin
LPS	Lipopolisacharide
NaOH	sodium hydroxide
NS/PC	Neural Stem/Progenitor cells
NSC	neural Stem cells
PCL	Poly(-caprolactone)
PECAM	Platelet Endothelial Cell Adhesion Molecule
PFA	Para-FormAldehyde
PGA	Poly(Glycolic Acid)
PLA	Poly(Lactic Acid)

PLGA	Poly(Lactic acid-co-Glycolic Acid)
PMMA	PoliMethyl MethAcrylate
PP	PoliPropilene
Q	Volumetric Swelling
RGD	Arginyl-glycyl-aspartic acid
SEM	Scanning Electron Microscopy
TE	Tissue Engineering
Tie-2	Tirosine Kinase receptor for angiopoietines
TBS	TrisBufferSaline
U373	Human glioblastoma-astrocytoma cell line
VEGF	Vascular Endothelial Growth Factor
vWF	von Willebrand Factor

LIST OF TABLES

Table 1.1 Normal concentrations (μg·g-1) of HA in various organs of different species..... 34

Table 2.1. Reaction conditions tested for hyaluronan crosslinking using 1,2,7,8-diepoxioctane 58

Table 2.2. Conditions for DEO crosslinking on hyaluronan 3D structures.... 60

Table 2.3. Shape of samples, protein coating and cultured cells onto HA-DVS materials 71

Table 3.1. Selected conditions for Hyaluronan crosslinking with 1,2,7,8-diepoxioctane and divinylsulfone for characterization .87

Table 3.2. Peaks in FTIR-ATR spectra for natural hyaluronan and their crosslinked structures HA-DEO and HA-DVS..... 89

Table 3.3. Physical properties for hyaluronan crosslinked matrices..... 94

Table 3.4. Physical properties for hyaluronan crosslinked matrices..... 96

Table 3.5. Porosity and standard deviation of scaffolds.. 102

Table 3.6. Shape of samples, protein coatings and human cell lines assayed on HA-DVS hydrogels. 107

Table 3.7. Assays performed to biological characterization of HA-DVS hydrogels..... 107

LIST OF FIGURES

Figure 1.1. “Rendering of human brain” created by Nicolas Rougier (Bat. C. INRIA Nancy - Grand Est research center). 25

Figure 1.2. Central and Peripheric Nervous system representation in the human body 26

Figure 1.3. Schematic representation of the cells composing the central nervous system, neurons, oligodendrocytes and astrocytes and their conexión between them and capillaries. 27

Figure 1.4. Cellular structure of the BBB (Figure from [31]) 28

Figure 1.5. Regeneration in the peripheral (A) and central nervous system. 30

Figure 2.1 Molecules of crosslinkers used for hyaluronan crosslinking… 56

Figure 2.2 Multidrilled Teflon® mold used to fabricate 3D structures of hyaluronan……..... ..61

Figure 2.3 Self-made Teflon® device to fabricate hyaluronan multichanneled scaffolds. …….61

Figure 3.1. EWC in HA_DEO crosslinked samples using a 1:50 ratio (w/w) (acetone:HCl 0,1N):HA during different times reactions…… ..82

Figure 3.2. EWC in 24h crosslinking reaction of HA_DEO hydrogels..... 84

Figure 3.3. The lower EWC for 1:5 HA_DEO molar ratio employed to crosslink hyaluronan during three times, 24, 48 and 72 h. 85

Figure 3.4. EWC of hyaluronan crosslinked films with DVS after ending the reaction by rinsing with different acetone-water solutions. 86

Figure 3.5. FTIR spectra of Hyaluronic acid and crosslinked derivates synthetized……..... 87

Figure 3.6. Different bond vibrations in the amide group. 88

Figure 3.7. EWC of HA-DEO and HA-DVS hydrogels by water immersion or by water vapour absorption at 37°C. 91

Figure 3.8. Volumetric swelling for HA-DEO and HA-DVS crosslinked hydrogels……..... 92

Figure 3.9.Typical stress-strain curve for hyaluronan crosslinked hydrogels……..... 93

Figure 3.10.In vitro enzymatic degradation of hyaluronan crosslinked hydrogels…….. 95

Figure 3.11.Optic microphotographs of a complete cylinder obtained by porogen leaching in a mold (a); b and c correspond to details of dry discs cut from the cylinder used for further studies. 96

Figure 3.12.Scanning electron microscopy of 1mm diameter porous cylinders made on HA-DEO.. 97

Figure 3.13.SEM of lyophylized HA-DEO scaffolds obtained by porogen leaching with low interconnection between pores…… 98

Figure 3.14.SEM of 3D structures with multiple parallel-like distributed channels made on HA-DEO. 99

Figure 3.15.3D matrix of HA-DVS with interconnected spherical porous inner structure..101

Figure 3.16.3D matrix of HA-DVS with interconnected spherical porous inner structure showing the fibrin coating. 101

Figure 3.17.Tubular channeled scaffold made on HA-DVS.. 103

Figure 3.18.Interconnected cylindrical channelled scaffold made on a co-polymer of poly(ethylacrylate-co-hydroxyethylacrylate) in a 9 to 1 ratio. . . 104

Figure 3.19.Microphotographs of acrylic co-polymer scaffold coated with hyaluronan DVS crosslinked layer.. 104

Figure 3.20.Evaluation of hyaluronan content in acrylic scaffolds after HA coating by alcian blue assay..... 105

Figure 3.21.8 days calcein stained hCMEC/D3 growing onto films of HA-DVS hydrogels LN or fb coated. 108

Figure 3.22.8 days calcein stained U373 cells growing onto films of HA-DVS hydrogels LN or fb coated. …… …..109

Figure 3.23.Expression of the endothelial specific cell adhesion molecule, E-selectin, by hCMEC/D3 growing on HA-DVS hydrogels without and upon activation by LPS as inflammatory response. 110

Figure 3.24.Endothelial cell specific markers expressed by hCMEC/D3 cultured *in vitro* in cover slides as control during 14 and 21 days..... 112

Figure 3.25.GFAP, an intermediate filament expressed by astrocytes thought to maintain astrocyte mechanical strength and shape in the CNS, was assayed in the U373 cell line..... 112

Figure 3.26.vWF expression by hCMEC/D3 cultured onto HA-DVS hydrogels coated either with LN or fb..... 114

Figure 3.27.PECAM expression by hCMEC/D3 cultured onto HA-DVS hydrogels coated either with LN or fb.. 115

Figure 3.28.GFAP expression by U373 cultured onto HA-DVS hydrogels coated either with LN or fb..... 116

Figure 3.29.Vascular Endothelial Growth Factor (VEGF) and Angiopoietins (Ang-1 and Ang-2) released by hCMEC and U373 into the supernatants

growing in monoculture onto 2D hyaluronan crosslinked hydrogels…… .....……118

Figure 3.30.8 days calcein stained hCMEC/D3 growing onto HA-DVS spherical interconnected porous scaffolds LN or fb coated.. 120

Figure 3.31.8 days calcein stained U373 cells growing onto HA-DVS spherical interconnected porous scaffolds LN or fb coated.. 121

Figure 3.32.vWF expression by hCMEC/D3 cultured onto HA-DVS scaffolds coated either with LN or fb. 123

Figure 3.33.PECAM expression by hCMEC/D3 cultured onto HA-DVS spherical interconnected scaffolds coated either with LN or fb.. 124

Figure 3.34.PECAM expression by hCMEC/D3 cultured onto HA-DVS spherical interconnected scaffolds coated either with LN or fb. 125

Figure 3.35.GFAP expression by U373 cultured onto hyaluronan DVS crosslinked hydrogels coated either with LN or fb..... 126

Figure 3.36.Angiogenic cytokines (Ang-1, Ang-2 and VEGF) released by hCMEC and U373 into the supernatants growing in monoculture onto 3D hyaluronan spherical interconnected porous scaffolds. 128

Figure 3.37.8 days calcein stained hCMEC/D3 growing onto acrylic based biomaterials both without and with HA-DVS coating. 130

Figure 3.38.8 days calcein stained U373 growing onto acrylic based biomaterials both without and with HA-DVS coating. 131

Figure 3.39.E-selectin was stained in green fluorescence in hCMEC growing on acrylic based scaffolds biomaterials without or with hyaluronan coating…….. 132

Figure 3.40.Immunofluorescent images of PECAM expression by hCMEC growing during 21 days onto acrylic based scaffolds with cylindrical interconnected inner structure both without and with HA-DVS coating.. .. 134

Figure 3.41.Immunofluorescent images of vWF expression by hCMEC/D3 growing on acrylic based scaffolds with cylindrical interconnected inner structure both without and with HA-DVS coating. 135

Figure 3.42.Immunofluorescent images of GFAP expression by U373 growing on acrylic based scaffolds with cylindrical interconnected inner structure both without and with HA-DVS coating. 136

Figure 3.43.Angiogenic growth factors (Ang-1, Ang-2 and VEGF) released by hCMEC and U373 into the supernatants growing in monoculture onto acrylic based scaffolds.. 138

Figure 3.44.Immunofluorescent analysis of co-culture control of hCMEC and U373 by successive cell seeding.. 141

Figure 3.45.Expression of vWF and GFAP in co-cultured hCMEC/D3 by simultaneous cell seeding. 141

Figure 3.46.Immunofluorescent analysis of co-culture of hCMEC/D3 and U373 by successive cell seeding. 143

Figure 3.47.Immunofluorescent analysis of co-culture of hCMEC/D3 and U373 by successive cell seeding……...144

Figure 3.48.Immunofluorescent analysis of co-culture of hCMEC/D3 and U373 by simultaneous cell seeding.. 145

Figure 3.49.SEM images of co-culture of hCMEC and U373 growing on hyaluronan based scaffolds.. 146

Figure 3.50.Angiogenic growth factors (Ang-1, Ang-2 and VEGF) released into the supernatants of co-cultured hCMEC and U373 growing in hyaluronan based scaffolds. 148

Figure 3.51.Immunofluorescent analysis of co-culture of hCMEC and U373 by successive cell seeding. 150

Figure 3.52.Immunofluorescent analysis of co-culture of hCMEC and U373 by successive cell seeding. 151

Figure 3.53.Immunofluorescent analysis of co-culture of hCMEC and U373 by simultaneous cell seeding. 152

Figure 3.54.SEM micrographs of hCMEC/D3 and U373 growing in co-culture on acrylic based scaffolds with interconnected cylindrical channels during 14 days. 153

Figure 3.55.SEM micrographs of hCMEC/D3 and U373 growing in co-culture on acrylic based scaffolds with interconnected cylindrical channels during 21 days.. 154

Figure 3.56.Angiogenic growth factors (Ang-1, Ang-2 and VEGF) released into the supernatants of co-cultured hCMEC and U373 growing in acrylic based scaffolds. 155

Figure 4.1.Reactions of hyaluronan..…… ……..160

Figure 4.2.Scheme for HA-DVS crosslinking reaction. 161

Figure 4.3.Schematic procedure to assess the influence of the solution employed for rinsing the HA-DVS hydrogels after crosslinking. 163

Figure 4.4.SEM photographs of hyaluronan scaffolds. 167